MODELS OF SPIN TORQUE USING SELF-CONSISTENT SOLUTIONS OF THE MAGNETISATION AND SPIN ACCUMULATION

PHANWADEE CHUREEMART

SUBMITTED FOR THE DEGREE OF DOCTOR OF PHILOSOPHY

THE UNIVERSITY OF YORK

DEPARTMENT OF PHYSICS

AUGUST 2013

ABSTRACT

A model of spin accumulation ($\mathbf{m}$) is proposed to develop theoretical approaches to calculate the $\mathbf{m}$ in any arbitrary magnetic structure. The model is based on generalising the approach of Zhang, Levy and Fert (PRL 88, 236601, 2002). The calculation involves the layer-wise discretisation of the structure and the development of semi-analytical approaches to solve for the equilibrium $\mathbf{m}$ throughout the structure. Interestingly, the layer discretisation allows the treatment of diffuse interfaces using a gradual variation of the magnetic and transport properties across the interface. The effect of the interfaces between a ferromagnet and a nonmagnet and between two ferromagnets on spin injection is investigated. The formalism for calculating the $\mathbf{m}$ is first generalised by taking $\mathbf{m}$ as the difference of spin-up and spin-down density of states, which is necessary for treating the interface between different ferromagnets. Then, the effect of atomic species interdiffusion at the interface is included by using Ficks law. It is shown that the discontinuity of the $\mathbf{m}$ at the interface depends strongly on the degree of interface mixing.

Subsequently, current-induced domain wall (DW) motion in a ferromagnetic thin film driven by a spin-polarised current is investigated using an atomistic model coupled with a standard Landau-Lifshitz-Gilbert equation. The inclusion of the spin-transfer torque is represented as an additional field. The $\mathbf{m}$ is calculated self-consistently and naturally includes the adiabatic and non-adiabatic contributions depending on the rate of change of magnetisation relative to the spin diffusion length. In this work, it is importantly found that the constants μ_x and β_x used in the standard micromagnetic model do not provide a good description of the spin torque phenomenon due to the non-physical behaviour. Therefore, it is suggested to describe the spin-transfer torque directly from the $\mathbf{m}$.

Finally, the evolution of the magnetisation and $\mathbf{m}$ are demonstrated by introducing a spin-polarised current into a material containing a DW whose width is varied by changing the anisotropy constant. It is found that the adiabatic spin torque tends to develop in the direction of the magnetisation whereas the non-adiabatic spin torque arising from the mistracking of conduction electrons and local magnetisation results in out-of-plane magnetisation components. However, the adiabatic spin torque significantly dominates the dynamics of magnetisation. The total spin torque acting on the magnetisation increases with anisotropy constant due to the increasing magnetisation gradient. This leads to increasing DW displacement.

TABLE OF CONTENTS

LIST OF FIGURES

ACKNOWLEDGEMENTS

It is a great opportunity to thank many people who have supported me and opened me up to the challenging magnetism. First and foremost I would like to express my deepest gratitude to my supervisor, Professor Roy Chantrell. It has been a great privilege and an honour to be his student. I appreciate his contribution of time, excellent ideas and enthusiasm. He also has provided the helpful discussion and guidance over the past five years with the most generous way that have made this thesis possible. I am also thankful for the exceptional example as a successful professor who has inspired me.

I would like to thank Dr. Irene D'Amico for a close collaboration. I am grateful for her useful discussions, excellent comments and constant interest in my work. I have to give a special thanks to Professor Kevin O'Grady for allowing me access to many places with my lovely husband, *Jessada Chureemart*. I would like to thank Dr. Atsufumi Hirohata for fruitful discussions and valuable suggestions. I am also grateful for the IEEE magnetics society for providing me the opportunity to attend the 2011 summer school in New Orleans, USA.

I have to thank all of the members of the computational magnetism group both past and present, who made my life in UK so enjoyable. I must give special mentions to my best friend, Weijia Fan. Thank you for being such a good friend. Dr. Richard Evans and Dr. Ramon Cuadrado are also deserved a special thanks. Working with them is a productive collaboration.

I gratefully acknowledge the provision of a PhD scholarship from the Royal Thai Government that gives me a superb opportunity to study at University of York. My parents must be thanked for their endless love and support towards my study. Lastly, and by no means least, this thesis could not have been possible without my encouraging and supportive husband who has never left me alone. Although he also has to complete his thesis, but he has still held my hands pass through the difficult times. I am truly and deeply indebted to him.

DECLARATION

I hereby declare that the following work presented in this thesis is based originally on my own research and effort. It has not been submitted for a degree in either this or any other university.

The following work was done in collaboration with others. The atomistic simulations of the domain wall structure and domain wall width with different anisotropy constants were done using the vampire software package developed by Dr. Richard Evans at the University of York. The calculations of spin density of states of Co and NiFe bulk alloys were performed by Dr. Ramon Cuadrado at the University of York.

Signed

Phanwadee Chureemart

August 2013

CHAPTER I

Introduction

The spin-transfer torque effect proposed by Slonczewski [1] and Berger [2] introduces an entirely new route for the control of the magnetisation of magnetic structures [3–5] and for spintronic device concepts. Its mechanism involving the spin-polarised current has been extensively studied both experimentally [6–8] and theoretically [9–17]. It is noted that spin electronics, using the spin of the electron in addition to its charge, is an emergent technology with exciting potential. Spin is the quantum mechanical property of the electron. Spin can carry information like charge among the devices and it has the advantage over the charge because of its easier manipulation by the external magnetic field. Spintronics is also potentially useful since it has two states, instead of one (charge). The spin orientation can be retained longer over the characteristic length scale the so-called spin diffusion length (λ_{sdl}) which is usually of the order of ten times larger than the electron mean free path (λ_{mfp}). On the other hand, charge can be easily destroyed by scattering or collision with defects, impurities or other charges [18,19]. This leads to the new class of device, known as *spintronics devices*, based on the electron spin rather than on charge.

The development of spin electronics follows the discovery of giant magnetoresistance (GMR) [20–22]. The GMR effect is associated with the spin-dependent scattering both at the interfaces and within the magnetic layers. GMR, and the subsequent discovery of tunnelling magnetoresistance (TMR) [23], led rapidly to applications such as spin-valve read heads for magnetic recording, giving rise to remarkable increases in storage density and revolutionising computer applications and efficiency. The spin-transfer torque resulting from the exchange interaction between the conduction electrons and the local magnetisation is an important phenomenon with potential applications as spin torque oscillators for telecommunications applications and in the switching of Magnetic Random Access Memory (MRAM) elements. MRAM provides an exciting technological advance, coupling fast speed, non-volatility and low power requirements [24]. The physics of the spin torque phenomenon can be described in terms of spin accumulation which

interacts with the local moment via a quantum mechanical exchange interaction. A polarised current is produced by a magnetic film and injected into a second layer, where its polarisation is rotated into the new magnetisation direction, exerting a reaction torque on the magnetisation. To gain deeper physical understanding in the mechanism of the spin-transfer torque, the effect of GMR and TMR will be presented first as the following.

1.1 Giant magnetoresistance (GMR)

The discovery of the GMR effect in the magnetic multilayer by Baibich *et al.* in 1988 [20] and Binash *et al.* in 1989 [21] opened the possibility to the development of spintronics field. They demonstrated the existence of GMR in multilayers of Fe/Cr which arises from the spin-dependent transmission of the conduction electrons from Fe layer through the Cr layer. Subsequently, the GMR effect in the trilayer magnetic system consisting of two ferromagnetic layers separated by a nonmagnetic layer known as *spin valves* was investigated by Dieny *et al.* [25]. The magnetisation of the first ferromagnet is pinned by coupling with an antiferromagnet whereas the magnetisation of the second ferromagnet is free to rotate. GMR represents the change in resistance through the layers of the magnetic system when the applied magnetic field is varied. Its mechanism based on the spin-dependent scattering can be theoretically explained by using "*two-current model*" proposed by Mott [26–28]. He showed that the electron transport in the ferromagnet is the result of the spin splitting of the energy bands in the ferromagnet. The conductivity of the ferromagnet can be described in terms of two independent conducting channels: spin-up (majority) and spin-down (minority) electrons expressed as the following equation

$$\sigma = \sigma^{\uparrow} + \sigma^{\downarrow} \tag{1.1}$$

and the resistivity can also be expressed as

$$\rho = \frac{\rho^{\uparrow}\rho^{\downarrow}}{\rho^{\uparrow} + \rho^{\downarrow}} \tag{1.2}$$

where σ denotes the conductivity of the ferromagnet. $\sigma^{\uparrow(\downarrow)}$ and $\rho^{\uparrow(\downarrow)}$ are the spin-dependent conductivities and the resistivities of the spin-up(down) channels respectively.

1.1.1 Band structure

The spin-dependent conduction of the ferromagnetic $3d$ transition metals can be qualitatively understood from the typical band structure as illustrated in figure 1.1. In the transition metals, the electron d band is split into the majority and minority d bands. As a result of the exchange splitting, the majority d band is fully occupied whereas the minority d band is partially occupied. This leads to a different spin-up and spin-down density of states at the Fermi energy leading to the magnetic moment. The electric current is carried by the sp electrons due to their low mass and high mobility giving rise to long mean free path and consequently high conductivity. The sp electrons can scatter into the unoccupied d band. Therefore, for majority spin channel the conductivity is governed by sp electrons with the long mean free path responsible for high conductivity whereas the low conductivity is enhanced for the minority spin channel due to the strong sp-d hybridisation [29,30] as shown in figure 1.1. Clearly, the d band plays an important role in the GMR.

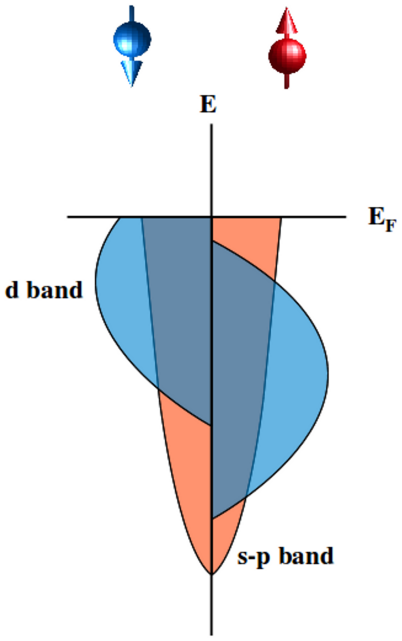

Figure 1.1: Illustration of a simplified band structure for the ferromagnet showing the splitting of the $3d$ band which gives rise to an unequal spin-up and spin-down density of states at the Fermi level: The exchange splitting leads to a different conductivity between majority (up, $\uparrow$) and minority (down, $\downarrow$) spins.

1.1.2 Resistor model

The GMR effect was first observed in the CIP (Current In Plane) geometry which is the magnetic multilayer structure consisting of alternating magnetic and nonmagnetic layers and the current is injected in the plane of the magnetic system. In the CIP geometry, GMR depends on the characteristic length scale, i.e., electron mean free path. To obtain nonzero GMR, the electron mean free path should be longer than the thickness of multilayer structure. Subsequently, the GMR in CPP (Current Perpendicular to the Plane) geometry was performed by injecting current perpendicular to the plane giving rise to higher GMR compared with CIP structure. Therefore, CPP structure is of particular interest in this thesis. Now consider the GMR in the trilayer system consisting of two ferromagnetic layers in between the nonmagnetic layer as illustrated in figure 1.2. The GMR can be determined by considering two configurations of structure: parallel (P) and antiparallel (AP) states.

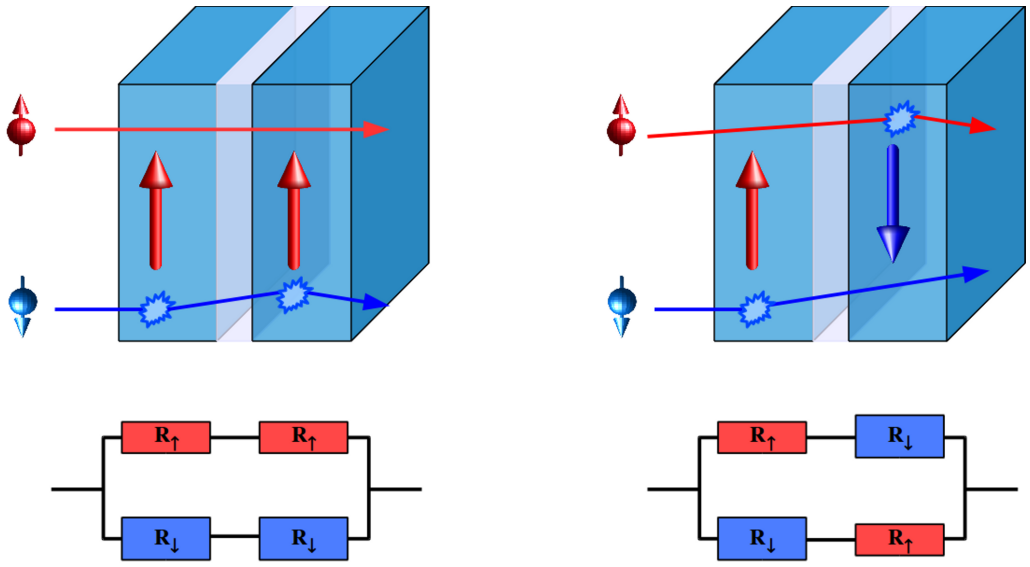

Figure 1.2: Schematic illustration of GMR using a simple resistor network model of parallel (P) and antiparallel (AP) configurations: (left) In parallel state(P), the majority spin or spin-up channel experiences a low resistance ($R_{\uparrow}$) throughout the layers whereas the minority spin or spin-down channel has a high resistance ($R_{\downarrow}$). (right) In antiparallel state (AP), both spin channels are of high resistance giving rise to high overall resistance state.

According to Mott's model, the GMR is generally considered from spin-dependent scattering. For reasons explained before, the minority spins carried by d electrons tend to be scattered more strongly than the majority spins governed by sp electrons. For the parallel configuration (P) in figure 1.2 (left panel), the spin-up electrons travel through the structure almost without the scattering due to the parallel orientation of spin and the magnetisation in both layers. This results in low resistance for the spin-up channel. On the other hand, strong scattering is experienced by the spin-down electrons as their spin direction is antiparallel to the magnetisation of the layers. The strong scattering is the description of the high resistance in the spin-down channel. The total resistance of the layers dominated by the spin-up channel becomes low. On the contrary, for the antiparallel state (AP) in figure 1.2 (right panel) both spin-up and spin-down electrons experience the strong scattering in one of ferromagnetic layers because of the antiparallel spin direction with respect to the magnetisation in ferromagnets. Consequently, the total resistance of the layers is high because of this reason [29, 30].

GMR can be observed when the magnetic structure is changed between the low to high resistance states. The magnetoresistance ratio of figure 1.2 can be determined by using the resistor model. The total resistance of P and AP states are represented by two-current channel with the resistance of different layers given by

$$\frac{\Delta R}{R} = \frac{R_{AP} - R_P}{R_P} = \frac{(R_\downarrow - R_\uparrow)^2}{4R_\uparrow R_\downarrow} \tag{1.3}$$

and the resistance of P and AP states are the following

$$\begin{aligned} R_P &= \frac{2R_\uparrow R_\downarrow}{R_\uparrow + R_\downarrow} \\ R_{AP} &= \frac{R_\uparrow + R_\downarrow}{2} \end{aligned} \tag{1.4}$$

where the low and high resistances are represented by $R_\uparrow$ and $R_\downarrow$ respectively. We note that the GMR normalised by the low resistance state (R_P) can be greater than 100 %.

Valet and Fert showed the enhancement of the spin accumulation around the interface region in the CPP geometry [31] arising from interface spin-dependent scattering. The effect of interface between layers with different band structures becomes significant to the GMR as the transmission of spins will be spin-dependent. Band matching plays an important role in the scattering process since the good band matching at the interface results in the high transmission of electrons across the interface which implies the small

scattering. Therefore, the interfaces between layers behave as spin-filters. As a consequence of spin-dependent scattering, the spin-up and spin-down density of states are out of equilibrium, exhibiting a so-called *spin accumulation*. GMR is associated with the spin accumulation propagating over the distance of the spin diffusion length. Therefore, the spin accumulation which is the quantity of interest will be investigated in this work to study the behaviour of spin transport.

1.2 Tunnel magnetoresistance (TMR)

The spin-dependent scattering significantly contributes to the magnetoresistance as explained in the previous section. Subsequently, various spintronic phenomena related to the interplay between magnetism and conduction electrons have been widely investigated. As a consequence of the advent of GMR, tunnel magnetoresistance (TMR) originating from the spin-dependent tunnelling occurs in a magnetic tunnel junction (MTJ) which consists of a thin insulator or semiconductor sandwiched between two ferromagnets. The thin insulating layer acting as a tunnel barrier enables the electrons to tunnel from one ferromagnet to the other. Similarly to GMR, the TMR is defined as the change in resistance with the relative orientation of magnetisation in two ferromagnetic layers.

The discovery of TMR dates back to the work of Julliere in 1975 [23]. He performed the TMR measurement of Fe/Ge/Co MTJ exhibiting a MR ratio of 14% at 4.2K. According to this model, the spin-polarised tunnelling effect was taken into account. The magnetoresistance ratio of the MTJ can be expressed in terms of the spin polarisation parameters of both ferromagnetic layers given by

$$TMR = \frac{R_{AP} - R_P}{R_P} = \frac{2P_1P_2}{1 - P_1P_2} \tag{1.5}$$

and

$$P_i = \frac{N_i^{\uparrow}(E_F) - N_i^{\downarrow}(E_F)}{N_i^{\uparrow}(E_F) + N_i^{\downarrow}(E_F)} \tag{1.6}$$

where P_i is the spin polarisation of the ferromagnet i and $N_i^{\uparrow(\downarrow)}(E_F)$ is the spin-up(down) density of state at the Fermi energy of the ferromagnet i.

From the above equation, it shows that the TMR value is based on the spin polarisation arising from the electrons tunnelling from one ferromagnet to the other

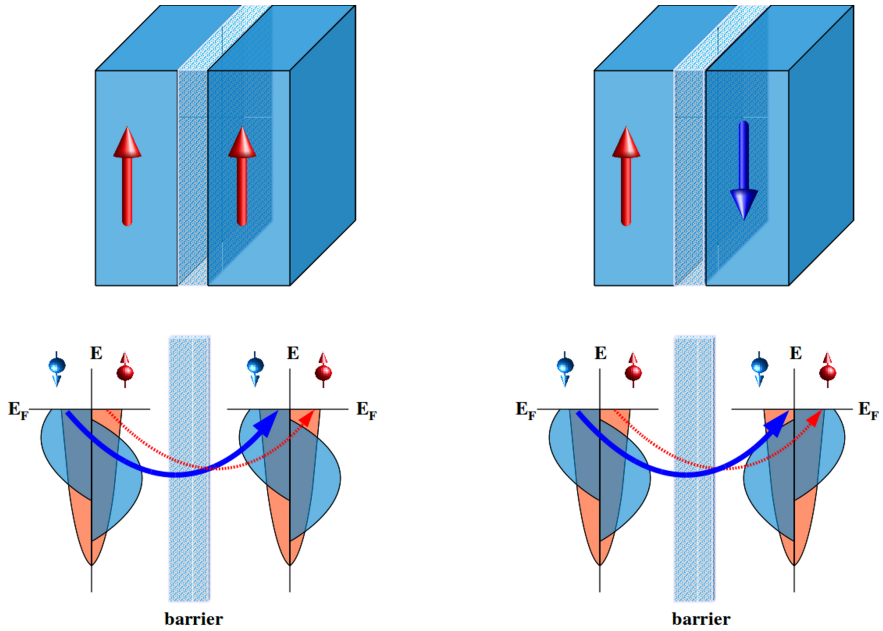

Figure 1.3: Schematic illustration of TMR effect in MTJ: (left) the parallel orientation of magnetisation in two ferromagnets known as P state (right) the antiparallel orientation or AP state

and the spin polarisation is given in terms of the spin-dependent density of states. The probability of electron tunnelling across the barrier depends on the relative orientation of magnetisation in two ferromagnets. As illustrated in figure 1.3 (left), for the parallel state the possibility of electron tunnelling from one ferromagnetic layer to the other through the barrier tends to be higher due to the availability of more free states leading to a large tunnelling current and subsequently a low resistance. In contrast, for the antiparallel orientation spin-up and spin-down channels encounter a bottleneck situation. This gives rise to a small current of electron tunnelling and also results in a high resistance as can be seen in figure 1.3 (right). It is interesting to note that the tunnelling current in TMR effect is mainly contributed from the itinerant *d* electrons due to the fact that the spin-split *d* bands are responsible for ferromagnetism. It is unlike the current in GMR which is carried by *sp* electrons.

The Julliere model is admittedly simple, and explained well the TMR effect of electrons tunnelling from Fe, Ni, and Co into a superconductor. However, it is not applicable for a a tunneling junction with a thin nonmagnetic metallic interlayer such as Cu or Ag which is inserted between one of the ferromagnetic layer and the insulating

barrier as it gives zero TMR inconsistent with the experiment [32]. TMR measurement at low temperature had received a little attention for more than a decade until the discovery of GMR in magnetic multilayer. The renewed attention of TMR results in the development of TMR effect at room temperature [33–35]. Recently, the high TMR in magnetic tunnel junction (MTJ) structures of CoFeB/MgO/CoFeB was investigated by S. Ikeda *et al.* [36, 37]. TMR in the MgO based magnetic tunnel junction can now be achieved over 600% at room temperature.

1.3 Motivation and thesis outline

The GMR and TMR investigations lead to a significant improvement in the potential applications in data storage technology and spintronic devices. The high resistance of TMR allows the development of magnetic random access memory (MRAM), which combines key advantages such as nonvolatility, exceptional endurance, and fast random access, making MRAM an important future technology. However, switching of the magnetic elements is difficult with conventional technology, and present devices predominantly use the spin-transfer torque phenomenon to achieve switching. The spin-transfer torque arising from the spin polarised current flowing through a spin valve or MTJ enables the magnetisation switching. Clearly, the full understanding of the spin torque phenomenon is important for the development of MRAM and other spin electronic technologies, which are currently a topic of extensive interest at the fundamental and technological levels. The mechanism behind GMR and TMR can be interpreted via spin accumulation. Essentially, the calculation of spin accumulation is required in order to have the knowledge insight into the spin transport behaviour in both GMR and TMR effect.

To understand the nature of spin accumulation, we review the previous work of ZLF (Zhang, Levy and Fert) [38]. They studied the spin transfer torque under the assumption that the longitudinal spin accumulation tended to decay to zero in the bulk of a ferromagnet as depicted in figure 1.4. In principle the spin accumulation represents the difference between spin up and spin down conduction electron populations. However, the spin accumulation is commonly defined as the deviation from the equilibrium value; $\delta\mathbf{m} = (n^{\uparrow} - n^{\uparrow}_{eq}) - (n^{\downarrow} - n^{\downarrow}_{eq})$, where n_{eq} refers to the equilibrium (bulk) populations, and $n^{\uparrow(\downarrow)}$ are the local spin-up(down) carrier densities. This definition was used by ZLF[1] in their study of the spin accumulation.

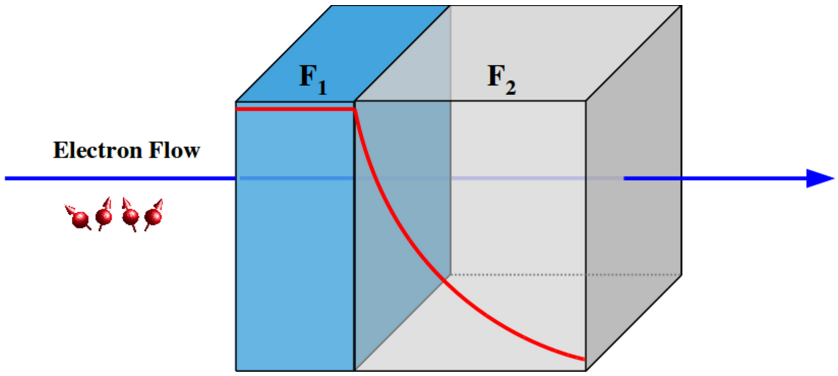

Figure 1.4: Schematic of the behaviour of spin accumulation in the bilayer magnetic system: The red line shows the longitudinal component of spin accumulation based on the model proposed by ZLF. Spin accumulation remains constant in the first ferromagnet as the spin current is fully polarised in this layer. It subsequently decays to zero in the second ferromagnet over the distance of spin diffusion length.

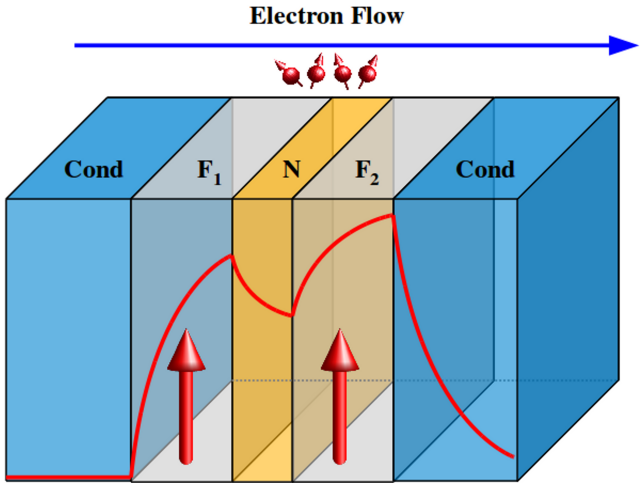

Figure 1.5: Schematic illustration of the behaviour of the spin accumulation throughout a multilayer system consisting of conductor/ferromagnet/nonmagnet/ferromagnet/conductor: The red line shows the development of spin accumulation allowed to increase or decrease to the equilibrium level appropriate for the material.

In this work, a modified equation is introduced by generalising the solutions for the spin accumulation. It is proposed to use the different definition of spin accumulation, $\mathbf{m} = n^{\uparrow} - n^{\downarrow}$. It clearly shows that two definitions used in ZLF and in this thesis differ only by the constant factor $n_{eq}^{\uparrow} - n_{eq}^{\downarrow}$ which is parallel to the local magnetisation. As a consequence, these two definitions give rise to the same spin torque and spin current depending only on the gradient of the spin accumulation. Interestingly, the advantage of using our definition is obviously seen when dealing with multiple layers with different equilibrium values, $\mathbf{m}_{\infty} \equiv n_{eq}^{\uparrow} - n_{eq}^{\downarrow}$. This is due to the fact that our treatment allows the longitudinal component of spin accumulation either to increase or decrease to a nonzero equilibrium value depending on the properties of a material. Figure 1.5 outlines the approach to be adopted. With the new form of the spin accumulation solution it is possible to model the development of spin accumulation from an unpolarised current as it transverses the polarising layer and its evolution throughout the multilayer stack. Consequently, it effectively describes the spin transfer torque in any magnetic material at any given position. This approach will be applied to the magnetic system to study the current-induced domain wall (DW) motion which is exciting for spintronic devices based on DW motion such as race-track memory. The work also allows the treatment of interfacial effects which, although important, have received little attention. The detail of this work will be explained in each chapter as the following.

Chapter 2 of this thesis will give more detail of the spin-dependent transport theory through *the drift-diffusion model* which is very important to understand the physics behind the behaviour of the spin transport. The definition and origin of spin current and spin accumulation will also be presented.

Chapter 3 will be devoted to the detail of the spin accumulation model proposed by ZLF. This model is based on the drift-diffusion equations for the charge and spin current and then applied to a FM/FM bilayer. The physics of this model is sound but limited in many aspects. Therefore, the limitation of this model will be addressed.

Chapter 4 will outline the modified spin accumulation model developed in this study. It gives the possibility to investigate the spatial variation of spin transport in multilayers. The modified model is proposed to develop theoretical approaches to calculate the spin accumulation in any arbitrary magnetic structure. Subsequently, the model is utilised to give the first calculation of the spin current and spin accumulation in the bilayer system with both collinear and non-collinear configurations.

Chapter 5 will present the approach of spin-transfer torque calculation. The spin-transfer torque which is the contribution of the adiabatic and non-adiabatic torques will be described directly through the transverse spin accumulation. The developed model of spin accumulation can be applied generally to a system of many layers, allowing studies of the spin accumulation as well as the spin torque in systems with spatially varying magnetisation structures, i.e., a domain wall. Furthermore, the effect of spin diffusion length and the influence of domain wall thickness will be studied. Importantly, the invalidity of the spin torque coefficients μ_x and β_x described adiabatic and non-adiabatic torques in the usual standard form of the micromagnetic model will be pointed out and discussed in this chapter.

In chapter 6 the effect of diffuse interfaces will be taken into account using the model of spin accumulation since the practical devices are generally produced by sputtering. It must be expected that the interfaces are not atomically smooth. In addition, the scaling of device dimensions leads to the influence of the interface effect. Consequently it is important to develop models of diffuse interfaces. This work suggests to use the solution of Fick's law to represent the interface region and then the modified solution of spin accumulation will be integrated with the diffuse interface model to observe the transport properties of the systems with different interface thicknesses. This is crucial as these systems tend to become important for future device design.

Chapter 7 will investigate the dynamic of magnetisation following the introduction of the spin polarised current by using atomistic model coupled with spin accumulation. It is worthwhile to note that the atomistic simulation of magnetic system increasingly becomes an essential tool in understanding the complex behaviour of the magnetic system such as the diffuse interface while the micromagnetic formalism cannot deal with this problem. The atomistic model including the effect of spin-transfer torque will be derived and then applied to the system containing domain walls to observe the current-induced domain wall motion.

Chapter 8 is the final part of this thesis which concludes the summary of this work as well as the future work. For the future work, the application of the atomistic model with spin accumulation to topics of special importance such as spin torque induced domain wall motion and systems with perpendicular anisotropy will be presented. The possibility to apply the proposed approach to the MTJ (Magnetic Tunnel Junction), CoFeB/MgO/CoFeB structrue, will be discussed.

CHAPTER II

Theory of Spin-dependent transport

This chapter will outline the spin transport theory to describe the physics behind the mechanism of the spin-polarised current travelling through the magnetic system as the spin transport phenomenon is of great interest in the potential applications to the spintronic devices. Evidently from both experimental and theoretical studies, injecting spin-polarised current from a ferromagnet (FM) to a nonmagnet (NM) results in the two main quantities of interest: spin accumulation and spin current [39, 40]. The origin and definition of the spin accumulation and spin current will be necessarily discussed first before explaining their behaviour by using the spin transport equation, a so-called "*drift-diffusion equation*".

2.1 Spin accumulation

The spin accumulation commonly defined as the nonequilibrium spin density can be described by the concept of the spin injection across the interface between a ferromagnet (FM) and a nonmagnet (NM). The spin accumulation phenomenon was first suggested by Aronov [41] and experimentally observed by Johnson and Silsbee [42]. This leads to a number of theoretical works extending the basic models to describe the spin accumulation. Initially, the basic understanding of the spin transport was provided by Mott [26–28]. He pointed out that the conductivity in the ferromagnet can be expressed as the sum of conductivities of the spin-up and spin-down electrons which are independent and unequal. It is known as "*two-current model*" and has been extended to describe the spin transport properties in the ferromagnet by Fert and Campbell [43]. This model also becomes important to provide the explanation of the magnetoresistance effect [31, 39] as mentioned in chapter 1.

According to the previous work of Van Son *et al.* [44], the spin transport can be described in terms of the two-current model. To explain the origin of the spin accumulation with this model, consider the spin transport through the interface between the

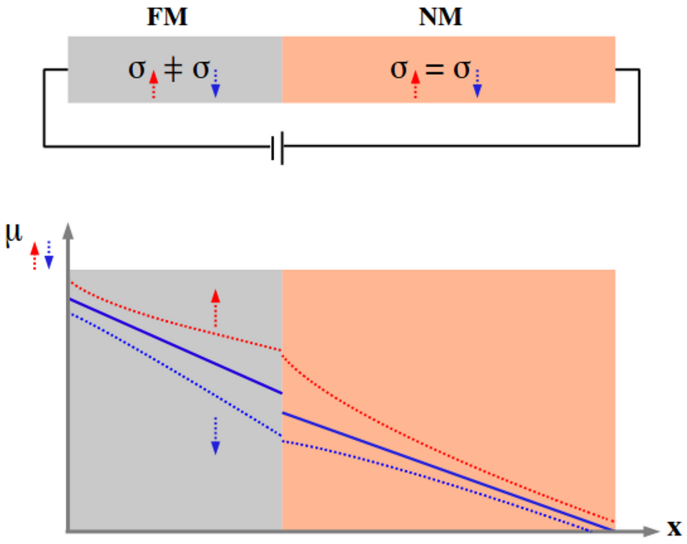

Figure 2.1: The spatial variation of the electrochemical potential for spin-up and spin-down electrons(dotted lines): The solid line shows the electrochemical potential difference for spin-up and spin-down electrons which is related to the spin accumulation [46].

ferromagnet and nonmagnet as depicted in figure 2.1 (top panel). Injecting an electric current into a ferromagnet results in a spin-polarised current, which subsequently flows across the interface into a nonmagnet giving rise the change in electrochemical potential (ECP). This change is associated with the distribution of the local spin-up and spin-down populations. In the absence of the magnetic field, the electrochemical potential (μ) is the contribution of the chemical potential (μ_{ch}) and the potential energy as the given equation.

$$\mu = \mu_{\text{ch}} - eV \tag{2.1}$$

where e denotes the absolute value of the electron charge and V is the electric potential. μ_{ch} is the chemical potential which is the energy required to add an electron to a system and accounts for the kinetic energy of the electrons. For small deviation from equilibrium, the chemical potential can be expressed in terms of the excess electron density and the density of state at the Fermi energy, $N(E_F)$, as follows [45]

$$\mu_{\text{ch}} = \frac{n - n_{eq}}{N(E_F)}. \tag{2.2}$$

In general, the spin accumulation defined as the deviation from the equilibrium value or excess electron density can be described via the two-current model given by

$$\delta\text{m} = n - n_{eq} = (n^{\uparrow} - n^{\uparrow}_{eq}) - (n^{\downarrow} - n^{\downarrow}_{eq}) \tag{2.3}$$

where δm is the spin accumulation, n_{eq} denotes the equilibrium (bulk) populations, and $n^{\uparrow(\downarrow)}$ are the local spin-up(down) carrier densities.

From the relation in equations (2.2) and (2.3), the spin accumulation can also be alternatively represented by the difference in electrochemical potential for spin-up and spin-down electrons, $\delta \mathrm{m} \propto \mu = \mu^{\uparrow} - \mu^{\downarrow}$. As shown in figure 2.1 (bottom panel), the spatial dependence of the ECP arises from the spin injection. Far from the interface, the spin-up and spin-down electrons will be in equilibrium whereas their distributions are significantly changed near the interface due to the mismatch of conductivity across the interface. As a consequence, the spin accumulation is enhanced close to the interfacial region. The spin accumulation diffuses into the nonmagnet from the interface and it tends to decays exponentially to $1/e$ of its magnitude at the interface over a length scale associated with the spin relaxation time [46–49].

In the next section, the important physics behind the behaviour of the spin current and spin accumulation will be outlined as we must implement the appropriate model to explain the spin transport in spintronic devices. Its underlying physics can be described through the theory of spin transport based on the drift-diffusion model. Also the transport parameters governing the development of the spin current and spin accumulation, such as the spin polarisation parameters, the spin diffusion length as well as the diffusion constant, will be introduced.

2.2 The drift-diffusion model

Electron transport results from the driving force on the conduction electrons in the system which is enhanced by the gradient of the electrochemical potential, $\nabla\mu$. The gradient in the ECP provides the driving force leading to the diffusion induced electron transport across the interface. It can be written from equation (2.1) as the following

$$\begin{aligned} \nabla\mu &= \nabla\mu_{\mathrm{ch}} - e\mathbf{E} \\ \nabla\mu &= \frac{\nabla n}{N(E_F)} - e\mathbf{E} \end{aligned} \tag{2.4}$$

where n denotes the spin density of state. $N(E_F)$ is the density of state at the Fermi energy, e is the absolute value of the electron charge and $\mathbf{E}$ is the electric field.

The above equation clearly shows that the driving force can arise from either a spatial varying electron density ∇n or the electric field $\mathbf{E}$. equation (2.4) can be

rewritten by substituting $\mathbf{j} = (-\sigma/e)\nabla\mu$ and the conductivity from the Einstein relation $\sigma = e^2 N(E_F) D$, then the current density driving the electron transport is as follows

$$\begin{aligned} -\frac{\mathbf{j}e}{\sigma} &= \frac{\nabla n}{N(E_F)} - e\mathbf{E} \\ \mathbf{j} &= \sigma\mathbf{E} - De\nabla n \end{aligned} \tag{2.5}$$

where σ is the conductivity and D is the diffusion constant.

Equation (2.5) is a so-called drift-diffusion model used to describe the spin transport in the magnetic system. The current density is contributed from two parts. The first term is the drift current density ($\mathbf{j}_{\text{drift}}$) due to the presence of the electric field. In the drift model, the spin density remains constant by imposing $\nabla n = 0$ whereas the difference in the electrochemical potential between two reservoirs related to ∇n is used to describe the diffusive transport via the diffusion current ($\mathbf{j}_{\text{diffusion}}$).

2.2.1 Charge current model

According to Mott's model, the transport in the magnetic system can also be described through the spin-dependent conductivities. Due to the difference in the spin-up and spin-down conductivities, the current density can be distributed over two spin channels as follows

$$\begin{aligned} \mathbf{j}^{\uparrow} &= \sigma^{\uparrow}\mathbf{E} - D^{\uparrow}e\nabla n^{\uparrow} \\ \mathbf{j}^{\downarrow} &= \sigma^{\downarrow}\mathbf{E} - D^{\downarrow}e\nabla n^{\downarrow}. \end{aligned} \tag{2.6}$$

Here the charge current and the spin current can be introduced via the two-current model. The charge current is determined first as the following

$$\begin{aligned} \mathbf{j}_e &= \mathbf{j}^{\uparrow} + \mathbf{j}^{\downarrow} \\ &= (\sigma^{\uparrow} + \sigma^{\downarrow})\mathbf{E} - D^{\uparrow}e\nabla n^{\uparrow} - D^{\downarrow}e\nabla n^{\downarrow}, \end{aligned}$$

and the spin-up and spin-down density of states can be rewritten as

$$\begin{aligned} n^{\uparrow} &= \left(\frac{n^{\uparrow} + n^{\downarrow}}{2}\right) + \left(\frac{n^{\uparrow} - n^{\downarrow}}{2}\right) \\ n^{\downarrow} &= \left(\frac{n^{\uparrow} + n^{\downarrow}}{2}\right) - \left(\frac{n^{\uparrow} - n^{\downarrow}}{2}\right), \end{aligned} \tag{2.7}$$

then the charge current is achieved by substituting equation (2.7) into equation (2.6) , giving

$$\begin{aligned}
\mathbf{j}_e &= (\sigma^{\uparrow}+\sigma^{\downarrow})\mathbf{E} - \frac{D^{\uparrow}e}{2}\nabla(n^{\uparrow}+n^{\downarrow}) - \frac{D^{\uparrow}e}{2}\nabla(n^{\uparrow}-n^{\downarrow}) - \frac{D^{\downarrow}e}{2}\nabla(n^{\uparrow}+n^{\downarrow}) \\
&\quad + \frac{D^{\downarrow}e}{2}\nabla(n^{\uparrow}-n^{\downarrow}) \\
&= (\sigma^{\uparrow}+\sigma^{\downarrow})E - \frac{e(D^{\uparrow}+D^{\downarrow})}{2}\nabla(n^{\uparrow}+n^{\downarrow}) - \frac{e(D^{\uparrow}-D^{\downarrow})}{2}\nabla(n^{\uparrow}-n^{\downarrow}) \\
&= \sigma\mathbf{E} - \frac{eD}{2}\nabla n - \frac{e\beta' D}{2}\nabla\delta\mathrm{m} \qquad (2.8)
\end{aligned}$$

and

$$\begin{aligned}
\sigma &= \sigma^{\uparrow}+\sigma^{\downarrow} \\
D &= D^{\uparrow}+D^{\downarrow} \\
\beta' &= \frac{D^{\uparrow}-D^{\downarrow}}{D^{\uparrow}+D^{\downarrow}} \\
n &= n^{\uparrow}+n^{\downarrow} \\
\delta\mathrm{m} &= n^{\uparrow}-n^{\downarrow}
\end{aligned}$$

where σ is the conductivity, D is the diffusion constant, β' is the spin polarisation parameter for diffusion constant, n is the charge accumulation and δm is the spin accumulation. $\sigma^{\uparrow(\downarrow)}$ and $D^{\uparrow(\downarrow)}$ denote the spin-dependent conductivities and the spin-dependent diffusion constants respectively.

From equation (2.8), it can be seen that the charge current arises from the contribution of the drift current in the first term, the charge accumulation and spin accumulation in the second and the last terms respectively [38, 50].

2.2.2 Spin current model

Similarly, the spin current can be determined in terms of the two spin channels. It is expressed as functions of the spin-up and spin-down current densities ($j^{\uparrow(\downarrow)}$) as follows

$$\begin{aligned}
\mathbf{j}_m &= \mathbf{j}^{\uparrow}-\mathbf{j}^{\downarrow} = (\sigma^{\uparrow}-\sigma^{\downarrow})\mathbf{E} - D^{\uparrow}e\nabla n^{\uparrow} + D^{\downarrow}e\nabla n^{\downarrow} \\
&= (\sigma^{\uparrow}-\sigma^{\downarrow})\mathbf{E} - \frac{D^{\uparrow}e}{2}\nabla(n^{\uparrow}+n^{\downarrow}) - \frac{D^{\uparrow}e}{2}\nabla(n^{\uparrow}-n^{\downarrow}) + \frac{D^{\downarrow}e}{2}\nabla(n^{\uparrow}+n^{\downarrow}) \\
&\quad - \frac{D^{\downarrow}e}{2}\nabla(n^{\uparrow}-n^{\downarrow}) \\
&= \left(\frac{\sigma^{\uparrow}-\sigma^{\downarrow}}{\sigma^{\uparrow}+\sigma^{\downarrow}}\right)(\sigma^{\uparrow}+\sigma^{\downarrow})\mathbf{E} - \frac{e(D^{\uparrow}-D^{\downarrow})}{2}\nabla(n^{\uparrow}+n^{\downarrow}) - \frac{e(D^{\uparrow}+D^{\downarrow})}{2}\nabla(n^{\uparrow}-n^{\downarrow})
\end{aligned}$$

$$
\begin{aligned}
&= \left(\frac{\sigma^{\uparrow}-\sigma^{\downarrow}}{\sigma^{\uparrow}+\sigma^{\downarrow}}\right)(\sigma^{\uparrow}+\sigma^{\downarrow})\mathbf{E} - \left(\frac{D^{\uparrow}-D^{\downarrow}}{D^{\uparrow}+D^{\downarrow}}\right)\frac{e(D^{\uparrow}+D^{\downarrow})}{2}\nabla(n^{\uparrow}+n^{\downarrow}) \\
&\quad -\frac{e(D^{\uparrow}+D^{\downarrow})}{2}\nabla(n^{\uparrow}-n^{\downarrow}) \\
&= \beta\sigma\mathbf{E} - \beta'\frac{eD}{2}\nabla n - \frac{eD}{2}\nabla\delta\mathrm{m}, \qquad (2.9)
\end{aligned}
$$

with the spin polarisation parameter for the conductivity (β) and the spin polarisation parameter for the diffusion constant (β') given by

$$
\begin{aligned}
\beta &= \frac{\sigma^{\uparrow}-\sigma^{\downarrow}}{\sigma^{\uparrow}+\sigma^{\downarrow}} \\
\beta' &= \frac{\beta-\beta''}{1-\beta\beta''}
\end{aligned}
$$

where $\beta'' = \frac{N^{\uparrow}(E_F)-N^{\downarrow}(E_F)}{N^{\uparrow}(E_F)+N^{\downarrow}(E_F)}$. For a nonmagnet, the spin polarisation parameters for the conductivity and for the diffusion constant are zero as the the distribution of two spin channels are equal, $\sigma^{\uparrow} = \sigma^{\downarrow}$.

The spin current can also be described by the drift-diffusion model. It originates from the drift current and the contributions of the charge accumulation and spin accumulation. The drift-diffusion model is a very useful implementation to study the transport across the interfaces between ferromagnet/nonmagnet and between two ferromagnets. Therefore, it is important to understand the continuity equation which will be used to solve the transport problems. The continuity equations for the charge and the spin in the steady state based on the current conservation are given by [40, 51]

$$
\begin{aligned}
\nabla\cdot(\mathbf{j}^{\uparrow}+\mathbf{j}^{\downarrow}) &= 0, \\
\nabla\cdot(\mathbf{j}^{\uparrow}-\mathbf{j}^{\downarrow}) &= -2e\frac{n^{\uparrow}}{\tau^{\uparrow\downarrow}} + 2e\frac{n^{\downarrow}}{\tau^{\downarrow\uparrow}} \qquad (2.10)
\end{aligned}
$$

where $n^{\uparrow(\downarrow)}$ denote the spin-up and spin-down density of states. The spin-relaxation rate at which the spin-up(down) electrons scatter to the spin-down(up) electrons is represented by $1/\tau^{\uparrow\downarrow}$ and $1/\tau^{\downarrow\uparrow}$. In equilibrium there is no net transfer of electrons between up and down states, giving

$$
\frac{N^{\uparrow}(E_F)}{\tau^{\uparrow\downarrow}} = \frac{N^{\downarrow}(E_F)}{\tau^{\downarrow\uparrow}}
$$

and the average spin-relaxation time(τ_{sf}) is introduced as

$$
\frac{1}{\tau_{\mathrm{sf}}} = \frac{1}{\tau^{\uparrow\downarrow}} + \frac{1}{\tau^{\downarrow\uparrow}} \ .
$$

In addition, the equation of the spin accumulation motion can be derived by considering the continuity equations for the spin-up and spin-down electron densities including the spin-flip scattering [46] given by

$$\begin{aligned} e\frac{\partial n^{\uparrow}}{\partial t} + \nabla \cdot \mathbf{j}^{\uparrow} &= -e\frac{n^{\uparrow}}{\tau^{\uparrow\downarrow}} + e\frac{n^{\downarrow}}{\tau^{\downarrow\uparrow}} \\ e\frac{\partial n^{\downarrow}}{\partial t} + \nabla \cdot \mathbf{j}^{\downarrow} &= -e\frac{n^{\downarrow}}{\tau^{\downarrow\uparrow}} + e\frac{n^{\uparrow}}{\tau^{\uparrow\downarrow}}. \end{aligned} \tag{2.11}$$

The motion of the spin accumulation can be obtained from the above equation under the assumption that $\tau^{\uparrow\downarrow} = \tau^{\downarrow\uparrow}$ and then the spin accumulation decays over the length scale of the average spin-relaxation time as the following

$$\frac{\partial \delta \mathrm{m}}{\partial t} + \frac{\partial j_m}{\partial x} = -\frac{\delta \mathrm{m}}{\tau_{\mathrm{sf}}}. \tag{2.12}$$

In this chapter, the basic theoretical aspect of the spin-dependent transport was discussed to understand the physics behind its behaviour. The spin current and spin accumulation are possible to derive via the two-current model suggested by Mott as mentioned earlier. Equation (2.12) shows the motion of the spin accumulation associated with the gradient of the spin current and the spin scattering event. The component of the spin accumulation will be solved firstly by reviewing the previous work of Zhang, Levy and Fert (ZLF). The detail will be addressed in the following chapter. ZLF also introduce the *s-d* exchange interaction between the conduction electron and the local magnetisation into the equation of the spin accumulation motion in order to describe the spin torque. Furthermore, mechanism of the spin-transfer torque arising from a spin-polarised current injected to the magnetic system will be discussed. The detail and limitation of the approach proposed by ZLF will be detailed in the following chapter.

CHAPTER III

Spin Accumulation in the ZLF Model

To understand the behaviour of spin transport in magnetic systems, this chapter will review the spin accumulation model proposed by Zhang, Levy and Fert (ZLF) in more detail [38, 52, 53]. They studied the mechanism of the magnetisation switching driven by spin polarised current in a magnetic bilayer system consisting of two ferromagnets separated by a nonmagnetic spacer layer. Subsequently, they proposed a model of spin accumulation based on diffusive transport in order to calculate the spin transfer torque acting on the local magnetisation of the ferromagnetic layer. The inclusion of the spin diffusion becomes very important to understand the magnetoresistance of the magnetic multilayers for current perpendicular to the plane of the system (CPP-MR). The solution of the ZLF model points out the important aspect that the spin transfer torque arises from the transverse spin accumulation which is perpendicular to the local magnetisation. In other words, the longitudinal spin accumulation does not play a role in the magnetisation switching [38]. In the last section of the chapter, the limitation of this approach will be addressed here.

3.1 A magnetic bilayer structure

A new method to manipulate the magnetisation by injecting a spin polarised current has attracted considerable attention in both theoretical [12–14] and experimental studies [37,54–56]. To understand the mechanism of the spin torque acting on the magnetisation, we first review the previous work of Zhang, Levy and Fert (ZLF) [38]. They proposed a spin torque model based on the spin accumulation and the effect of the spin diffusion is taken into account in the model. The common usage essentially defines the spin accumulation as the deviation from the equilibrium value; $\delta\mathbf{m} = (n^{\uparrow} - n^{\uparrow}_{eq}) - (n^{\downarrow} - n^{\downarrow}_{eq})$, where n_{eq} refers to the equilibrium (bulk) populations [38, 57–59]. This definition was used by ZLF in their study of the spin accumulation.

The motion of the spin accumulation was considered in a magnetic bilayer structure consisting of two ferromagnetic layers separated by a nonmagnetic layer. The magnetisation of the first ferromagnet (F1) regarded as "*the pinned layer*" and that of the second ferromagnet (F2) referred to as "*the free layer*"are noncollinear as depicted in figure 3.1. To simplify the calculation, the pinned layer is assumed to be very thick, exceeding the spin diffusion length (λ_{sdl}), which is the average distance of electron travel before a spin flip event. This means that current achieves maximum polarisation. ZLF also assume the pinned layer to be a half metal, resulting in a 100% polarised current. In addition, the nonmagnetic layer is vanishingly thin to conserve the spin current across the layer and to avoid the spin flip scattering within this layer.

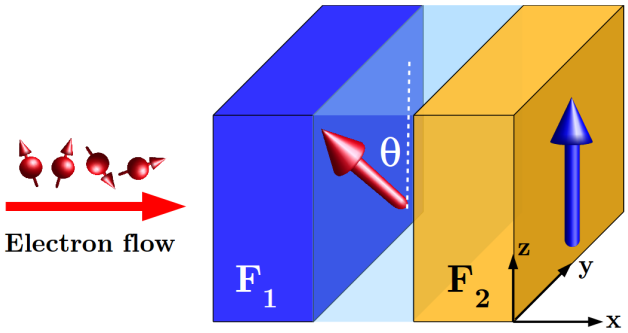

Figure 3.1: Schematic of a magnetic bilayer system consisting of two ferromagnetic layers separated by a nonmagnetic layer: A thick ferromagnetic layer (F_1) behaves as a pinned layer of which the magnetisation is $\mathbf{M}_p = \cos\theta\mathbf{e}_z - \sin\theta\mathbf{e}_y$. The magnetisation of the second ferromagnetic layer (F_2) regarded as the free layer is aligned in the z direction, $\mathbf{M} = \mathbf{e}_z$.

The mechanism of magnetisation switching starts with injecting the spin current perpendicular to the plane of the layers which is defined as the x direction. Initially, the spin current flows into the pinned layer causing it to be polarised via the *s-d* exchange interaction between the itinerant electrons and the local magnetisation. Subsequently, the spin-polarised current flows through the free layer and the spin-transfer torque acts on the spin current to align it in the direction of the free-layer magnetisation. Simultaneously, a reaction torque is exerted on the magnetisation of the free layer, causing magnetisation reorientation.

3.2 Motion of spin accumulation

Firstly, consider the magnetic bilayer system as shown in figure 3.1. The current is injected along the x direction which is perpendicular to the plane of the layers. The linear response of the current to the electrical field including the diffusive transport can be written in a spinor form,

$$\hat{j}(x) = \hat{\sigma}E(x) - \hat{D}\frac{\partial \hat{n}}{\partial x}, \tag{3.1}$$

where $E(x)$ is the electric field, $\hat{j}$, $\hat{\sigma}$, $\hat{D}$ and $\hat{n}$ are the 2×2 matrices representing the current, the conductivity, the diffusion constant, and the accumulation at a given position. The diffusion constant and the conductivity are related via the Einstein relation $\hat{\sigma} = e^2\hat{N}(E_F)\hat{D}$ for a degenerate metal, where $\hat{N}(E_F)$ is the density of states at the Fermi level. These matrices can be expressed in terms of the Pauli spin matrices [38].

The magnetisation current or spin current ($\mathbf{j}_m$) can be written in terms of the modulus of the electrical current (j_e) and the spin accumulation [38] ($\mathbf{m}$) as,

$$\mathbf{j}_m = \beta j_e \mathbf{M} - 2D_0\left[\frac{\partial \mathbf{m}}{\partial x} - \beta\beta'\mathbf{M}\left(\mathbf{M}\cdot\frac{\partial \mathbf{m}}{\partial x}\right)\right] \tag{3.2}$$

where $\mathbf{M}$ is the normalised magnetisation of the free layer. The spin polarisation parameter β for the conductivity is defined as $\boldsymbol{\sigma} = \beta\sigma_0\mathbf{M}$ and β' is the spin polarisation for the diffusion constant defined as $\mathbf{D} = \beta' D_0\mathbf{M}$. Coefficients σ_0 and D_0 are $\sigma/2$ and $D/2$ respectively.

The motion of the spin accumulation is described via the *s-d* exchange interaction between the spin accumulation and the local magnetisation, $\mathcal{H}_{int} = -J\mathbf{m}\cdot\mathbf{M}$. The equation of motion of the spin accumulation can be expressed as,

$$\frac{d\mathbf{m}}{dt} + (J/\hbar)\mathbf{m}\times\mathbf{M} = -\frac{\mathbf{m}}{\tau_{sf}} \tag{3.3}$$

where $\mathbf{m}$ is the spin accumulation, $\mathbf{M}$ is the unit vector for the local magnetisation of the free layer, J is the exchange energy between the electron spin and the local magnetisation, $\hbar$ is the reduced Planck constant and τ_{sf} is the spin-flip relaxation time of the conduction electrons.

As shown in equation (3.3), the spin accumulation is assumed to precess about the local magnetisation in the presence of damping with non-conservation of the magnitude of $\mathbf{m}$. Specifically, the damping term is of the Bloch form $-\frac{\mathbf{m}}{\tau_{sf}}$ with (τ_{sf}) the spin

relaxation time of the conduction electrons. The magnitude of the spin accumulation tends to decay to zero since it is defined as the nonequilibrium spin density and measured from the equilibrium value, $(n_{eq}^{\uparrow} - n_{eq}^{\downarrow})$. Note that this definition of the accumulation is equivalent to the quantity $\delta\mathbf{m}$ given earlier. However, for convenience of notation we use the symbol $\mathbf{m}$, for consistency with ZLF.

3.3 Formalism of spin accumulation

The components of the spin accumulation can be derived from equation (3.3) by replacing $\frac{d\mathbf{m}}{dt}$ with $\frac{\partial\mathbf{m}}{\partial t} + \frac{\partial\mathbf{j}_m}{\partial x}$. Subsequently, we obtain,

$$\frac{1}{2D_0}\frac{\partial\mathbf{m}}{\partial t} = \frac{\partial^2\mathbf{m}}{\partial x^2} - \beta\beta'\mathbf{M}\left(\mathbf{M}\cdot\frac{\partial^2\mathbf{m}}{\partial x^2}\right) - \frac{\mathbf{m}}{\lambda_{sf}^2} - \frac{\mathbf{m}\times\mathbf{M}}{\lambda_J^2} \tag{3.4}$$

where $\lambda_{sf} = \sqrt{2D_0\tau_{sf}}$ and $\lambda_J = \sqrt{2\hbar D_0/J}$.

The spin accumulation is time and position dependent. Because the timescale of magnetisation changes is much slower than changes in spin accumulation, the stationary solution of spin accumulation can be obtained with the assumption that the local magnetisation is fixed. Then its components can be separated into two parts: longitudinal ($\mathbf{m}_{\parallel}$) and transverse ($\mathbf{m}_{\perp}$) modes which are parallel and perpendicular to the direction of the local magnetisation. Each component of the spin accumulation can be written as,

$$\frac{\partial^2\mathbf{m}_{\parallel}}{\partial x^2} - \frac{\mathbf{m}_{\parallel}}{\lambda_{sdl}^2} = 0 \tag{3.5}$$

where $\lambda_{sdl} = \sqrt{(1-\beta\beta')}\lambda_{sf}$, and

$$\frac{\partial^2\mathbf{m}_{\perp}}{\partial x^2} - \frac{\mathbf{m}_{\perp}}{\lambda_{sf}^2} - \frac{\mathbf{m}_{\perp}\times\mathbf{M}}{\lambda_J^2} = 0. \tag{3.6}$$

From equations (3.5) and (3.6), the longitudinal accumulation decays at the length scale of the spin diffusion length λ_{sdl} while the transverse spin accumulation decays at the length scale of λ_J in the case of $\lambda_{sf} \gg \lambda_J$.

To simplify the solution of the spin accumulation, a magnetic bilayer is considered as depicted in figure 3.1. It consists of two ferromagnetic layers separated by a nonmagnetic spacer. The first ferromagnetic material taken as a “pinned layer” is very thick and

assumed to be half metallic so that the spin current is fully polarised by virtue of the *s-d* exchange interaction. The spacer layer is sufficiently thin to retain the spin-polarized current across the layer. Furthermore, the simple calculation is made by neglecting the spin-dependent reflection at the interfaces. The spin accumulation in the free layer (F2), of which the magnetisation orients in the z direction, is calculated. Meanwhile the magnetisation of the pinned layer is aligned on $-yz$ plane, $\mathbf{M}_p = \cos\theta\mathbf{e}_z - \sin\theta\mathbf{e}_y$, where θ is the angle between the magnetisation of the pinned layer and the that of the free layer. For this specific configuration, the solution of the spin accumulation comprising the longitudinal component and the transverse component is found. The longitudinal accumulation parallel to the magnetisation of the free layer is in the z direction whereas the transverse component perpendicular to the magnetisation consists of the x and y components as given by,

$$\begin{aligned} m_x(x) &= G_2\exp(-x/l_+) + G_3\exp(-x/l_-) \\ m_y(x) &= -iG_2\exp(-x/l_+) + iG_3\exp(-x/l_-) \\ m_z(x) &= G_1\exp(-x/\lambda_{sdl}) \end{aligned} \tag{3.7}$$

where the coefficients G_1, G_2 and G_3 can be calculated by imposing continuity of the spin current and $1/l_\mp = \sqrt{(1/\lambda_{sf}^2) \pm (i/\lambda_J^2)}$.

3.4 Formalism of spin current

The spin current is the next important physical quantity being determined. From equation (3.2), in the case that the magnetisation of the free layer is in the z direction, the spin current at any position of the free layer which is related to the gradient of the spin accumulation can be determined as follows,

$$\begin{aligned} j_{mx}(x) &= \beta j_e M_x - 2D_0\left[\frac{\partial m_x}{\partial x} - \beta\beta' M_x\left(M_x\cdot\frac{\partial m_x}{\partial x} + M_y\cdot\frac{\partial m_y}{\partial x} + M_z\cdot\frac{\partial m_z}{\partial x}\right)\right] \\ j_{my}(x) &= \beta j_e M_y - 2D_0\left[\frac{\partial m_y}{\partial x} - \beta\beta' M_y\left(M_x\cdot\frac{\partial m_x}{\partial x} + M_y\cdot\frac{\partial m_y}{\partial x} + M_z\cdot\frac{\partial m_z}{\partial x}\right)\right] \\ j_{mz}(x) &= \beta j_e M_z - 2D_0\left[\frac{\partial m_z}{\partial x} - \beta\beta' M_z\left(M_x\cdot\frac{\partial m_x}{\partial x} + M_y\cdot\frac{\partial m_y}{\partial x} + M_z\cdot\frac{\partial m_z}{\partial x}\right)\right] \end{aligned}$$

and $\mathbf{M} = \mathbf{e}_z$, therefore we obtain,

$$\begin{aligned} j_{mx}(x) &= -2D_0 \frac{\partial m_x}{\partial x} \\ j_{my}(x) &= -2D_0 \frac{\partial m_y}{\partial x} \\ j_{mz}(x) &= \beta j_e - 2D_0(1-\beta\beta')\frac{\partial m_z}{\partial x}. \end{aligned} \tag{3.8}$$

The first derivative of the spin accumulation with respect to the distance x can be calculated from equation (3.7) as follows,

$$\begin{aligned} \frac{\partial m_x(x)}{\partial x} &= -\left[\frac{G_2}{l_+}e^{-x/l_+} + \frac{G_3}{l_-}e^{-x/l_-}\right] \\ \frac{\partial m_y(x)}{\partial x} &= -i\left[-\frac{G_2}{l_+}e^{-x/l_+} + \frac{G_3}{l_-}e^{-x/l_-}\right] \\ \frac{\partial m_z(x)}{\partial x} &= -\frac{G_1}{\lambda_{sdl}}e^{-x/\lambda_{sdl}} \end{aligned} \tag{3.9}$$

substituting the derivative of the spin accumulation as equation (3.9) into equation (3.8) one obtains the spin current expressed in terms of the coefficients G_1, G_2 and G_3 which is given by,

$$\begin{aligned} j_{mx}(x) &= 2D_0\left[\frac{G_2}{l_+}e^{-x/l_+} + \frac{G_3}{l_-}e^{-x/l_-}\right] \\ j_{my}(x) &= 2D_0 i\left[-\frac{G_2}{l_+}e^{-x/l_+} + \frac{G_3}{l_-}e^{-x/l_-}\right] \\ j_{mz}(x) &= \beta j_e + \frac{2D_0(1-\beta\beta')}{\lambda_{sdl}}G_1 e^{-x/\lambda_{sdl}}. \end{aligned} \tag{3.10}$$

3.5 Boundary condition: continuity of the spin current

The coefficients G_1, G_2 and G_3 can be evaluated by using the boundary condition between layers which is the continuity of spin current [18,38]. Therefore, the boundary condition at the interface between the pinned layer (PL) and the free layer (FL) is shown below,

$$\mathbf{j}_m^{PL}(0^-) = \mathbf{j}_m^{FL}(0^+)$$

where 0^- and 0^+ define the position entering and leaving the interface between the pinned layer and the free layer. The entering spin current is fully polarised since the pinned layer is half metallic with the spin polarisation parameter $\beta^{PL} = 1$. It results in $\mathbf{j}_m^{PL}(0^-) = (0, \ -j_e \sin\theta, \ j_e \cos\theta)$. The continuity of the spin current at the interface $(x = 0)$ is given as,

$$\begin{aligned} 0 &= 2D_0\left[\frac{G_2}{l_+}+\frac{G_3}{l_-}\right] \\ -j_e\sin\theta &= 2D_0 i\left[-\frac{G_2}{l_+}+\frac{G_3}{l_-}\right] \\ j_e\cos\theta &= \beta j_e + 2D_0(1-\beta\beta')\frac{G_1}{\lambda_{sdl}}. \end{aligned} \tag{3.11}$$

Consequently, the coefficients G_1, G_2 and G_3 can be obtained by solving the above equation.

$$\begin{aligned} G_1 &= \frac{-j_e\lambda_{sdl}(\beta-\cos\theta)}{2D_0(1-\beta\beta')} \\ G_2 &= \frac{j_e l_+\sin\theta}{4iD_0} \\ G_3 &= -\frac{j_e l_-\sin\theta}{4iD_0} \end{aligned} \tag{3.12}$$

3.6 Spin accumulation and spin current

Here, the spin accumulation and spin current in the free layer of the magnetic bilayer structure are examined to understand their behaviours. The collinear and non-collinear configurations are investigated by using the formalism of the spin accumulation and the spin current proposed by Zhang *et al.* in Ref. [38].

3.6.1 Collinear configuration

The spin accumulation and spin current in the bilayer structure (F1/F2) as described in Sec. 3.1 are considered. The calculation for a simplified system is performed by neglecting the effect of the nonmagnetic layer. The first ferromagnet (F1) is assumed to be half metallic leading to fully spin-polarised current in this layer whereas the second ferromagnetic (F2) layer is cobalt.

For the collinear configuration, let the magnetisation of the pinned layer be oriented in the same direction as that of the free layer, i.e., the z direction. The spin-polarised current travels through the free layer in the x direction perpendicular to the plane of the layers. The value of transport parameters of cobalt (Co) is taken from Ref. [53]. The spin polarisation parameter (β) for conductivity is 0.5, the spin polarisation for diffusion constant (β') is 0.9, the exchange energy (J) is 0.25 eV and the spin diffusion length (λ_{sdl}) is 60 nm. The length scale of λ_{sf} and λ_J are 80 nm and 4 nm respectively.

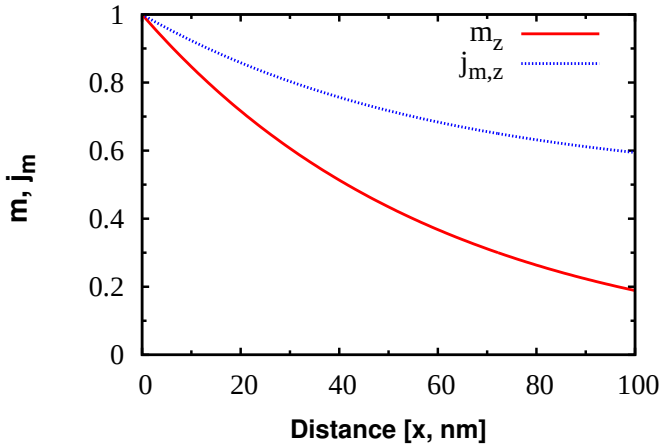

Figure 3.2: Normalised spin accumulation $\mathbf{m}/[j_e\lambda_{sdl}(1-\beta)/(2D_0(1-\beta\beta')]$ and spin current $\mathbf{j}_m/j_e$ at any position of the ferromagnetic (free) layer for the collinear configuration: The magnetisation in the pinned layer and that in the free layer orient in the same direction, $\theta = 0$.

As illustrated in figure 3.2, the pinned layer serves as the polariser providing the spin-polarised current. It tends to follow the direction of the magnetisation in the pinned layer, i.e., z direction due to the exchange coupling. The spin-polarised current next flows into, and acts on, the free layer. In this case the magnetisation of two ferromagnets are aligned exactly, giving rise to zero torque acting on the magnetisation of the free layer. It results in only longitudinal spin accumulation which is parallel to the local magnetisation in the free layer. The longitudinal spin accumulation and spin current decay at the length scale of the spin diffusion length λ_{sdl} about 60 nm, while the transverse spin accumulation disappears for this case.

3.6.2 Non-collinear configuration

Next consider the case of non-collinear configuration. The misalignment angle (θ) between the magnetisation of two ferromagnets is assumed to be 30° off from z axis. The magnetisation of the pinned layer is $\mathbf{M}_p = -0.5\mathbf{e}_y + 0.877\mathbf{e}_z$ and that of the free layer is $\mathbf{M} = \mathbf{e}_z$. To observe the effect of the misalignment on the spin accumulation and spin current, the treatment discussed above is applied. The results are shown in figure 3.3.

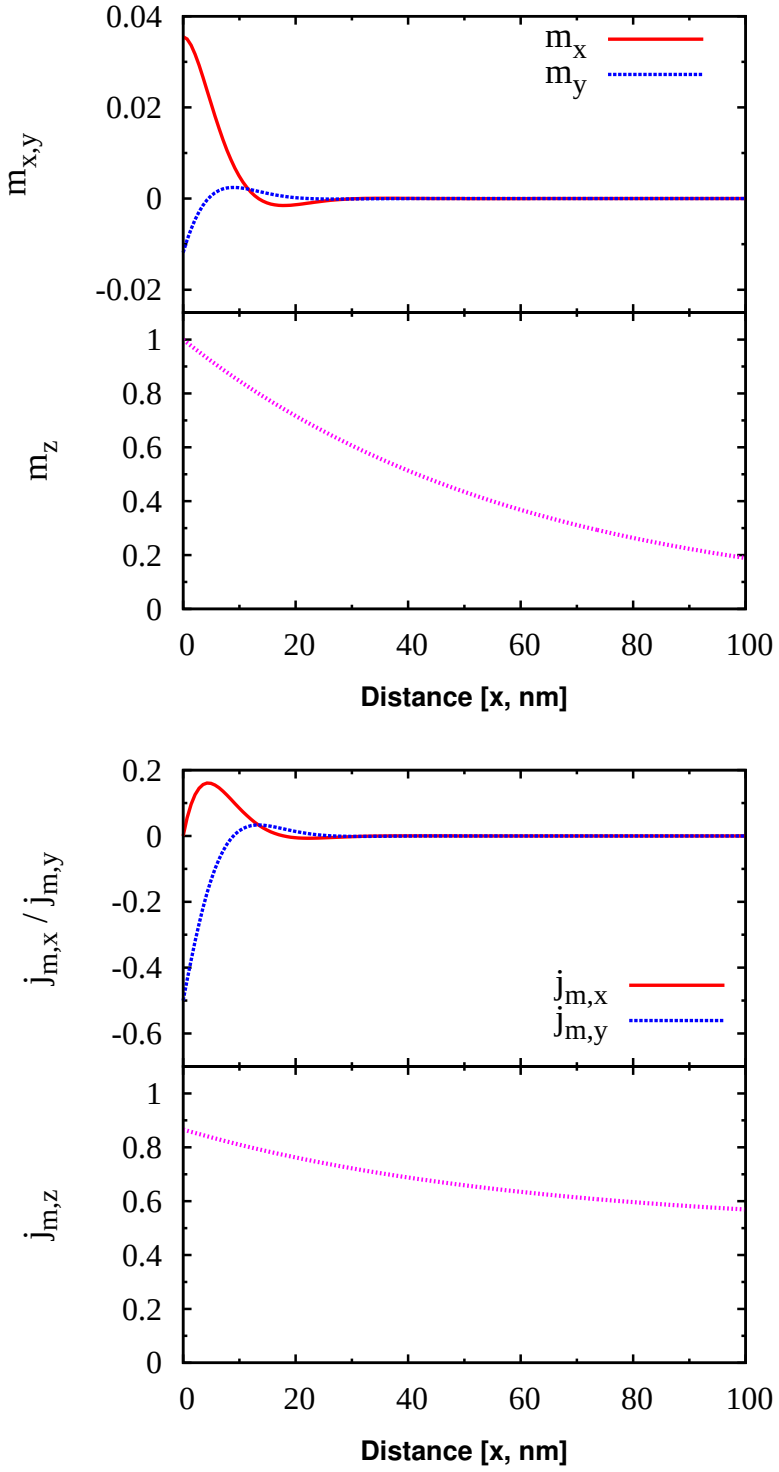

Figure 3.3: Component of normalised spin accumulation $\mathbf{m}/[-j_e\lambda_{sdl}(\beta-\cos\theta)/(2D_0(1-\beta\beta')]$ and spin current $\mathbf{j}_m/j_e$ at any position of the ferromagnetic(free) layer for the non-collinear configuration: The magnetisation of the pinned layer and the that of the free layer are misaligned at the angle of $\theta = 30°$ off from z axis

The spin-polarised current leaving the pinned layer is fully polarised, since the pinned layer is initially assumed to be half metallic, having a spin polarisation parameter $\beta = 1$. Similar to the collinear configuration, the longitudinal spin accumulation decays at the length scale of the spin diffusion length. Interestingly, the transverse spin accumulation comprising x and y components is oscillatory before decaying at the length scale of $\frac{1.414}{\sqrt{\lambda_{sf}^{-2}+\sqrt{\lambda_{sf}^{-4}+\lambda_J^{-4}}}}$ which is about 5.6 nm. In the case of $\lambda_{sf} \gg \lambda_J$, the transverse spin accumulation tends to decay at the length scale at about λ_J. Similarly to the behaviour of the spin accumulation, at the interface $x = 0$ the incoming spin-polarised current orients in the direction of magnetisation of the pinned layer, ($-yz$ plane). Subsequently, it flows into the free layer and interacts with the local magnetisation. The transverse component of the spin current is oscillatory and then decays to zero whereas the longitudinal component tends to follow the magnetisation in the free layer and decay with the length scale of spin diffusion length as the response of the longitudinal spin accumulation.

3.7 Limitation of the ZLF model

As discussed earlier, the oversimplified case is chosen to consider the analytical solution of the spin accumulation. The longitudinal and the transverse spin accumulation are expressed in terms of the coefficients G_1, G_2 and G_3 which can be obtained from the boundary conditions of the continuity of the spin current. For this simple case, the solution of the spin accumulation in the free layer (F_2) is determined in the local coordinate system in which the magnetisation of the free layer is in the z and that of the pinned layer (F_1) orients in the $-yz$ plane.

Therefore, there are two limitations for the model of spin accumulation suggested by ZLF. Firstly, the formalism of spin accumulation is valid for the simple case with the specific configuration based on the local coordinate system. In the case of magnetisations orienting differently from the local coordinate system, the different boundary conditions will need to be considered. Secondly, longitudinal spin accumulation is allowed to decay to zero over the length scale of the spin diffusion length since the spin accumulation is defined as the deviation from the equilibrium value. As shown in equation (3.3), the equation of motion of the spin accumulation, the damping term drives the system to zero as $-\mathbf{m}/\tau_{sf}$. However, for the multilayer structure, each having a different and nonzero

equilibrium value, the spin accumulation calculated by this approach is not allowed to increase at any point in the layer. This is not physically realistic. For example, consider the case of a non-polarised current flowing into a magnet. The form of equation (3.3) does not allow a spin accumulation to develop as it must.

Consequently, we will generalise the model of spin accumulation being able to consider the transport behaviour in the multilayer structure with different materials. The detail of the modified model will be discussed in the next chapter.

CHAPTER IV

Generalised Spin Accumulation Model

In this chapter, a general approach to determine the transport phenomena in a magnetic multilayer structure is proposed. This approach is developed as a model of the spin accumulation which can be applied generally to a system of many layers, allowing studies of the spin accumulation in systems not only with spatially varying magnetisation structures but also with different materials. The proposed approach is based on generalising the approach of Zhang, Levy and Fert (ZLF) including the diffusive transport as discussed in the previous chapter.

In this work, I generalise the treatment in two important aspects. Firstly, in the conventional method the magnetisation is assumed to be homogeneous within each magnetic layer of the system [38, 53]. To examine the transport across the layer in which the magnetisation continuously rotates, i.e., a domain wall, it is suggested to discretise the multilayer system into many thin layers, a so-called "layer by layer method" [60]. This technique allows us to consider the transport across the system in which the magnetisation is non-uniform throughout the layer. Subsequently, the modified solution of the spin accumulation will be applied to each discretised layer.

Secondly, the multilayer system comprises different materials, leading to the different equilibrium values of the spin accumulation. The solution of spin accumulation of the ZLF model is not applicable to this problem. Importantly, the different equilibrium values of different materials are taken into account in the modified model. Consequently, the spin accumulation at any position of the system is obtained. The current approach has successfully explained the behaviour of spin transport across the multilayer system with different materials [61]. Importantly, it is also applicable to the treatment of interfaces, as shown in chapter 6.

4.1 Modified ZLF model

To deal with the multiple layers of different materials, one must consider the nature of the spin accumulation. In principle the spin accumulation represents the difference between spin up and spin down conduction electron populations. However, the common usage essentially defines the spin accumulation as the deviation from the equilibrium value; $\delta\mathbf{m} = (n^{\uparrow} - n^{\uparrow}_{eq}) - (n^{\downarrow} - n^{\downarrow}_{eq})$, where n_{eq} refers to the equilibrium (bulk) populations as mentioned in the previous chapter, and $n^{\uparrow(\downarrow)}$ are the local spin-up (down) carrier densities. This definition was used in the ZLF model and is convenient when a polarised current is injected. In Ref. [38] the spin accumulation is assumed to precess about the local magnetisation in the presence of damping with non-conservation of the magnitude of $\delta\mathbf{m}$. Specifically, the damping term is of the Bloch form $-\delta\mathbf{m}/\tau_{sf}$ with (τ_{sf}) the spin relaxation time of the conduction electrons. Here I propose to use the definition $\mathbf{m} = n^{\uparrow} - n^{\downarrow}$. Clearly $\mathbf{m}$ and $\delta\mathbf{m}$ differ only by the constant factor $n^{\uparrow}_{eq} - n^{\downarrow}_{eq}$. As a result the two definitions give rise to the same spin torque (since $n^{\uparrow}_{eq} - n^{\downarrow}_{eq}$ is parallel to the local magnetisation) and spin current (dependent only on the gradient of the spin accumulation). The advantage of using this definition is seen when dealing with multiple layers with different $\mathbf{m}_{\infty} \equiv n^{\uparrow}_{eq} - n^{\downarrow}_{eq}$.

4.1.1 Modified motion of spin accumulation

In this work the spin accumulation is defined as $\mathbf{m} = n^{\uparrow} - n^{\downarrow}$. This requires that the damping term drives the system to an equilibrium value $\mathbf{m}_{\infty} = n^{\uparrow}_{eq} - n^{\downarrow}_{eq}$, leading to the following equation of motion including a damping term of modified Bloch form

$$\frac{d\mathbf{m}}{dt} + (J/\hbar)\mathbf{m} \times \mathbf{M} = -\frac{\mathbf{m} - \mathbf{m}_{\infty}}{\tau_{sf}}, \tag{4.1}$$

where $\mathbf{M}$ is a unit vector along the local magnetisation direction. It is important to note that the new definition, used consistently throughout the rest of the thesis, differs from that used by ZLF (and many others). The spin current expressed in terms of the modulus of the electric current and the spin accumulation is given by

$$\mathbf{j}_m = \beta j_e \mathbf{M} - 2D_0 \left[\frac{\partial \mathbf{m}}{\partial x} - \beta\beta' \mathbf{M} \left(\mathbf{M} \cdot \frac{\partial \mathbf{m}}{\partial x} \right) \right], \tag{4.2}$$

with β the spin polarisation of the conductivity, and β' the spin polarisation of the diffusion constant. In order to describe the system with continuously varying magnetisation the system is discretised into thin layers in which the magnetisation and transport

properties are assumed piecewise constant. Therefore, the magnetisation is conserved throughout the layer, $\frac{\partial \mathbf{M}}{\partial x} = 0$, and

$$\frac{\partial \mathbf{j}_m}{\partial x} = -2D_0 \left[\frac{\partial^2 \mathbf{m}}{\partial x^2} - \beta\beta' \mathbf{M} \left(\mathbf{M} \cdot \frac{\partial^2 \mathbf{m}}{\partial x^2} \right) \right].$$

Similarly to the ZLF model, to determine the components of the spin accumulation $\frac{d\mathbf{m}}{dt} = \frac{\partial \mathbf{m}}{\partial t} + \frac{\partial \mathbf{j}_m}{\partial x}$ is next replaced into equation (4.1), therefore one obtains

$$\frac{1}{2D_0} \frac{\partial \mathbf{m}}{\partial t} = \frac{\partial^2 \mathbf{m}}{\partial x^2} - \beta\beta' \mathbf{M} \left(\mathbf{M} \cdot \frac{\partial^2 \mathbf{m}}{\partial x^2} \right) - \frac{\mathbf{m} - \mathbf{m}_\infty}{\lambda_{sf}^2} - \frac{\mathbf{m} \times \mathbf{M}}{\lambda_J^2}. \tag{4.3}$$

The relaxation time τ_{sf} of the spin accumulation, i.e., of the order of picoseconds, is much shorter than the characteristic timescale associated with magnetisation changes, and as a result one can search for a stationary solution for $\mathbf{m}$. The solution can conveniently be determined by separating $\mathbf{m}$ into longitudinal and transverse components with respect to $\mathbf{M}$. The aim is to relax the ZLF assumption that the magnetisation of the two magnetic layers are coplanar. Specifically, the equations for the spin accumulation for any arbitrary orientation of the magnetisation are derived. This allows application of the formalism to general magnetisation structures, for example domain walls.

4.1.2 Basis coordinate system

As discussed in the limitation of the ZLF model, the solution is applicable for the specific configuration considered in their paper. To generalise the expressions for the spin accumulation in a magnetic layer arising from an incoming spin polarised current, the local magnetisation in the magnetic layer may align in any direction, $\mathbf{M} = M_x\hat{\mathbf{e}}_x + M_y\hat{\mathbf{e}}_y + M_z\hat{\mathbf{e}}_z$. To derive the components of spin accumulation for this arbitrary orientation of the magnetisation, a modified solution is sought by using the coordinate system $\hat{\mathbf{b}}_1$, $\hat{\mathbf{b}}_2$ and $\hat{\mathbf{b}}_3$ which are parallel and perpendicular to the *local* magnetisation as illustrated in figure 4.1 (right). Therefore, the longitudinal spin accumulation will be along the direction $\hat{\mathbf{b}}_1$, and the two components of the transverse spin accumulation along the directions $\hat{\mathbf{b}}_2$ and $\hat{\mathbf{b}}_3$. The basis $\hat{\mathbf{b}}_1$, $\hat{\mathbf{b}}_2$ and $\hat{\mathbf{b}}_3$ can be expressed in the global coordinate system as follows,

$$\begin{aligned}
\hat{\mathbf{b}}_1 &= b_{1x}\hat{\mathbf{e}}_x + b_{1y}\hat{\mathbf{e}}_y + b_{1z}\hat{\mathbf{e}}_z \\
\hat{\mathbf{b}}_2 &= b_{2x}\hat{\mathbf{e}}_x + b_{2y}\hat{\mathbf{e}}_y + b_{2z}\hat{\mathbf{e}}_z \\
\hat{\mathbf{b}}_3 &= b_{3x}\hat{\mathbf{e}}_x + b_{3y}\hat{\mathbf{e}}_y + b_{3z}\hat{\mathbf{e}}_z.
\end{aligned}$$

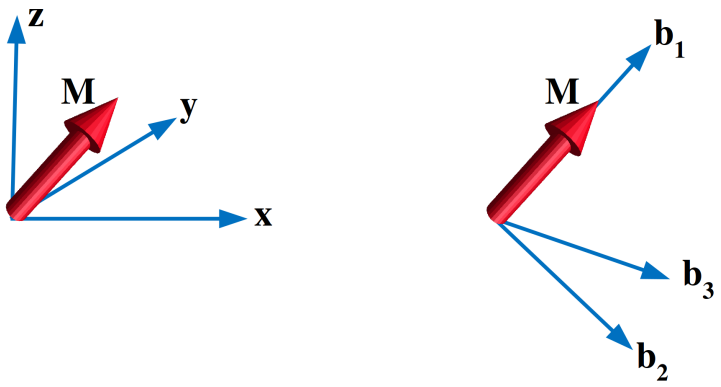

Figure 4.1: (left) Magnetisation in the global coordinate system, and (right) in the rotated basis system

It can be rewritten in the general form as follows, with $i = 1, 2, 3$ and $\alpha = x, y, z$

$$\begin{aligned} \hat{\mathbf{b}}_i &= \sum_{\alpha} b_{i\alpha}\hat{\mathbf{e}}_\alpha, \\ \left[\hat{\mathbf{b}}\right] &= [b_{i\alpha}][\hat{\mathbf{e}}_x \;\; \hat{\mathbf{e}}_y \;\; \hat{\mathbf{e}}_z]^T. \end{aligned} \tag{4.4}$$

Clearly the coefficients $b_{i\alpha}$ cannot be determined unambiguously. They can be chosen as convenient subject to the constraints $b_{1\alpha} = M_\alpha$ (ensures $\hat{\mathbf{b}}_1 // \mathbf{M}$) and that the $\hat{\mathbf{b}}_2$ and $\hat{\mathbf{b}}_3$ are orthogonal to $\hat{\mathbf{b}}_1$. The basis system can be easily achieved by rotating the z axis of the Cartesian coordinate system into the direction of the local magnetisation. Subsequently as depicted in figure 4.1 (right), the basis $\hat{\mathbf{b}}_1$, $\hat{\mathbf{b}}_2$ and $\hat{\mathbf{b}}_3$ correspond to the rotated z, x and y axes respectively. As a result of rotating the z axis, the transformation matrix $[T]$ involving the direction of magnetisation is employed to calculate the coefficients $b_{i\alpha}$ as follows

$$\begin{aligned} [b_{i\alpha}] &= [T][I_i] \\ &= \begin{bmatrix} \frac{1}{D_2^2} & 0 & \frac{M_x}{D_2} \\ \frac{-M_x M_y}{D_1 D_2} & \frac{M_z}{D_1} & \frac{M_y}{D_2} \\ \frac{-M_x M_z}{D_1 D_2} & \frac{-M_y}{D_1} & \frac{M_z}{D_2} \end{bmatrix} [I_i] \\ &= \begin{bmatrix} \frac{M_x}{D_2} & \frac{M_y}{D_2} & \frac{M_z}{D_2} \\ \frac{1}{D_2^2} & \frac{-M_x M_y}{D_1 D_2} & \frac{-M_x M_z}{D_1 D_2} \\ 0 & \frac{M_z}{D_1} & \frac{-M_y}{D_1} \end{bmatrix}, \end{aligned} \tag{4.5}$$

where matrices $[I_1] = [0\ 0\ 1]^T$, $[I_2] = [1\ 0\ 0]^T$, $[I_3] = [0\ 1\ 0]^T$, $D_1 = \sqrt{M_y^2 + M_Z^2}$ and $D_2 = \sqrt{M_x^2 + M_y^2 + M_z^2}$.

Finally, the basis coordinate system for the arbitrary orientation of the magnetisation is obtained by substituting equation (4.5) into equation (4.4). Consequently, the direction of the longitudinal and transverse component of the spin accumulation can be calculated, as in the following sections.

4.1.3 Component of spin accumulation

4.1.3.1 Longitudinal component of spin accumulation ($\mathbf{m}_{\parallel}$)

The basis coordinate system is required in order to determine the longitudinal and transverse component of the spin accumulation for the arbitrary orientation of the magnetisation. Using this basis and following the ZLF model, the parallel component of the spin accumulation from equation (4.3) can be rewritten as

$$\frac{\partial^2 \mathbf{m}_{\parallel}}{\partial x^2} - \frac{\mathbf{m}_{\parallel} - \mathbf{m}_{\parallel}(\infty)}{\lambda_{sdl}^2} = 0 \tag{4.6}$$

The solution of the longitudinal spin accumulation along the direction of basis $\hat{\mathbf{b}}_1$ can be solved as the following equation.

$$\mathbf{m}_{\parallel}(x) = [m_{\parallel}(\infty) + [m_{\parallel}(0) - m_{\parallel}(\infty)]e^{-x/\lambda_{sdl}}]\ \hat{\mathbf{b}}_1 \tag{4.7}$$

• *Equilibrium value of spin accumulation* ($\mathbf{m}_{\infty}$)

The nonzero equilibrium value of spin accumulation, $m_{\parallel}(\infty)$ is the difference between the spin up and spin down density of states (DOS) at the Fermi energy as follows,

$$m_{\parallel}(\infty) = \frac{[N^{\uparrow}(E_F) - N^{\downarrow}(E_F)]k_B T e}{V}. \tag{4.8}$$

where k_B is the Boltzmamn constant, T is the temperature, e is the electron charge and V is the unit cell volume.

This quantity can be calculated by means of Density Functional Theory (DFT) calculations. Values of $m_{\parallel}(\infty)$ determined from DFT calculations (provided by Dr. R. Cuadrado) will be used later in calculations involving Co and NiFe. An example is shown in figure 4.2 for Co bulk.

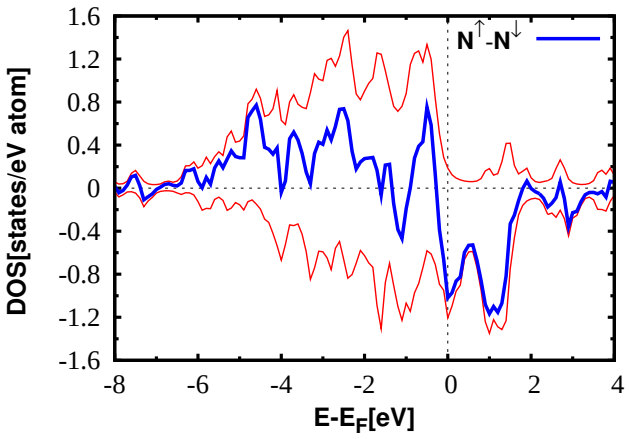

Figure 4.2: Spin resolved density of states of Co bulk [61, 62]: The red lines show the spin up and spin down density of states, $N^{\uparrow(\downarrow)}$. The thick blue line shows the different of $N^{\uparrow} - N^{\downarrow}$, (courtesy of Dr. R. Cuadrado).

4.1.3.2 Transverse component of spin accumulation ($\mathbf{m}_{\perp}$)

The transverse component of spin accumulation is perpendicular to the local magnetisation which will be along the direction $\hat{\mathbf{b}}_2$ and $\hat{\mathbf{b}}_3$. Its form is preserved as the ZLF model given by

$$\frac{\partial^2 \mathbf{m}_{\perp}}{\partial x^2} - \frac{\mathbf{m}_{\perp}}{\lambda_{sf}^2} - \frac{\mathbf{m}_{\perp} \times \mathbf{M}}{\lambda_J^2} = 0, \tag{4.9}$$

but the transverse spin accumulation consists of two components along the directions $\hat{\mathbf{b}}_2$ and $\hat{\mathbf{b}}_3$, $\mathbf{m}_{\perp} = \mathbf{m}_{\perp,2} + \mathbf{m}_{\perp,3} = m_2\hat{\mathbf{b}}_2 + m_3\hat{\mathbf{b}}_3$. Therefore the cross product of the transverse spin accumulation and the magnetisation in the third term of equation (4.9) can be expressed as,

$$\begin{aligned} \mathbf{m}_{\perp} \times \mathbf{M} &= (m_2\hat{\mathbf{b}}_2 + m_3\hat{\mathbf{b}}_3) \times (\hat{\mathbf{b}}_1) \\ &= -m_2\hat{\mathbf{b}}_3 + m_3\hat{\mathbf{b}}_2 \end{aligned}$$

and then substituting the cross product into equation (4.9), one obtain

$$\begin{aligned} \frac{\partial^2 (m_2\hat{\mathbf{b}}_2 + m_3\hat{\mathbf{b}}_3)}{\partial x^2} - \frac{(m_2\hat{\mathbf{b}}_2 + m_3\hat{\mathbf{b}}_3)}{\lambda_{sf}^2} - \frac{(-m_2\hat{\mathbf{b}}_3 + m_3\hat{\mathbf{b}}_2)}{\lambda_J^2} &= 0 \\ \left[\frac{\partial^2 m_2}{\partial x^2} - \frac{m_2}{\lambda_{sf}^2} - \frac{m_3}{\lambda_J^2}\right]\hat{\mathbf{b}}_2 + \left[\frac{\partial^2 m_3}{\partial x^2} - \frac{m_3}{\lambda_{sf}^2} + \frac{m_2}{\lambda_J^2}\right]\hat{\mathbf{b}}_3 &= 0. \end{aligned}$$

The basis $\hat{\mathbf{b}}_2$ and $\hat{\mathbf{b}}_3$ are orthogonal to each other. As a result, $\mathbf{m}_\perp$ can be represented as a complex quantity. Finally the above equation can be rewritten as;

$$\left[\frac{\partial^2 m_2}{\partial x^2} - \frac{m_2}{\lambda_{sf}^2} - \frac{m_3}{\lambda_J^2}\right] + \left[\frac{\partial^2 m_3}{\partial x^2} - \frac{m_3}{\lambda_{sf}^2} + \frac{m_2}{\lambda_J^2}\right] i = 0 \tag{4.10}$$

From equation (4.10), the magnitude of the transverse spin accumulation along the direction $\hat{\mathbf{b}}_2$ and $\hat{\mathbf{b}}_3$ which are m_2 and m_3 respectively can be calculated.

• *Solution of the transverse spin accumulation*

The magnitude of the transverse spin accumulation m_2 along the direction $\hat{\mathbf{b}}_2$ can be obtained by collecting terms in m_2 from the above equation.

$$\begin{aligned} \frac{\partial^2 m_2}{\partial x^2} - \frac{m_2}{\lambda_{sf}^2} + \frac{i m_2}{\lambda_J^2} &= 0 \\ \frac{\partial^2 m_2}{\partial x^2} - m_2\left(\frac{1}{\lambda_{sf}^2} - \frac{i}{\lambda_J^2}\right) &= 0 \end{aligned} \tag{4.11}$$

Similarly, collecting terms in m_3, the magnitude of the transverse spin accumulation m_3 along the direction $\hat{\mathbf{b}}_3$ can be obtained as follows,

$$\begin{aligned} \frac{\partial^2 i m_3}{\partial x^2} - \frac{i m_3}{\lambda_{sf}^2} - \frac{m_3}{\lambda_J^2} &= 0 \\ i\left[\frac{\partial^2 m_3}{\partial x^2} - m_3\left(\frac{1}{\lambda_{sf}^2} - \frac{i}{\lambda_J^2}\right)\right] &= 0 \end{aligned} \tag{4.12}$$

Subsequently, equations (4.11) and (4.12) can be solved and one seek the solution of the following form,

$$\begin{aligned} \mathbf{m}_{\perp,2}(x) &= \left[G_2 e^{-x/l_+} + G_3 e^{-x/l_-}\right] \hat{\mathbf{b}}_2 \\ \mathbf{m}_{\perp,3}(x) &= \left[-iG_2 e^{-x/l_+} + iG_3 e^{-x/l_-}\right] \hat{\mathbf{b}}_3, \end{aligned} \tag{4.13}$$

where,

$$\begin{aligned} G_2 &= \frac{\mathbf{m}_{\perp,2}(0) + i\mathbf{m}_{\perp,3}(0)}{2} = u + iv \\ G_3 &= \frac{\mathbf{m}_{\perp,2}(0) - i\mathbf{m}_{\perp,3}(0)}{2} = u - iv \\ 1/l_+ &= \sqrt{(1/\lambda_{sf}^2) - (i/\lambda_J^2)} = k_1 - ik_2 \\ 1/l_- &= \sqrt{(1/\lambda_{sf}^2) + (i/\lambda_J^2)} = k_1 + ik_2. \end{aligned}$$

As shown in equation (4.13), the transverse component is expressed in the inconvenient form of the complex number. Alternatively, the solution of transverse component can be rewritten in a sinusoidal function by substituting $G_2, G_3, 1/l_+$ and $1/l_-$ into the above equation. Therefore, the solution of transverse component is in the following form

$$\begin{aligned} m_{\perp,2}(x) &= [G_2 \exp(-x/l_+) + G_3 \exp(-x/l_-)] \\ &= (u+iv)e^{-x(k_1-ik_2)} + (u-iv)e^{-x(k_1+ik_2)} \\ &= (u+iv)e^{-k_1x}e^{ik_2x} + (u-iv)e^{-k_1x}e^{-ik_2x} \\ &= (ue^{-k_1x} + ive^{-k_1x})[\cos(k_2x) + i\sin(k_2x)] \\ &\quad +(ue^{-k_1x} - ive^{-k_1x})[\cos(k_2x) - i\sin(k_2x)] \\ &= 2e^{-k_1x}[u\cos(k_2x) - v\sin(k_2x)] \end{aligned}$$

and similarly,

$$\begin{aligned} m_{\perp,3}(x) &= [-iG_2 \exp(-x/l_+) + iG_3 \exp(-x/l_-)] \\ &= -i(u+iv)e^{-x(k_1-ik_2)} + i(u-iv)e^{-x(k_1+ik_2)} \\ &= -i(u+iv)e^{-k_1x}e^{ik_2x} + i(u-iv)e^{-k_1x}e^{-ik_2x} \\ &= -i(ue^{-k_1x} + ive^{-k_1x})[\cos(k_2x) + i\sin(k_2x)] \\ &\quad +i(ue^{-k_1x} - ive^{-k_1x})[\cos(k_2x) - i\sin(k_2x)] \\ &= 2e^{-k_1x}[u\sin(k_2x) + v\cos(k_2x)]. \end{aligned}$$

4.1.3.3 Solution of spin accumulation

Consequently, the total spin accumulation is the contribution of the longitudinal and transverse components, $\mathbf{m}(x) = \mathbf{m}_\parallel(x) + \mathbf{m}_{\perp,2}(x) + \mathbf{m}_{\perp,3}(x)$, shown as the following equations.

$$\begin{aligned} \mathbf{m}_\parallel(x) &= [m_\parallel(\infty) + [m_\parallel(0) - m_\parallel(\infty)]e^{-x/\lambda_{sdl}}]\ \hat{\mathbf{b}}_1 \\ \mathbf{m}_{\perp,2}(x) &= 2e^{-k_1x}\left[u\cos(k_2x) - v\sin(k_2x)\right]\hat{\mathbf{b}_2} \\ \mathbf{m}_{\perp,3}(x) &= 2e^{-k_1x}\left[u\sin(k_2x) + v\cos(k_2x)\right]\hat{\mathbf{b}_3}, \end{aligned} \tag{4.14}$$

with $(k_1 \pm ik_2) = \sqrt{\lambda_{sf}^{-2} \pm i\lambda_J^{-2}}$, where $\lambda_{sf} = \sqrt{2D_0\tau_{sf}}$ and $\lambda_J = \sqrt{2\hbar D_0/J}$. Here $\lambda_{sdl} = \sqrt{1-\beta\beta'}\lambda_{sf}$ is the spin diffusion length of the material, D_0 the diffusion constant, $m_\parallel(0)$, u and v are constants which will be determined shortly. The equilibrium value of the spin accumulation, $m_\parallel(\infty)$, can be calculated as discussed previously.

4.2 The determination of the coefficients

The spin accumulation in the magnetic layer requires determination of $m_{\parallel}(0)$, u and v, which is achieved by imposing continuity of the spin current at the interface. The spin current for the arbitrary direction of magnetisation, $\mathbf{M} = M_x\hat{\mathbf{e}_x} + M_y\hat{\mathbf{e}_y} + M_z\hat{\mathbf{e}_z}$ can be obtained from equation (3.2). It is given by

$$\begin{aligned}
j_{mx}(x) &= \beta j_e M_x - 2D_0\left[\frac{\partial m_x}{\partial x} - \beta\beta' M_x\left(\mathbf{M}\cdot\frac{\partial \mathbf{m}}{\partial x}\right)\right] \\
j_{my}(x) &= \beta j_e M_y - 2D_0\left[\frac{\partial m_y}{\partial x} - \beta\beta' M_y\left(\mathbf{M}\cdot\frac{\partial \mathbf{m}}{\partial x}\right)\right] \\
j_{mz}(x) &= \beta j_e M_z - 2D_0\left[\frac{\partial m_z}{\partial x} - \beta\beta' M_z\left(\mathbf{M}\cdot\frac{\partial \mathbf{m}}{\partial x}\right)\right],
\end{aligned}$$

with

$$\mathbf{M}\cdot\frac{\partial \mathbf{m}}{\partial x} = M_x\frac{\partial m_x}{\partial x} + M_y\frac{\partial m_y}{\partial x} + M_z\frac{\partial m_z}{\partial x}.$$

Therefore, the component of spin current in the global coordinate system is written as follows,

$$\begin{aligned}
j_{mx}(x) &= \beta j_e M_x - 2D_0\left[\frac{\partial m_x}{\partial x} - \beta\beta' M_x\left(M_x\frac{\partial m_x}{\partial x} + M_y\frac{\partial m_y}{\partial x} + M_z\frac{\partial m_z}{\partial x}\right)\right] \\
j_{my}(x) &= \beta j_e M_y - 2D_0\left[\frac{\partial m_y}{\partial x} - \beta\beta' M_y\left(M_x\frac{\partial m_x}{\partial x} + M_y\frac{\partial m_y}{\partial x} + M_z\frac{\partial m_z}{\partial x}\right)\right] \\
j_{mz}(x) &= \beta j_e M_z - 2D_0\left[\frac{\partial m_z}{\partial x} - \beta\beta' M_z\left(M_x\frac{\partial m_x}{\partial x} + M_y\frac{\partial m_y}{\partial x} + M_z\frac{\partial m_z}{\partial x}\right)\right].
\end{aligned}$$

4.2.1 Spin current at the interface

The spin current at the interface between the layers ($x = 0$) is as follows

$$\begin{aligned}
j_{mx}(0) - \beta j_e M_x &= 2D_0(\beta\beta' M_x^2 - 1)\frac{\partial m_x(0)}{\partial x} + 2D_0\beta\beta' M_x M_y\frac{\partial m_y(0)}{\partial x} \\
&\quad + 2D_0\beta\beta' M_x M_z\frac{\partial m_z(0)}{\partial x} \\
j_{my}(0) - \beta j_e M_y &= 2D_0\beta\beta' M_x M_y\frac{\partial m_x(0)}{\partial x} + 2D_0(\beta\beta' M_y^2 - 1)\frac{\partial m_y(0)}{\partial x} \\
&\quad + 2D_0\beta\beta' M_y M_z\frac{\partial m_z(0)}{\partial x} \\
j_{mz}(0) - \beta j_e M_z &= 2D_0\beta\beta' M_x M_z\frac{\partial m_x(0)}{\partial x} + 2D_0\beta\beta' M_y M_z\frac{\partial m_y(0)}{\partial x} \\
&\quad + 2D_0(\beta\beta' M_z^2 - 1)\frac{\partial m_z(0)}{\partial x}.
\end{aligned}$$

Then one finds the first derivative of the spin accumulation with respect to the distance at $x = 0$ in the matrix form as below. It is expressed in terms of the transport parameters of the layer and the incoming spin current $j_m(0)$ from the previous layer.

$$\begin{bmatrix} \frac{\partial m_x(0)}{\partial x} \\ \frac{\partial m_y(0)}{\partial x} \\ \frac{\partial m_z(0)}{\partial x} \end{bmatrix} = \begin{bmatrix} 2D_0(\beta\beta' M_x^2 - 1) & 2D_0\beta\beta' M_x M_y & 2D_0\beta\beta' M_x M_z \\ 2D_0\beta\beta' M_x M_y & 2D_0(\beta\beta' M_y^2 - 1) & 2D_0\beta\beta' M_y M_z \\ 2D_0\beta\beta' M_x M_z & 2D_0\beta\beta' M_y M_z & 2D_0(\beta\beta' M_z^2 - 1) \end{bmatrix}^{-1} \begin{bmatrix} j_{mx}(0) - \beta j_e M_x \\ j_{my}(0) - \beta j_e M_y \\ j_{mz}(0) - \beta j_e M_z \end{bmatrix} \tag{4.15}$$

The first derivative of spin accumulation in the above equation is easily obtained. All transport parameters of the magnetic layer depending on the property of material are known. The incoming spin current ($\mathbf{j}_m$) is calculated from the boundary condition by imposing continuity of the spin current at the interface between layers. In principle, the transport parameters may vary from layer to layer. However, for clarity I leave the layer variation as implicit rather than adding label such as β_i. Equation (4.15) gives the gradient of the accumulation at the interface with the previous layer, as determined by the spin current from the previous layer. From this the unknown coefficients $m_\parallel(0)$, u and v can be determined as in the following section.

4.2.2 Spin accumulation at the interface

The final step is to use the derivatives of $\mathbf{m}$, determined, using the interface conditions as equation (4.15) to evaluate the constants $m_\parallel(0)$, u and v which completely determine the solution for $\mathbf{m}$. The solution of spin accumulation from equation (4.14) is in the basis coordinate system, $\mathbf{b}_1$, $\mathbf{b}_2$ and $\mathbf{b}_3$. It can be rewritten to represent in the global coordinate system.

$$\begin{aligned} m_x(x)\hat{\mathbf{e}}_x + m_y(x)\hat{\mathbf{e}}_y + m_z(x)\hat{\mathbf{e}}_z &= m_\parallel(x)\hat{\mathbf{b}}_1 + m_{\perp,2}(x)\hat{\mathbf{b}}_2 + m_{\perp,3}(x)\hat{\mathbf{b}}_3 \\ &= m_\parallel(x)\left[b_{1x}\hat{\mathbf{e}}_x + b_{1y}\hat{\mathbf{e}}_y + b_{1z}\hat{\mathbf{e}}_z\right] \\ &\quad + m_{\perp,2}(x)\left[b_{2x}\hat{\mathbf{e}}_x + b_{2y}\hat{\mathbf{e}}_y + b_{2z}\hat{\mathbf{e}}_z\right] \\ &\quad + m_{\perp,3}(x)\left[b_{3x}\hat{\mathbf{e}}_x + b_{3y}\hat{\mathbf{e}}_y + b_{3z}\hat{\mathbf{e}}_z\right] \end{aligned}$$

Consider each component of the spin accumulation in the global coordinate system

$$\begin{aligned} m_x(x) &= b_{1x}m_\parallel(x) + b_{2x}m_{\perp,2}(x) + b_{3x}m_{\perp,3}(x) \\ m_y(x) &= b_{1y}m_\parallel(x) + b_{2y}m_{\perp,2}(x) + b_{3y}m_{\perp,3}(x) \\ m_z(x) &= b_{1z}m_\parallel(x) + b_{2z}m_{\perp,2}(x) + b_{3z}m_{\perp,3}(x). \end{aligned}$$

Determine the first derivative of the spin accumulation with respect to the distance x,

$$\begin{aligned}
\frac{\partial m_x(x)}{\partial x} &= b_{1x}\frac{\partial m_{\parallel}(x)}{\partial x} + b_{2x}\frac{\partial m_{\perp,2}(x)}{\partial x} + b_{3x}\frac{\partial m_{\perp,3}(x)}{\partial x} \\
\frac{\partial m_y(x)}{\partial x} &= b_{1y}\frac{\partial m_{\parallel}(x)}{\partial x} + b_{2y}\frac{\partial m_{\perp,2}(x)}{\partial x} + b_{3y}\frac{\partial m_{\perp,3}(x)}{\partial x} \\
\frac{\partial m_z(x)}{\partial x} &= b_{1z}\frac{\partial m_{\parallel}(x)}{\partial x} + b_{2z}\frac{\partial m_{\perp,2}(x)}{\partial x} + b_{3z}\frac{\partial m_{\perp,3}(x)}{\partial x},
\end{aligned} \tag{4.16}$$

where

$$\begin{aligned}
\frac{\partial m_{\parallel}(x)}{\partial x} &= \frac{\left[m_{\parallel}(\infty) - m_{\parallel}(0)\right]}{\lambda_{sdl}} e^{-x/\lambda_{sdl}} \\
\frac{\partial m_{\perp,2}(x)}{\partial x} &= -\left[\frac{G_2}{l_+}e^{-x/l_+} + \frac{G_3}{l_-}e^{-x/l_-}\right] \\
\frac{\partial m_{\perp,3}(x)}{\partial x} &= -i\left[-\frac{G_2}{l_+}e^{-x/l_+} + \frac{G_3}{l_-}e^{-x/l_-}\right].
\end{aligned}$$

At the interface ($x = 0$), one obtains

$$\begin{aligned}
\frac{\partial m_{\parallel}(0)}{\partial x} &= \frac{\left[m_{\parallel}(\infty) - m_{\parallel}(0)\right]}{\lambda_{sdl}} \\
\frac{\partial m_{\perp,2}(0)}{\partial x} &= -\left[\frac{G_2}{l_+} + \frac{G_3}{l_-}\right] = -2k_1u - 2k_2v \\
\frac{\partial m_{\perp,3}(0)}{\partial x} &= -i\left[-\frac{G_2}{l_+} + \frac{G_3}{l_-}\right] = 2k_2u - 2k_1v
\end{aligned} \tag{4.17}$$

and substitute equation (4.17) into equation (4.16), subsequently one has the following relationships.

$$\begin{aligned}
\frac{\partial m_x(0)}{\partial x} &= b_{1x}\frac{\left[m_{\parallel}(\infty) - m_{\parallel}(0)\right]}{\lambda_{sdl}} + b_{2x}(-2k_1u - 2k_2v) + b_{3x}(2k_2u - 2k_1v) \\
&= \frac{b_{1x}m_{\parallel}(\infty)}{\lambda_{sdl}} - \frac{b_{1x}m_{\parallel}(0)}{\lambda_{sdl}} + (-2b_{2x}k_1 + 2b_{3x}k_2)u + (-2b_{2x}k_2 - 2b_{3x}k_1)v
\end{aligned}$$

$$\begin{aligned}
\frac{\partial m_x(0)}{\partial x} &= b_{1y}\frac{\left[m_{\parallel}(\infty) - m_{\parallel}(0)\right]}{\lambda_{sdl}} + b_{2y}(-2k_1u - 2k_2v) + b_{3y}(2k_2u - 2k_1v) \\
&= \frac{b_{1y}m_{\parallel}(\infty)}{\lambda_{sdl}} - \frac{b_{1y}m_{\parallel}(0)}{\lambda_{sdl}} + (-2b_{2y}k_1 + 2b_{3y}k_2)u + (-2b_{2y}k_2 - 2b_{3y}k_1)v
\end{aligned}$$

$$\begin{aligned}
\frac{\partial m_x(0)}{\partial x} &= b_{1z}\frac{\left[m_{\parallel}(\infty) - m_{\parallel}(0)\right]}{\lambda_{sdl}} + b_{2z}(-2k_1u - 2k_2v) + b_{3z}(2k_2u - 2k_1v) \\
&= \frac{b_{1z}m_{\parallel}(\infty)}{\lambda_{sdl}} - \frac{b_{1z}m_{\parallel}(0)}{\lambda_{sdl}} + (-2b_{2z}k_1 + 2b_{3z}k_2)u + (-2b_{2z}k_2 - 2b_{3z}k_1)v
\end{aligned}$$

The above equations can be represented in the matrix form as follows

$$\begin{bmatrix} \frac{\partial m_x(0)}{\partial x} \\ \frac{\partial m_y(0)}{\partial x} \\ \frac{\partial m_z(0)}{\partial x} \end{bmatrix} = \frac{m_{\parallel}(\infty)}{\lambda_{sdl}} \begin{bmatrix} b_{1x} \\ b_{1y} \\ b_{1z} \end{bmatrix} + \begin{bmatrix} -\frac{b_{1x}}{\lambda_{sdl}} & (-2b_{2x}k_1 + 2b_{3x}k_2) & (-2b_{2x}k_2 - 2b_{3x}k_1) \\ -\frac{b_{1y}}{\lambda_{sdl}} & (-2b_{2y}k_1 + 2b_{3y}k_2) & (-2b_{2y}k_2 - 2b_{3y}k_1) \\ -\frac{b_{1z}}{\lambda_{sdl}} & (-2b_{2z}k_1 + 2b_{3z}k_2) & (-2b_{2z}k_2 - 2b_{3z}k_1) \end{bmatrix} \begin{bmatrix} m_{\parallel}(0) \\ u \\ v \end{bmatrix}$$

Consequently,

$$\begin{bmatrix} m_{\parallel}(0) \\ u \\ v \end{bmatrix} = \begin{bmatrix} -\frac{b_{1x}}{\lambda_{sdl}} & (-2b_{2x}k_1 + 2b_{3x}k_2) & (-2b_{2x}k_2 - 2b_{3x}k_1) \\ -\frac{b_{1y}}{\lambda_{sdl}} & (-2b_{2y}k_1 + 2b_{3y}k_2) & (-2b_{2y}k_2 - 2b_{3y}k_1) \\ -\frac{b_{1z}}{\lambda_{sdl}} & (-2b_{2z}k_1 + 2b_{3z}k_2) & (-2b_{2z}k_2 - 2b_{3z}k_1) \end{bmatrix}^{-1} \begin{bmatrix} \frac{\partial m_x(0)}{\partial x} - \frac{b_{1x}m_{\parallel}(\infty)}{\lambda_{sdl}} \\ \frac{\partial m_y(0)}{\partial x} - \frac{b_{1y}m_{\parallel}(\infty)}{\lambda_{sdl}} \\ \frac{\partial m_z(0)}{\partial x} - \frac{b_{1z}m_{\parallel}(\infty)}{\lambda_{sdl}} \end{bmatrix} \tag{4.18}$$

Finally, the unknown coefficients $m_{\parallel}(0)$, u and v can be calculated by substituting the first derivative of the spin accumulation at interface, $\frac{\partial \mathbf{m}(0)}{\partial x}$, as equation (4.15) into equation (4.18).

4.3 Summarised step of calculation

To calculate the spin accumulation of any magnetic system, with spatially varying magnetisation structures, the modified solution of spin accumulation is proposed for a general case. The procedure of this approach is not complicated to follow, but many calculations in the procedure will be performed. To assist understanding, the steps of the calculation are summarised here.

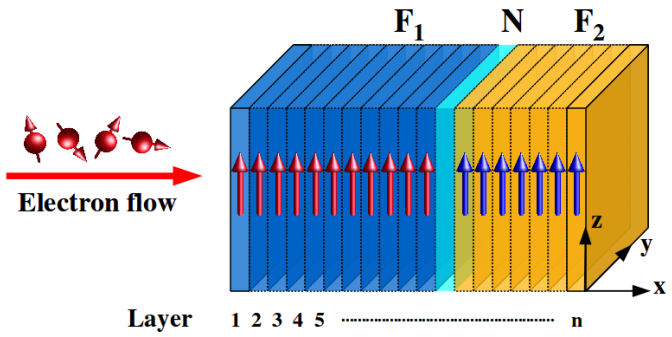

Figure 4.3: Schematic of a magnetic bilayer system discretised into a series of thin layers: In this case magnetisation in the thick ferromagnetic layer (F_1) is collinear with that in the thin ferromagnet (F_2), but the numerical procedure applies to structures with spatially varying magnetisation.

The precedure works by dividing the system into a series of thin layers, $i = 0,\ 1,\ 2, \ldots,\ n$ with the thickness t_F for each layer and the average magnetisation within each thin layer is used to calculate the spin accumulation as illustrated in figure 4.3. This

method allows us to calculate the spin accumulation and spin current at any position of the system. They can be calculated easily in 7 steps by applying the modified solution to each thin layer as shown in figure 4.4. One settled on the following procedure.

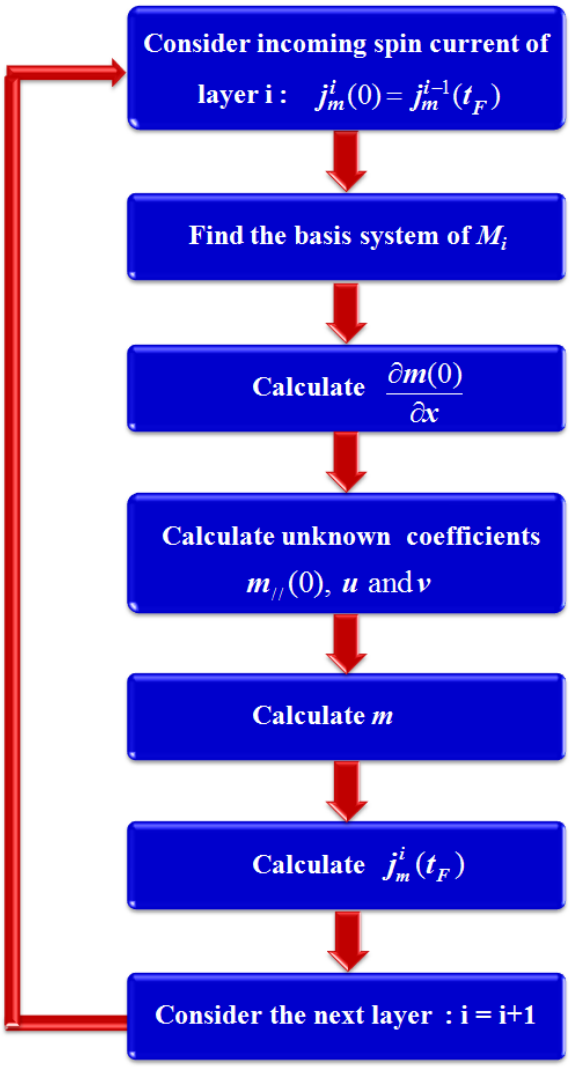

Figure 4.4: Diagram of the procedure of the spin accumulation calculation

Step 1: To calculate the spin accumulation of the layer i, the incoming spin current used as the input parameter is required. It flows from the previous layer $i-1$ and can be determined by imposing the boundary condition at the interface between layers ($x = 0$) which is the continuity of the spin current given by

$$\mathbf{j}_m^i(0) = \mathbf{j}_m^{i-1}(t_F).$$

Step 2: Consider the basis coordinate system for the local magnetisation aligned to any direction, $\mathbf{M}_i$. As mentioned in details in Sec. 4.1.2, the basis system expressed in term of the component of magnetisation can be determined as the following relationship

$$\left[\hat{\mathbf{b}}\right] = \begin{bmatrix} \frac{M_x}{D_2} & \frac{M_y}{D_2} & \frac{M_z}{D_2} \\ \frac{1}{D_2^2} & \frac{-M_xM_y}{D_1D_2} & \frac{-M_xM_z}{D_1D_2} \\ 0 & \frac{M_z}{D_1} & \frac{-M_y}{D_1} \end{bmatrix} [\hat{\mathbf{e}}_x \quad \hat{\mathbf{e}}_y \quad \hat{\mathbf{e}}_z]^T$$

where $D_1 = \sqrt{M_y^2 + M_z^2}$ and $D_2 = \sqrt{M_x^2 + M_y^2 + M_z^2}$.

Step 3: To determine the unknown coefficients used to describe the spin accumulation as seen in equation (4.14), the first derivative of the spin accumulation at $x = 0$ with respect to the distance is evaluated as the following relationship in matrix form.

$$\begin{bmatrix} \frac{\partial m_x(0)}{\partial x} \\ \frac{\partial m_y(0)}{\partial x} \\ \frac{\partial m_z(0)}{\partial x} \end{bmatrix} = \begin{bmatrix} 2D_0(\beta\beta' M_x^2 - 1) & 2D_0\beta\beta' M_xM_y & 2D_0\beta\beta' M_xM_z \\ 2D_0\beta\beta' M_xM_y & 2D_0(\beta\beta' M_y^2 - 1) & 2D_0\beta\beta' M_yM_z \\ 2D_0\beta\beta' M_xM_z & 2D_0\beta\beta' M_yM_z & 2D_0(\beta\beta' M_z^2 - 1) \end{bmatrix}^{-1} \begin{bmatrix} j_{mx}(0) - \beta j_e M_x \\ j_{my}(0) - \beta j_e M_y \\ j_{mz}(0) - \beta j_e M_z \end{bmatrix}$$

Step 4: Subsequently, the unknown coefficients $m_\parallel(0)$, u and v are calculated by substituting $\frac{\partial \mathbf{m}(0)}{\partial x}$ from the previous step, all elements of the basis coordinate system as well as the constants k_1 and k_2 obtained from the transport parameters into the following relationship.

$$\begin{bmatrix} m_\parallel(0) \\ u \\ v \end{bmatrix} = \begin{bmatrix} -\frac{b_{1x}}{\lambda_{sdl}} & (-2b_{2x}k_1 + 2b_{3x}k_2) & (-2b_{2x}k_2 - 2b_{3x}k_1) \\ -\frac{b_{1y}}{\lambda_{sdl}} & (-2b_{2y}k_1 + 2b_{3y}k_2) & (-2b_{2y}k_2 - 2b_{3y}k_1) \\ -\frac{b_{1z}}{\lambda_{sdl}} & (-2b_{2z}k_1 + 2b_{3z}k_2) & (-2b_{2z}k_2 - 2b_{3z}k_1) \end{bmatrix}^{-1} \begin{bmatrix} \frac{\partial m_x(0)}{\partial x} - \frac{b_{1x}m_\parallel(\infty)}{\lambda_{sdl}} \\ \frac{\partial m_y(0)}{\partial x} - \frac{b_{1y}m_\parallel(\infty)}{\lambda_{sdl}} \\ \frac{\partial m_z(0)}{\partial x} - \frac{b_{1z}m_\parallel(\infty)}{\lambda_{sdl}} \end{bmatrix}$$

Step 5: Consequently, the spin accumulation in the basis coordinate system at $x = t_F$ can be worked out by substituting the unknown coefficients achieved from step 4 into the equations below.

$$\begin{aligned} \mathbf{m}_\parallel(x) &= [m_\parallel(\infty) + [m_\parallel(0) - m_\parallel(\infty)]e^{-x/\lambda_{sdl}}]\ \hat{\mathbf{b}}_1 \\ \mathbf{m}_{\perp,2}(x) &= 2e^{-k_1x}\left[u\cos(k_2x) - v\sin(k_2x)\right]\hat{\mathbf{b}}_2 \\ \mathbf{m}_{\perp,3}(x) &= 2e^{-k_1x}\left[u\sin(k_2x) + v\cos(k_2x)\right]\hat{\mathbf{b}}_3, \end{aligned}$$

with $(k_1 \pm ik_2) = \sqrt{\lambda_{sf}^{-2} \pm i\lambda_J^{-2}}$, where $\lambda_{sf} = \sqrt{2D_0\tau_{sf}}$ and $\lambda_J = \sqrt{2\hbar D_0/J}$. Here $\lambda_{sdl} = \sqrt{1 - \beta\beta'}\lambda_{sf}$ denotes the spin diffusion length of the material, D_0 is the diffusion constant and $m_\parallel(\infty)$ is the equilibrium value of the spin accumulation.

In addition, the component of the spin accumulation in the global coordinate system is also determined as follows

$$\begin{aligned} m_x(x) &= b_{1x}m_{\parallel}(x) + b_{2x}m_{\perp,2}(x) + b_{3x}m_{\perp,3}(x) \\ m_y(x) &= b_{1y}m_{\parallel}(x) + b_{2y}m_{\perp,2}(x) + b_{3y}m_{\perp,3}(x) \\ m_z(x) &= b_{1z}m_{\parallel}(x) + b_{2z}m_{\perp,2}(x) + b_{3z}m_{\perp,3}(x). \end{aligned}$$

Step 6: The spin current of the layer i at the distance $x = t_F$ is the next quantity of interest. It can be determined directly from the gradient of the spin accumulation as shown in the following equation. It will be used as the incoming spin current for the next layer, $i + 1$.

$$\begin{aligned} j_{mx}(x) &= \beta j_e M_x - 2D_0 \left[\frac{\partial m_x}{\partial x} - \beta\beta' M_x \left(M_x \frac{\partial m_x}{\partial x} + M_y \frac{\partial m_y}{\partial x} + M_z \frac{\partial m_z}{\partial x} \right) \right] \\ j_{my}(x) &= \beta j_e M_y - 2D_0 \left[\frac{\partial m_y}{\partial x} - \beta\beta' M_y \left(M_x \frac{\partial m_x}{\partial x} + M_y \frac{\partial m_y}{\partial x} + M_z \frac{\partial m_z}{\partial x} \right) \right] \\ j_{mz}(x) &= \beta j_e M_z - 2D_0 \left[\frac{\partial m_z}{\partial x} - \beta\beta' M_z \left(M_x \frac{\partial m_x}{\partial x} + M_y \frac{\partial m_y}{\partial x} + M_z \frac{\partial m_z}{\partial x} \right) \right]. \end{aligned}$$

where

$$\begin{aligned} \frac{\partial m_x(x)}{\partial x} &= b_{1x}\frac{\partial m_{\parallel}(x)}{\partial x} + b_{2x}\frac{\partial m_{\perp,2}(x)}{\partial x} + b_{3x}\frac{\partial m_{\perp,3}(x)}{\partial x} \\ \frac{\partial m_y(x)}{\partial x} &= b_{1y}\frac{\partial m_{\parallel}(x)}{\partial x} + b_{2y}\frac{\partial m_{\perp,2}(x)}{\partial x} + b_{3y}\frac{\partial m_{\perp,3}(x)}{\partial x} \\ \frac{\partial m_z(x)}{\partial x} &= b_{1z}\frac{\partial m_{\parallel}(x)}{\partial x} + b_{2z}\frac{\partial m_{\perp,2}(x)}{\partial x} + b_{3z}\frac{\partial m_{\perp,3}(x)}{\partial x}, \end{aligned}$$

and

$$\begin{aligned} \frac{\partial m_{\parallel}(x)}{\partial x} &= \frac{\left[m_{\parallel}(\infty) - m_{\parallel}(0)\right]}{\lambda_{sdl}} e^{-x/\lambda_{sdl}} \\ \frac{\partial m_{\perp,2}(x)}{\partial x} &= 2e^{-k_1 x}\sin(k_2 x)\left[k_1 v - k_2 u\right] - 2e^{-k_1 x}\cos(k_2 x)\left[k_1 u + k_2 v\right] \\ \frac{\partial m_{\perp,3}(x)}{\partial x} &= -2e^{-k_1 x}\sin(k_2 x)\left[k_1 u + k_2 v\right] + 2e^{-k_1 x}\cos(k_2 x)\left[-k_1 v + k_2 u\right]. \end{aligned}$$

Step 7: Repeat step 1 - 6 for all thin layers. Consequently, the spin accumulation and spin current at any position of the magnetic system are calculated.

4.4 Spin accumulation and spin current in the bilayer system

In this section, the applicability of the modified solution of the spin accumulation is investigated in a bilayer system of Co/Co. In the first ferromagnetic layer of Co regarded as the "*pinned layer*", the magnetisation orients in the y direction whereas the magnetisation in the second Co layer rotates its direction uniformly to 90°, as illustrated in figure 4.5.

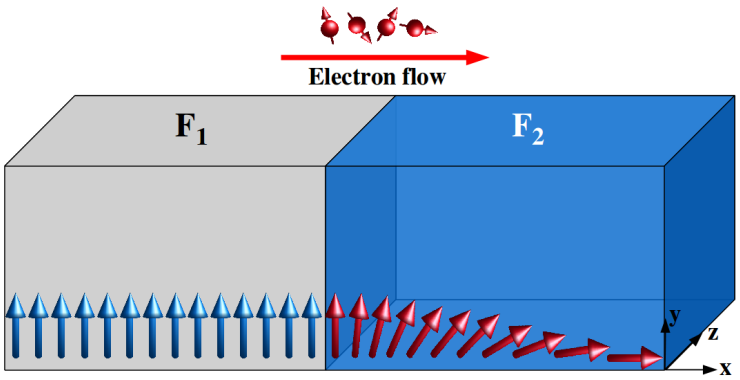

Figure 4.5: Schematic illustration of the bilayer system (Co/Co): The magnetisation of the first ferromagnetic layer is fixed in the y direction and that of the second one gradually changes throughout the layer.

The behaviour of the spin accumulation is investigated not only to check the validity of the modified solution but also to describe the effect of the spin torque arising from the spin accumulation in the next chapter. Therefore, I first consider the system shown in figure 4.5 containing a domain wall. The system is spatially discretised into many thin layers with the distance between the layers of 5 atomic spacings. The magnetisation in the second Co layer is allowed to gradually change giving rise to a domain wall within this layer. The domain wall motion resulting from the spin current will be considered later. Here I simply evaluate the spatial variation of $\mathbf{m}$ and $\mathbf{j}_m$ throughout the wall. The spin accumulation is investigated by applying the modified solution to each thin layer discussed previously.

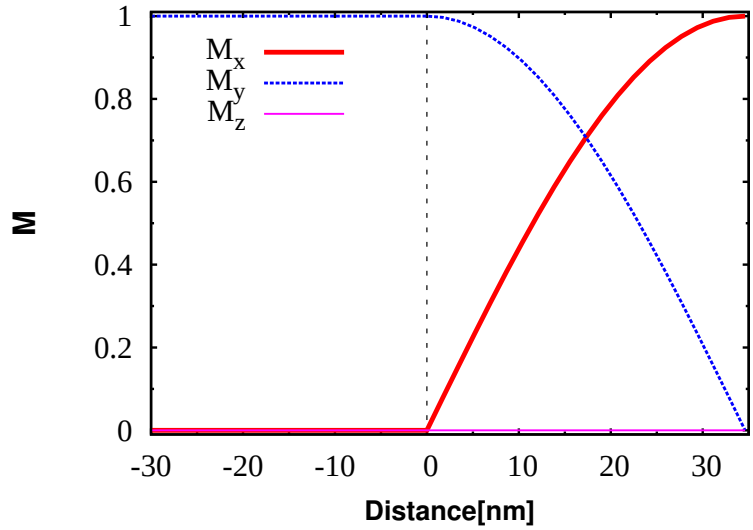

Figure 4.6: Normalised magnetisation at any position in the bilayer system (Co/Co): The position $x = 0$ is the center of the interface. The position $x < 0$ and $x > 0$ show the first ferromagnetic layer of Co and the second ferromagnetic layer of Co respectively.

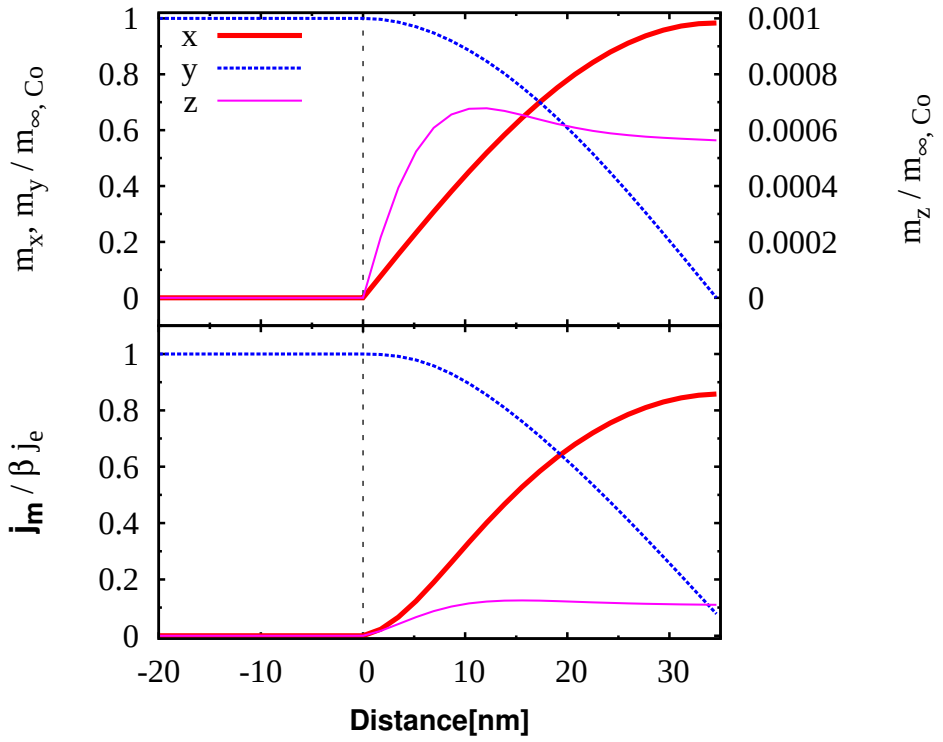

Figure 4.7: Normalised spin accumulation and spin current at any position of the Co/Co system in the global coordinate system

The static domain wall profile is shown in figure 4.6. The transport parameters of Co used in spin accumulation calculation are taken from Ref. [53] as the following values, $\beta = 0.5,\ \beta' = 0.9,\ D_0 = 0.003\ m^2/s,\ \lambda_{sdl} = 60\ nm$ and $\lambda_J = 4\ nm$. The equilibrium value of spin accumulation (m_∞) can be calculated from equation (4.8). The *fcc* lattice parameter of the Co bulk used here is $a_{\mathrm{Co}} = 3.46\ \mathring{A}$ and the difference of the spin up and spin down density of states$(N^{\uparrow}(E_F) - N^{\downarrow}(E_F))$ is 1.02 states/eV atom [62]. It results in the equilibrium value of the spin accumulation of $m_{\parallel}(\infty) = 3.945 \times 10^7\ C/m^3$ with $k_BT = 10\ meV$

The spin current is introduced to the bilayer system in the x direction. Subsequently, it flows through the layer and interacts via the *s-d* exchange interaction with the local magnetisation giving rise to a spatially varying spin accumulation. This can be calculated by applying the generalised ZLF model based on the diffusive transport with the appropriate boundary condition at the interface, and the results are shown in figure 4.7. The component of the spin accumulation can be resolved into the *in-plane* and the *out-of-plane* components. It shows that the spin accumulation and spin current tend to adiabatically follow the direction of magnetisation in both Co layers due to the exchange interaction between the spin-polarised current and the local magnetisation. Interestingly, in the second Co layer with the smoothly varying magnetisation, an out-of-plane (z) component is exhibited owing to the mistracking of conduction electrons, a so-called "*non-adiabatic component*". This is due to the large spin diffusion length. It is generally much smaller than the in-plane component but significant. The effect of both components will be discussed fully in the next chapter.

4.5 Summary

In conclusion, the modified solution proposed here can be effectively used to explain the behaviour of the spin transport at any position of the system by dividing the system into many thin layers. Specifically, the modified spin accumulation model can be applied to any arbitrary orientation of the magnetisation by using the transformation matrix to rotate the magnetisation in the global coordinate system into the basis coordinate system. Furthermore, it also can be applied to the multilayer structure with different material by the introduction of the nonzero equilibrium value, $m_{\parallel}(\infty)$. The solution of the ZLF model can be obtained from the general solution as well. It indicates that the modified solution is valid for any system.

This approach will be applied to a bilayer system to calculate the spin torque coeffecients which are often-used in micromagnetic model in the following chapter. Also, the modified solution of spin accumulation allowing the inclusion of the effect of diffuse interface will be studied in chapter 6. Finally, the current-induced domain wall motion will be investigated by using the proposed model as details in chapter 7.

CHAPTER V

Spin-transfer torque on a domain wall

In this chapter, the main interest is associated with the spin-transfer torque calculation. As explained in chapter 1, it can be represented in terms of an interaction between the local magnetisation and a spin accumulation which is calculated self-consistently and naturally includes the adiabatic and non-adiabatic contributions. The first section of the chapter is organised to give an understanding of the spin-transfer torque component related to Slonczewski's original model. Then the spin-transfer torque parameters a and b corresponding to the adiabatic and non-adiabatic torques [12, 13, 16, 38, 58, 63, 64] are formulated directly from the spin accumulation. Subsequently, the formalism of spin torque derived from the spin accumulation is applied to the magnetic bilayer system containing a domain wall (DW) to investigate its behaviour under the influence of the spin-transfer torque. In this approach, the spin torque parameters a and b are found to be nonuniform throughout the magnetic layer. The details and importance of this aspect will be discussed in relation to the usual micromagnetic approach assuming fixed empirical constants determining the strength of the adiabatic and non-adiabatic terms.

Specifically, the coefficients of adiabatic and non-adiabatic torques in the standard form [6, 65–68], μ_x and β_x respectively, are considered as a function of the spin torque parameters a and b. Interestingly, the adiabatic and non-adiabatic contributions depend on the rate of change of magnetisation. It leads to a divergence of the spin torque parameters for the case of small gradient of magnetisation. This stresses the importance of the new route to calculate adiabatic and non-adiabatic torques directly from spin accumulation instead of the often-used method, assuming that the coefficients μ_x and β_x are constant. A suitable criterion for the validity of the standard approach will be presented.

Finally, the influence of the spin diffusion length and the domain wall thickness on the spin accumulation and spin torque is also studied to deeply understand its behaviour in a magnetic bilayer system.

5.1 Spin-transfer torque

The spin-transfer torque, extensively used to manipulate magnetisation and control domain wall dynamics, was first proposed theoretically by Berger [2] and Slonczewski [1,69]. Physically, the spin-transfer torque arises from the *s-d* exchange interaction between the conduction electron and the local magnetisation. As a result of this interaction, the spin-transfer torque acting on the local magnetisation contributes two components of torque: *adiabatic* and *non-adiabatic* torques. The first originates from the conduction electron spins tending to align in the direction of the local magnetisation, whereas the latter can be interpreted as arising from the mistracking of conduction electron spins and local magnetisation [70–72]. The qualitative understanding and determination of both adiabatic and non-adiabatic torques have been discussed by many research groups; although the adiabatic torque is theoretically well understood, the physics of the non-adiabatic torque remains ambiguous [9, 64, 73–75].

5.1.1 Slonczewski spin torque

According to Slonczewski's model based on ballistic transport [1, 69, 76–78], the spin-transfer torque is exerted on the local magnetisation by injecting the spin current into the magnetic bilayer structure. It arises from the conservation of the spin angular momentum carried by the conduction electrons. This spin torque is referred to *" a Slonczewski torque"*(T_S) given by,

$$\mathbf{T}_S = \left(\frac{\partial \mathbf{M}}{\partial t}\right)_{STT} = \gamma a \mathbf{M} \times (\mathbf{M} \times \mathbf{M}_p), \tag{5.1}$$

where $a = \frac{\hbar PI}{M_s V e}$ is a spin torque parameter, I is the electric current, $P = \frac{N^{\uparrow} - N^{\downarrow}}{N^{\uparrow} + N^{\downarrow}}$ is the spin polarisation parameter of spin current at the Fermi level, $\gamma = g\mu_B/\hbar$ is the gyromagnetic ratio, M_s is the saturation magnetisation, V is the volume of the sample and e is the electron charge. $\mathbf{M}$ and $\mathbf{M}_p$ denote the unit vectors of magnetisation in the free and pinned layers respectively.

As seen in equation (5.1), the Slonczewski spin torque can be a source of damping motion forcing the magnetisation of the free layer towards the orientation of magnetisation in the pinnned layer. This torque is extensively used to describe the mechanism of the spin torque in the magnetic system [12–14, 63], also namely "*adiabatic spin torque*" (AST). If this torque points in the same direction as the natural damping, it can either

increase or decrease the natural damping of the spin motion depending on the direction of the injected current. The effect of this torque on the dynamics of magnetisation will be discussed in more detail in chapter 7.

5.1.2 Field-like torque

Apart from the adiabatic torque, an additional torque enhanced in the magnetic system via the *s-d* exchange interaction is introduced as a *field-like torque* or a *perpendicular spin torque* [11, 38, 68, 76, 79], given by

$$\mathbf{T}_F = b(\mathbf{M} \times \mathbf{M}_p). \tag{5.2}$$

It behaves the same way as the external magnetic field leading to precessional motion around the magnetisation in the pinned layer. The strength of this torque is characterised by the parameter b. In general, the field-like torque is known as a "*non-adiabatic spin torque*" (NAST). It has been explained by various mechanisms such as momentum transfer, spin mistracking and spin flip scattering [6]. However, its origin is still controversial. By considering equations (5.1) and (5.2), the non-adiabatic torque is perpendicular to the adiabatic spin-transfer torque and the magnetisation as shown in figure 5.1.

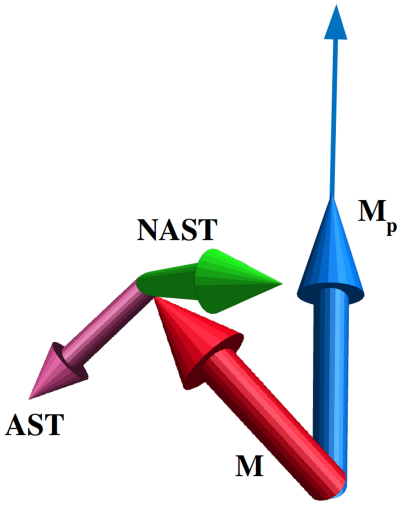

Figure 5.1: The contribution of adiabatic and non-adiabatic spin torques to the local magnetisation in the free layer **M**: The adiabatic torque orients in the plane of **M** and $\mathbf{M}_p$ whereas the non-adiabatic torque or field-like torque points to the direction perpendicular to that plane.

5.2 Spin torque calculation

As discussed in the previous section, the total spin torque arises from the contribution of the adiabatic and non-adiabatic torques characterised by parameters a and b. These parameters have been considered by many authors by means of various transport theories [11,12,38]. The spin-transfer torque can be represented in terms of an interaction between the local magnetisation and the spin accumulation as the following equation

$$\mathcal{H} = -J\mathbf{m} \cdot \mathbf{M} \tag{5.3}$$

where J is the s-d exchange integral, $\mathbf{m}$ is the spin accumulation and $\mathbf{M}$ is the unit vector along the local magnetisation direction.

In this section, I will formulate the spin torque in the system as well as the coefficients a and b describing the adiabatic and non-adiabatic spin torque directly from the spin accumulation. I first consider the relationship between the accumulation and spin torque by making a decomposition into adiabatic and non-adiabatic components. The additional magnetic field arising from the spin accumulation, $J \cdot \mathbf{m}$, can be written in terms of the transverse spin accumulation since the longitudinal accumulation does not induce any torque to affect the motion of magnetisation. Hence, following the approach of the ZLF [38, 53], the additional field ($\mathbf{H}_{\mathrm{ST}}$) can be introduced as a function of the magnetisation of the current ($\mathbf{M}$) and previous ($\mathbf{M}_p$) layers as

$$\begin{aligned} \mathbf{H}_{\mathrm{ST}} &= -\frac{\partial \mathcal{H}}{\partial \mathbf{M}} = J\mathbf{m}_{\perp} \\ &= a(\mathbf{M}_p \times \mathbf{M}) + b(\mathbf{M} \times \mathbf{M}_p) \times \mathbf{M}. \end{aligned} \tag{5.4}$$

5.2.1 Total spin torque

To investigate the influence of spin accumulation on the local magnetisation, the additional field in the above equation can be introduced in the Landau-Lifschitz-Gilbert equation (LLG) [12–14,38,63] representing adiabatic and non-adiabatic spin torque contributions as follows

$$\begin{aligned} \frac{\partial \mathbf{M}}{\partial t} &= -\gamma \mathbf{M} \times (\mathbf{H}_{\mathrm{eff}} + J\mathbf{m}_{\perp}) + \alpha \mathbf{M} \times \frac{\partial \mathbf{M}}{\partial t} \\ &= -\gamma(\mathbf{M} \times \mathbf{H}_{\mathrm{eff}}) + \alpha \mathbf{M} \times \frac{\partial \mathbf{M}}{\partial t} - \gamma a \mathbf{M} \times (\mathbf{M}_p \times \mathbf{M}) - \gamma b(\mathbf{M} \times \mathbf{M}_p). \end{aligned} \tag{5.5}$$

From equation (5.5), one can decompose the total spin torque arising from the additional field $\mathbf{H}_{\mathrm{ST}}$ as follows

$$\begin{aligned} \mathrm{ST}_{\mathrm{total}} &= \mathrm{AST} + \mathrm{NAST} \\ &= -\gamma a \mathbf{M} \times (\mathbf{M}_p \times \mathbf{M}) - \gamma b \mathbf{M} \times \mathbf{M}_p, \end{aligned} \tag{5.6}$$

where the first and second terms of the right hand side represent the adiabatic and non-adiabatic spin torques, denoted AST and NAST respectively. The above equation shows that the spin torque can be expressed in terms of spin accumulation and the angle between the magnetisation of both ferromagnets. In the following sections I consider the relationship between the micromagnetic representation and the spin accumulation. Firstly, I relate the coefficients a and b and the spin accumulation.

5.2.2 Spin torque parameters a and b

To calculate the spin torque parameters a and b describing the adiabatic and non-adiabatic spin torques, one considers the basis coordinate system introduced in chapter 4. The total spin torque arising from the contribution of the adiabatic (AST) and non-adiabatic spin torques (NAST) can be considered conveniently in the basis coordinate system.

The local magnetisation in the current layer ($\mathbf{M}$) is along the direction $\hat{\mathbf{b}}_1$ as explained in chapter 4. Therefore, the magnetisation in the previous layer ($\mathbf{M}_p$) is needed to be transformed into the basis coordinate system by using the transformation matrix expressed in terms of components of magnetisation in the current layer. The relationship of magnetisation components in the global and rotated coordinate systems can be determined as follows

$$M_{p,x}\hat{\mathbf{e}}_x + M_{p,y}\hat{\mathbf{e}}_y + M_{p,z}\hat{\mathbf{e}}_z = M_{p\parallel}\hat{\mathbf{b}}_1 + M_{p\perp,2}\hat{\mathbf{b}}_2 + M_{p\perp,3}\hat{\mathbf{b}}_3.$$

The magnetisation of the previous layer ($\mathbf{M}_p$) in the global coordinate system can be expressed in terms of the longitudinal and transverse components of the magnetisation in the basis coordinate system, which are parallel and perpendicular to $\mathbf{M}$ respectively, as below,

$$\begin{aligned} M_{p,x} &= b_{1x}M_{p\parallel} + b_{2x}M_{p\perp,2} + b_{3x}M_{p\perp,3} \\ M_{p,y} &= b_{1y}M_{p\parallel} + b_{2y}M_{p\perp,2} + b_{3y}M_{p\perp,3} \\ M_{p,z} &= b_{1z}M_{p\parallel} + b_{2z}M_{p\perp,2} + b_{3z}M_{p\perp,3}. \end{aligned}$$

Therefore, the component of magnetisation in the basis coordinate system can be rewritten in the matrix form as follows,

$$\begin{aligned}\begin{bmatrix} M_{p\parallel} \\ M_{p\perp,2} \\ M_{p\perp,3} \end{bmatrix} &= \begin{bmatrix} b_{1x} & b_{2x} & b_{3x} \\ b_{1y} & b_{2y} & b_{3y} \\ b_{1z} & b_{2z} & b_{3z} \end{bmatrix}^{-1} \begin{bmatrix} M_{p,x} \\ M_{p,y} \\ M_{p,z} \end{bmatrix} \\ &= \begin{bmatrix} \frac{M_x}{D_2} & \frac{1}{D_2^2} & 0 \\ \frac{M_y}{D_2} & \frac{-M_xM_y}{D_1D_2} & \frac{M_z}{D_1} \\ \frac{M_z}{D_2} & \frac{-M_xM_z}{D_1D_2} & \frac{-M_y}{D_1} \end{bmatrix}^{-1} \begin{bmatrix} M_{p,x} \\ M_{p,y} \\ M_{p,z} \end{bmatrix}, \end{aligned} \tag{5.7}$$

where M_x, M_y and M_z are the x, y and z components of magnetisation in the current layer respectively. $D_1 = \sqrt{M_y^2 + M_Z^2}$ and $D_2 = \sqrt{M_x^2 + M_y^2 + M_z^2}$.

The total spin torque can be calculated in the basis coordinate system by substituting $\mathbf{M} = \hat{\mathbf{b}}_1$ and $\mathbf{M}_p = M_{p\parallel}\hat{\mathbf{b}}_1 + M_{p\perp,2}\hat{\mathbf{b}}_2 + M_{p\perp,3}\hat{\mathbf{b}}_3$ into the equation (5.6) as follows

$$\mathbf{M} \times J\mathbf{m}_\perp = a\left[\mathbf{M} \times (\mathbf{M}_p \times \mathbf{M})\right] + b\left[\mathbf{M} \times \mathbf{M}_p\right],$$

where

$$\begin{aligned}[\mathbf{M} \times \mathbf{M}_p] &= \hat{\mathbf{b}}_1 \times (M_{p\parallel}\hat{\mathbf{b}}_1 + M_{p\perp,2}\hat{\mathbf{b}}_2 + M_{p\perp,3}\hat{\mathbf{b}}_3) \\ &= M_{p\perp,2}\hat{\mathbf{b}}_3 - M_{p\perp,3}\hat{\mathbf{b}}_2 \qquad (5.8) \\ [\mathbf{M} \times (\mathbf{M}_p \times \mathbf{M})] &= \hat{\mathbf{b}}_1 \times (-M_{p\perp,2}\hat{\mathbf{b}}_3 + M_{p\perp,3}\hat{\mathbf{b}}_2) \\ &= M_{p\perp,2}\hat{\mathbf{b}}_2 + M_{p\perp,3}\hat{\mathbf{b}}_3. \qquad (5.9)\end{aligned}$$

Subsequently one obtains the following equation,

$$\begin{aligned}\mathbf{M} \times J\mathbf{m}_\perp &= a\left[\mathbf{M} \times (\mathbf{M}_p \times \mathbf{M})\right] + b\left[\mathbf{M} \times \mathbf{M}_p\right] \\ \hat{\mathbf{b}}_1 \times (Jm_{\perp,2}\hat{\mathbf{b}}_2 + Jm_{\perp,3}\hat{\mathbf{b}}_3) &= a(M_{p\perp,2}\hat{\mathbf{b}}_2 + M_{p\perp,3}\hat{\mathbf{b}}_3) + b(M_{p\perp,2}\hat{\mathbf{b}}_3 - M_{p\perp,3}\hat{\mathbf{b}}_2)\end{aligned}$$

$$Jm_{\perp,2}\hat{\mathbf{b}}_3 - Jm_{\perp,3}\hat{\mathbf{b}}_2 = (aM_{p\perp,2} - bM_{p\perp,3})\hat{\mathbf{b}}_2 + (aM_{p\perp,3} + bM_{p\perp,2})\hat{\mathbf{b}}_3. \tag{5.10}$$

From equation (5.10), the coefficients a and b can be determined as follows

$$\begin{aligned}-Jm_{\perp,3} &= aM_{p\perp,2} - bM_{p\perp,3} \\ Jm_{\perp,2} &= aM_{p\perp,3} + bM_{p\perp,2}.\end{aligned}$$

Therefore, the coefficients a and b are given by

$$\begin{aligned} a &= \frac{J(m_{\perp,2}M_{p\perp,3} - m_{\perp,3}M_{p\perp,2})}{{M_{p\perp,2}}^2 + {M_{p\perp,3}}^2} \\ b &= \frac{J(m_{\perp,2}M_{p\perp,2} + m_{\perp,3}M_{p\perp,3})}{{M_{p\perp,2}}^2 + {M_{p\perp,3}}^2}, \end{aligned}$$

where $M_{p\perp,2}$ and $M_{p\perp,3}$ are the perpendicular component of the magnetisation of the previous layer along the basis $\hat{\mathbf{b}}_2$ and $\hat{\mathbf{b}}_3$ respectively. Clearly these can be written as

$$\begin{aligned} a &= \frac{J\hat{\mathbf{b}}_1 \cdot (\mathbf{m}_\perp \times \mathbf{M}_{p\perp})}{|\mathbf{M}_{p\perp}|^2} = \frac{J|\mathbf{m}_\perp|\sin\theta}{|\mathbf{M}_{p\perp}|} \\ b &= \frac{J(\mathbf{m}_\perp \cdot \mathbf{M}_{p\perp})}{|\mathbf{M}_{p\perp}|^2} = \frac{J|\mathbf{m}_\perp|\cos\theta}{|\mathbf{M}_{p\perp}|}, \end{aligned} \tag{5.11}$$

where $\mathbf{m}_\perp$ and $\mathbf{M}_{p\perp}$ are the transverse components of the spin accumulation and the magnetisation in the previous layer respectively and θ is the phase angle between $\mathbf{m}_\perp$ and $\mathbf{M}_{p\perp}$.

In order to achieve the units of spin torque parameter a and b in tesla as the magnetic field, the volume of the unit cell (a_0^3), the electric charge (e) and Bohr magnetron (μ_B) are inserted into the above equation [38]. Consequently, one obtains

$$\begin{aligned} a &= \frac{J|\mathbf{m}_\perp|\sin\theta}{|\mathbf{M}_{p\perp}|}\frac{a_0^3}{e\mu_B} \\ b &= \frac{J|\mathbf{m}_\perp|\cos\theta}{|\mathbf{M}_{p\perp}|}\frac{a_0^3}{e\mu_B}. \end{aligned} \tag{5.12}$$

Equation (5.12) describes the magnitude and character of the spin torque. The magnitude of the spin torque is determined by $|\ \mathbf{m}_\perp\ |\ /\ |\ \mathbf{M}_{p\perp}\ |$, while the relative strengths of the AST and NAST terms are determined by the phase angle θ. These quantities might be expected to depend on the spatial location for the case of non-uniform magnetisation structures. This will be investigated in the next section along with consideration of the implication for the usual micromagnetic representation.

To explain the behaviour of the coefficients a and b, it is important to consider the phase angle θ in above equation. The effect of phase angle can be determined from the orientation of the transverse spin accumulation and that of magnetisation in the previous layer as depicted in figure 5.2. For clarity, the magnetisation in the current layer ($\mathbf{M}$) and that in the previous layer ($\mathbf{M}_p$) are assumed to align in the $\hat{\mathbf{b}}_1\hat{\mathbf{b}}_2$ plane of the basis coordinate system. Therefore, the transverse component of magnetisation in the previous layer ($\mathbf{M}_{p,\perp}$) and the transverse spin accumulation ($\mathbf{m}_\perp$) must be oriented along the direction of basis $\hat{\mathbf{b}}_2$ and in the $\hat{\mathbf{b}}_2\hat{\mathbf{b}}_3$ plane respectively.

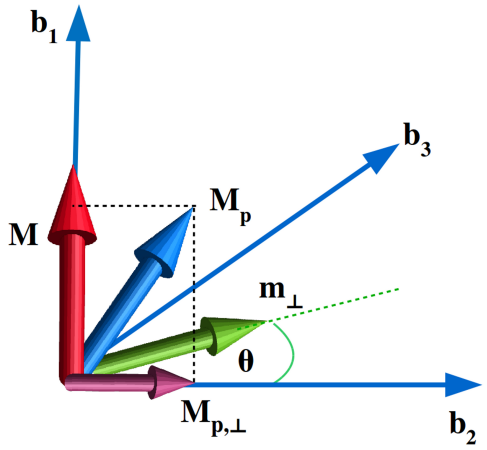

Figure 5.2: The orientation of magnetisation and transverse spin accumulation representing the phase effect on the spin torque parameters

Clearly, the adiabatic torque is along in the direction which is perpendicular to $\mathbf{M}$ and oriented along basis $\hat{\mathbf{b}}_2$. Its magnitude is characterised by parameter a depending on the phase angle $(\sin\theta)$. Hence, the non-adiabatic torque must be along the direction of basis $\hat{\mathbf{b}}_3$. In addition, the dependence of a and b on θ suggests that a and b may change sign, as will be demonstrated later.

5.2.3 Divergence of the spin torque parameters

Physically, the origin of the adiabatic and non-adiabatic spin torque terms must be related to the phase difference between the magnetisation and spin accumulation. There are many theoretical studies investigating the adiabatic and non-adiabatic torques [9,64, 73–75]. Generally the approach comprises the introduction of terms in the LLG equation representing adiabatic and non-adiabatic spin torque contributions. These terms involve constants whose ratio is determined by a phenomenological non-adiabatic parameter β_x.

Berger theoretically studied the effect of reaction torque on the system containing a non-uniform magnetisation [2,80]. The gradient of magnetisation corresponds to change in spin current to conserve the angular momentum carried by the conduction electron. The spin torque acting on the magnetisation can be quantitatively described in the Gilbert form of the LLG equation given by

$$\Gamma = -\mu_x \frac{\partial \mathbf{M}}{\partial x} + \mu_x \beta_x \mathbf{M} \times \frac{\partial \mathbf{M}}{\partial x}. \tag{5.13}$$

In the standard form as shown in the above equation, the adiabatic and non-adiabatic torques are expressed in terms of μ_x and β_x [6, 65, 66, 76, 80, 81] respectively. Typically, the phenomenological non-adiabaticity parameter β_x is an unknown variable and its value has been assumed. The parameters μ_x and β_x which are unknown variables in the standard Gilbert form can be considered as functions of the coefficients a and b. Consider the modified LLG equation including the spin torque expressed in terms of the magnetisation gradient in equation (5.14) given by

$$\frac{d\mathbf{M}}{dt} = -\gamma\mathbf{M}\times\mathbf{H}_{\text{eff}} + \alpha\mathbf{M}\times\frac{d\mathbf{M}}{dt} - \mu_x\frac{\partial\mathbf{M}}{\partial x} + \beta_x\mu_x\mathbf{M}\times\frac{\partial\mathbf{M}}{\partial x}. \tag{5.14}$$

The modified LLG taking the Slonczewski torque and the field-like torque into account can be expressed as a function of the spin torque parameters a and b as follows

$$\frac{d\mathbf{M}}{dt} = -\gamma\mathbf{M}\times\mathbf{H}_{\text{eff}} + \alpha\mathbf{M}\times\frac{d\mathbf{M}}{dt} - a\gamma\left[\mathbf{M}\times(\mathbf{M}\times\mathbf{M}_p)\right] + b\gamma(\mathbf{M}\times\mathbf{M}_p). \tag{5.15}$$

Therefore, the coefficient μ_x and β_x in the standard form can be represented as functions of parameters a and b by comparing the last two terms in equation (5.14) with those in equation (5.15) as follows

$$-\mu_x\frac{\partial\mathbf{M}}{\partial x} = -a\gamma\left[\mathbf{M}\times(\mathbf{M}\times\mathbf{M}_p)\right]$$

and

$$\beta_x\mu_x\mathbf{M}\times\frac{\partial\mathbf{M}}{\partial x} = b\gamma(\mathbf{M}\times\mathbf{M}_p).$$

The coefficients μ_x and β_x can be obtained by solving the above equations given by

$$\mu_x = \frac{a\gamma\frac{\partial\mathbf{M}}{\partial x}\cdot\left[\mathbf{M}\times(\mathbf{M}\times\mathbf{M}_p)\right]}{\left|\frac{\partial\mathbf{M}}{\partial x}\right|^2} \tag{5.16}$$

$$\beta_x = \frac{b\gamma(\mathbf{M}\times\frac{\partial\mathbf{M}}{\partial x})\cdot(\mathbf{M}\times\mathbf{M}_p)}{\mu_x\left|\mathbf{M}\times\frac{\partial\mathbf{M}}{\partial x}\right|^2}. \tag{5.17}$$

where $\frac{\partial\mathbf{M}}{\partial x}$ is the gradient of the local magnetisation with respect to the distance along the direction of the injected spin current.

Consider the relationship of μ_x and β_x by putting $\mathbf{M} = \mathbf{M}_p + \frac{\partial\mathbf{M}}{\partial x}\Delta x$ into the cross product term as follows

$$\begin{aligned}\mathbf{M}\times(\mathbf{M}\times\mathbf{M}_p) &= (\mathbf{M}\cdot\mathbf{M}_p)\mathbf{M} - (\mathbf{M}\cdot\mathbf{M})\mathbf{M}_p \\ &= (\mathbf{M}\cdot(\mathbf{M} - \frac{\partial\mathbf{M}}{\partial x}\Delta x))\mathbf{M} - |\mathbf{M}|^2\mathbf{M}_p\end{aligned}$$

$$
\begin{aligned}
&= (1 - \mathbf{M} \cdot \frac{\partial \mathbf{M}}{\partial x} \Delta x)\mathbf{M} - (\mathbf{M} - \frac{\partial \mathbf{M}}{\partial x} \Delta x) \\
&= -(\mathbf{M} \cdot \frac{\partial \mathbf{M}}{\partial x})\Delta x \mathbf{M} + \frac{\partial \mathbf{M}}{\partial x} \Delta x.
\end{aligned}
$$

Therefore, the coefficient μ_x in equation (5.16) can be rewritten as

$$
\begin{aligned}
\mu_x &= \frac{a\gamma \frac{\partial \mathbf{M}}{\partial x} \cdot \left[-(\mathbf{M} \cdot \frac{\partial \mathbf{M}}{\partial x})\Delta x \mathbf{M} + \frac{\partial \mathbf{M}}{\partial x} \Delta x \right]}{\left| \frac{\partial \mathbf{M}}{\partial x} \right|^2} \\
&= a\gamma \Delta x [1 - \frac{(\mathbf{M} \cdot \frac{\partial \mathbf{M}}{\partial x})^2}{\left| \frac{\partial \mathbf{M}}{\partial x} \right|^2}], \qquad (5.18)
\end{aligned}
$$

and straightforwardly

$$
\beta_x = -\frac{b\gamma \Delta x}{\mu_x}. \qquad (5.19)
$$

In general, the parameter μ_x in the standard form is assumed to be constant throughout the layer and proportional to the spin current density (j_e) given by $\mu_x = \frac{\gamma \hbar P j_e}{2eM_s}$. The non-adiabatic contribution characterised by parameter β_x has been in debate. In this work as shown in equations (5.18) and (5.19), these parameters can be written in terms of the coefficients a and b. The unknown variable μ_x in the standard form is obtained explicitly since the spin torque parameters a and b can be calculated directly from the spin accumulation using equation (5.12). Moreover, the parameters μ_x and β_x depend on the gradient of magnetisation which means that they tend to be nonuniform and divergent for small gradients, as will be discussed in detail later.

5.3 Spin torque in domain wall structure

Initially the calculation of spin accumulation in the domain wall (DW) structure is presented in order to verify the modified solution of spin accumulation derived in chapter 4. It will be applied generally to a system of a series of layers, allowing studies of the spin accumulation in systems with spatially varying magnetisation structures. In this computational study I also investigate the behaviour of the spin current, the adiabatic and non-adiabatic torque components, the spin torque parameters a and b in the proposed model and the coefficients μ_x and β_x in the standard form at any position of the system in detail in the following.

5.3.1 Domain wall structure

To demonstrate the use of the formalism in the case of a spatially dependent magnetisation structure, a bilayer structure consisting of two non-collinear ferromagnets (a pinned layer F_1 and a free layer F_2) is considered here. The system is first discretised into small grids with a cell size of 1.5×1.5×1.5 nm^3. The magnetic moment in each cell is then calculated by averaging over the spins within the cell. As shown in figure 5.3 (a), the pinned layer is not considered explicitly; its role is simply to provide a spin-polarised current through the layer under investigation. Meanwhile, a domain wall into the free layer, which is a single thin film of 60×30×1.5 nm^3, is forced by pinning the magnetisation in the $\pm y$ direction at $x = 0,\ L$ where L (= 60 nm) is the extent of the free layer in the x-direction.

The magnetisation structure is formed by minimizing the total energy using the atomistic model with a Heisenberg form of the exchange in a Hamiltonian $\mathcal{H}$ which also includes the anisotropy energy and is given by

$$\mathcal{H} = -\sum_{i \neq j} J_{ij} \mathbf{S}_i \cdot \mathbf{S}_j - \sum_i K_u (\mathbf{S}_i{}^2 \cdot \mathbf{e}^2), \tag{5.20}$$

with the corresponding parameters expressed as energies per atom. Here J_{ij} is the nearest neighbour exchange integral between the spin site i and j, $\mathbf{S}_i$ is the local normalised spin moment at site i, $\mathbf{S}_j$ is the normalised spin moment of the neighbouring atom at site j, K_u is the uniaxial anisotropy constant and $\mathbf{e}$ is the unit vector of the easy axis.

The studied system is based on a material with a uniaxial anisotropy constant of $K_u = 2.52 \times 10^6\ J/m^3$ with the y direction as the easy axis, an exchange stiffness constant of $A = 1.4 \times 10^{-11}\ J/m$ and a lattice constant of $a = 3.49\ \mathring{A}$ [82]. The domain walls are investigated by observing the magnetisation components at any grid point of the discretised system. As illustrated figure 5.3 (b), at the centre of the DW the x component of magnetisation is maximum and the y component is zero, consistent with the formation of a Néel wall and previous study of the similar system [15].

In order to test the atomistic model the domain wall width is first calculated for comparison with the analytical expression. The effective DW width (δ) in terms of the uniaxial anisotropy can be obtained using a micromagnetic approach as follows [82, 83]

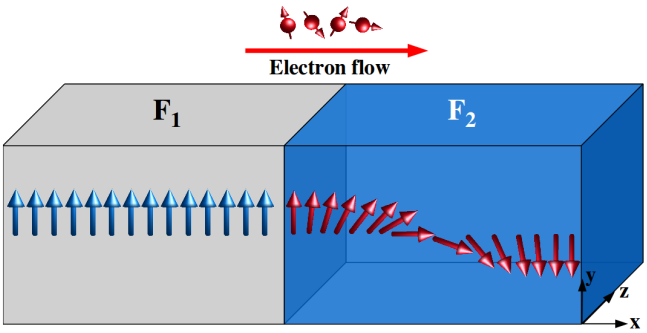

(a)

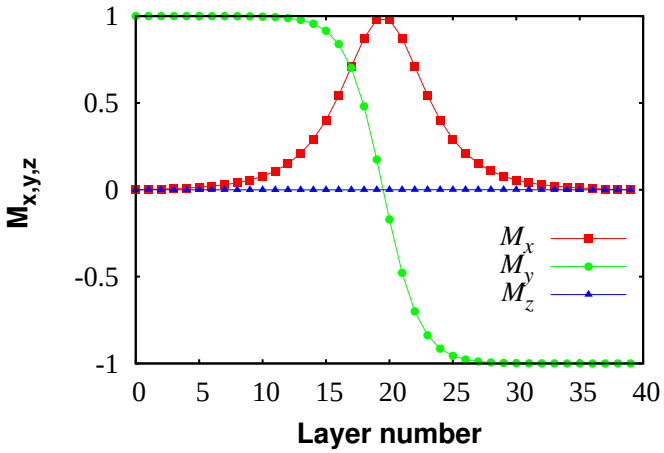

(b)

Figure 5.3: (a) The investigated structure containing the zero field equilibrium domain wall: The bilayer structure comprises of two ferromagnetic layers divided into many thin layers of 5 atomic spacings. The tail-to-tail domain wall is in the free layer with the zero field and the easy axis is in the y direction. (b) The magnetisation components of the domain wall in the free layer obtained from atomistic calculation: The distance between layer is given in units of cells. Lines provide a guide to the eye.

$$\delta = \pi \sqrt{\frac{A}{K_u}} \tag{5.21}$$

where K_u is the uniaxial anisotropy constant and A is the exchange stiffness constant.

The calculated domain wall width using atomistic model is approximately 6.86 nm, slightly lower than the analytical value of 7.42 nm due to the finite system size. From this point, the uniaxial anisotropy constant of $K_u = 2.52 \times 10^6\ J/m^3$ is applied to all of the computational test systems in this section.

5.3.2 Spin accumulation and spin current

After considering the initially equilibrium configuration of domain wall in the free layer, the average magnetisation within each cell of the discretised system is then used to calculate the spin accumulation and spin current. The spin accumulation is introduced by the injection of a spin current along the x-axis, with a spin current density of $j_e = 5 \times 10^{11} A/m^2$ as illustrated in figure 5.3 (a).

As mentioned in chapter 4, the spin accumulation is calculated in the basis coordinate system ($\hat{\mathbf{b}}_1$, $\hat{\mathbf{b}}_2$ and $\hat{\mathbf{b}}_3$), with the direction of the local magnetisation as the direction $\hat{\mathbf{b}}_1$. Therefore, equation (4.4) is then applied to each thin layer of the system to find the basis coordinate system. Subsequently, the modified solution of spin accumulation in equations (4.14) and (4.18) are applied to a series of layers representing the spatial variation of the magnetisation in a domain wall. Therefore the spin accumulation at any position is calculated in the rotated basis in the form

$$\begin{aligned}
\mathbf{m}_{\parallel}(x) &= [m_{\parallel}(\infty) + [m_{\parallel}(0) - m_{\parallel}(\infty)]e^{-x/\lambda_{sdl}}]\ \hat{\mathbf{b}}_1 \\
\mathbf{m}_{\perp,2}(x) &= 2e^{-k_1 x}\left[u\cos(k_2 x) - v\sin(k_2 x)\right]\hat{\mathbf{b}_2} \\
\mathbf{m}_{\perp,3}(x) &= 2e^{-k_1 x}\left[u\sin(k_2 x) + v\cos(k_2 x)\right]\hat{\mathbf{b}_3}
\end{aligned}$$

where the coefficients $m_{\parallel}(0)$, u and v are determined from equation (4.18). The transport parameters of Co use the values of $m_{\parallel}(\infty) = 3.945 \times 10^7\ C/m^3$, $\beta = 0.5$ and $\beta' = 0.9$. The spin diffusion length (λ_{sdl}) is taken to be 60 nm from Ref. [53].

Figure 5.4 shows a result of the calculated spin accumulation and spin current at any position of domain wall in the free layer. The current entering the free layer is polarised in the direction of the magnetisation of the pinned layer (y direction). This gives rise to a spin accumulation and spin current whose polarisations tend to follow the direction of the magnetisation. However, it should be noted that the spin current and spin accumulation also develop an out-of-plane component. Although the out-of-plane component of spin accumulation is generally small, it significantly induces the spin torque in the system. Its influence will be discussed in the next section.

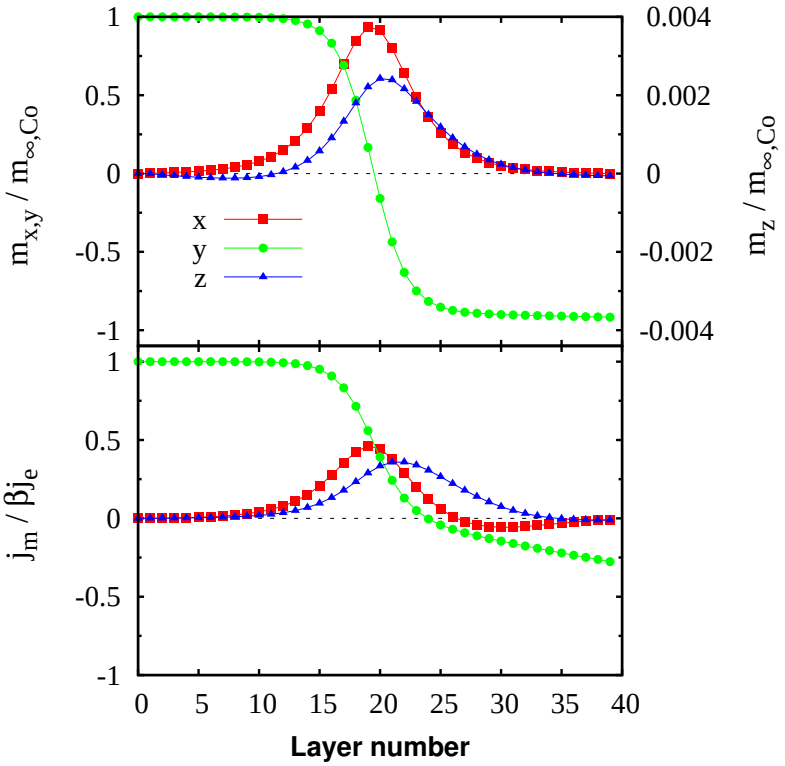

Figure 5.4: The spin accumulation ($\mathbf{m}$) and spin current ($\mathbf{j}_m$) at any position of the free layer in the global coordinate system after the introduction of spin current density of $j_e = 5 \times 10^{11}\ A/m^2$ to the system along the x direction

5.3.3 Spin torque parameters

5.3.3.1 Spin torque parameters a and b

The spin torque parameters a and b in this approach, measuring the strength of the spin transfer torque arising from the s-d exchange interaction, are investigated next. So far the magnitude of both spin torque parameters have been under debate and roughly estimated. However, they can be calculated directly from the spin accumulation as shown in equation (5.12). These spin torque parameters are proportional to the ratio of $|\ \mathbf{m}_\perp\ |\ /\ |\ \mathbf{M}_{p\perp}\ |$ and characterised by the phase angle θ given by

$$
\begin{aligned}
a &= \frac{J|\mathbf{m}_\perp|\sin\theta}{|\mathbf{M}_{p\perp}|}\frac{a_0^3}{e\mu_B} \\
b &= \frac{J|\mathbf{m}_\perp|\cos\theta}{|\mathbf{M}_{p\perp}|}\frac{a_0^3}{e\mu_B}.
\end{aligned}
$$

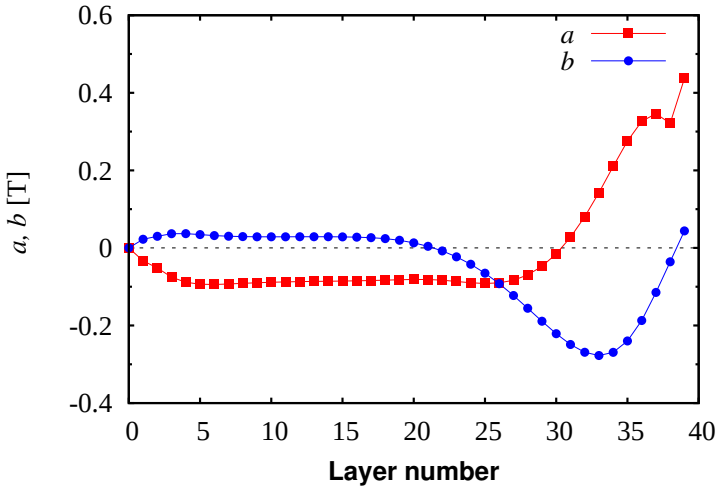

Figure 5.5: The spin torque parameters a and b as a function of the position in the domain wall

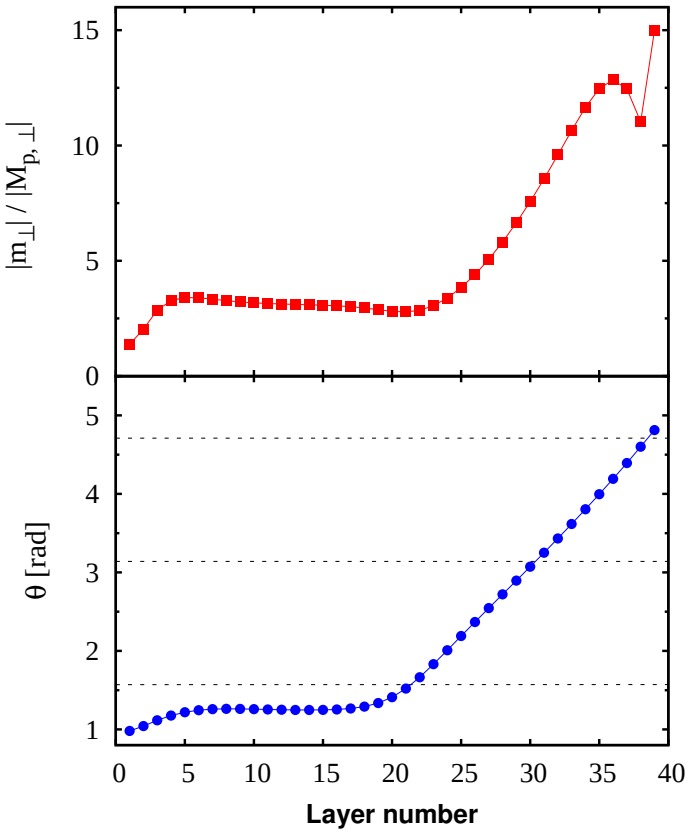

Figure 5.6: (top) The spatial variation of ratio $\frac{|\mathbf{m}_\perp|}{|\mathbf{M}_{p\perp}|}$ (bottom) the angle $\theta_{\mathbf{m}_\perp \mathbf{M}_{p,\perp}}$ between the transverse component of spin accumulation and that of magnetisation in previous layer as a function of position in the domain wall. Horizental lines indicate the angles $\pi/2$, π and $3\pi/2$.

Figure 5.5 depicts the spin torque parameters a and b at any position within the domain wall calculated from the transverse spin accumulation. The result shows that they are not uniform throughout the domain wall. At the boundary of the free layer $x = 0$, there is no torque due to collinear configuration of the pinning layer leading to zero value of spin torque parameters. a and b are approximately constant up to the middle of the domain wall. After the centre of the DW a and b become non-uniform. The coefficient a varies relatively slowly in the regime where the magnetisation gradient is approximately constant, followed by a more rapid variation, including a change of sign at layer number 31. However, b varies significantly from the centre of the wall (layer number 20).

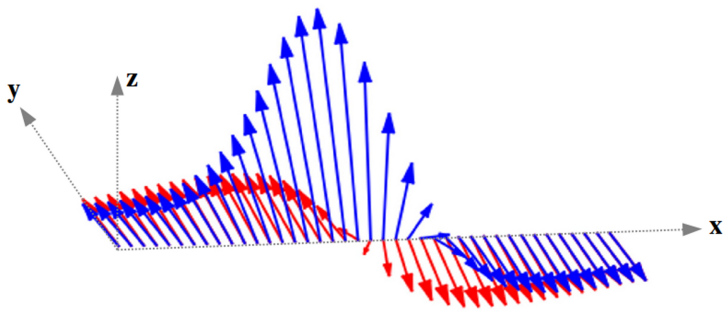

Figure 5.7: The spatial variation of spin accumulation (blue arrows) with respect to the local magnetisation (red arrows)

The behaviours of a and b are spatially dependent. Their values correspond to the spatial variation of the ratio $\frac{|\mathbf{m}_\perp|}{|\mathbf{M}_{p\perp}|}$ as seen in figure 5.6 (top). The sign of the spin torque coefficients indicate the direction of the spin accumulation which varies spatially due to precessional motion. The positions in the domain wall where a and b change in sign can be considered from the angle θ as illustrated in figure 5.6 (bottom). The motion of spin accumulation at any position with respect to the local magnetisation direction is shown in figure 5.7.

5.3.3.2 Spin torque parameters μ_x and β_x

Let us now consider in more detail of the coefficients μ_x and β_x in the representation of the AST and NAST. In the current approach, equations (5.12), (5.18) and (5.19) allow us to evaluate these coefficients from the spin accumulation. It is important to consider the magnitude of the spin accumulation, which is determined by $\mid \mathbf{m}_\perp \mid / \mid \mathbf{M}_{p\perp} \mid$ as well as the phase angle. This angle partially determines the values of μ_x and β_x which is taken as a (unknown) constant (i.e. spatially independent) in the usual formalism.

Figure 5.8 shows the values of μ_x and β_x through the domain wall. It can be seen that the coefficient μ_x is roughly constant in the first half of the domain wall and then its trend is to exhibit a strong spatial dependence. Also its divergence appears at the position with the small angle between the magnetisation corresponding to the behaviour of a.

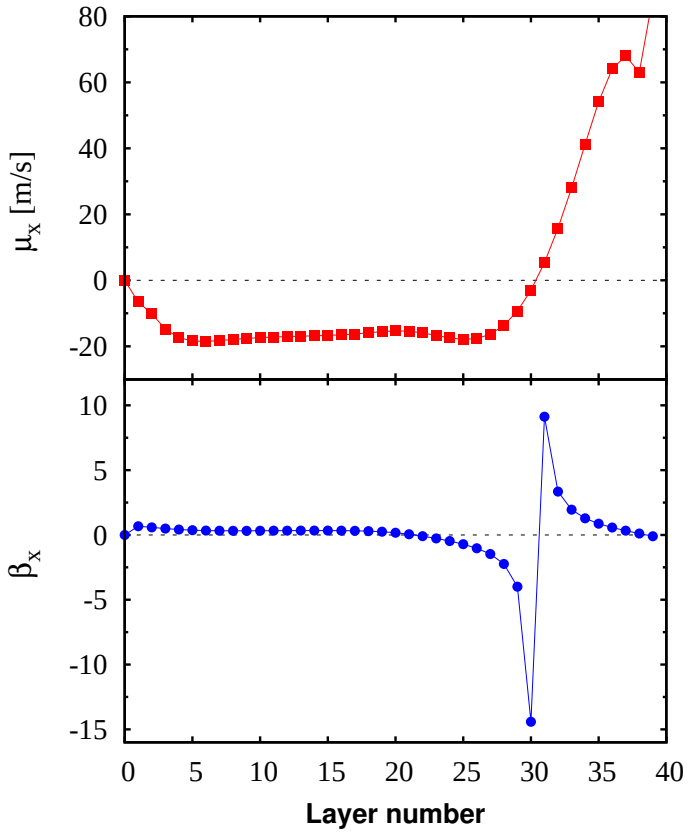

Figure 5.8: The spin torque coefficients μ_x and β_x in the standard form at any position of domain wall in the free layer

Similarly, the coefficient β_x can be determined by the relative strength of the non-adiabatic and adiabatic terms $b/a = \cot\theta$ associated with the "*phase angle*" between the transverse spin accumulation and the magnetisation. In the first half of the domain wall, the non-adiabatic coefficient β_x is approximately constant, consistent with the behaviour of θ and $\mid \mathbf{m}_\perp \mid / \mid \mathbf{M}_{p\perp} \mid$ in figure 5.6. Interestingly, at around layer number 30, μ_x goes to zero, leading to a divergence of β_x as seen in figure 5.8 (low panel). This effect arises from the fact that at around layer 30, $\theta = \pi$ and consequently a vanishes while b remains non-zero as can be seen from equations (5.22). In other words, the divergence must arise from the disappearance of the adiabatic term a ($\sin\theta \to 0$). This can arise from the projection of $\mathbf{m}$ onto orthogonal components of the magnetisation, as is essentially done in equations (5.16) and (5.17). As pointed out by Claudio-Gonzalez *et al.* [67] this is a non-physical effect arising from the projection technique itself. Claudio-Gonzalez *et al.* take the divergence from $\mid \frac{\partial \mathbf{M}}{\partial x} \mid^2$ but equation (5.18) shows that a can go to zero, as will be discussed further in section 5.4.4.

The nonuniform adiabatic and non-adiabatic coefficients μ_x and β_x observed in this calculation are consistent with the work proposed by Claudio-Gonzalez *et al.* [67]. They also demonstrate that the divergence of these coefficients strongly depends on the spatial variation of magnetisation gradient. This aspect agrees with the current approach since $|\partial \mathbf{M}/\partial x| = |\mathbf{M}_{p,\perp}|$. Therefore, to avoid this situation instead Claudio-Gonzalez *et al.* [67] calculate the effective non-adiabatic coefficient β_{diff} by averaging with the weight function, $\mid \partial \mathbf{M}/\partial x \mid^2$.

However, in this work it is suggested to consider the magnitude of the transverse spin accumulation $\mid \mathbf{m}_\perp \mid$ as functions of transport parameters and the factor which is determined by $\mid \mathbf{m}_\perp \mid / \mid \mathbf{M}_{p\perp} \mid$ to investigate the influence of spin diffusion on the divergence of spin torque coefficients. In general, determination of $\mathbf{m}_\perp$ requires numerical solution. However, reducing to the case of two layers with in-plane magnetisation (the case treated by Zhang, Levy and Fert [38]) it is straightforward to show that

$$\begin{aligned} \mid \mathbf{m}_\perp \mid &\propto \frac{1}{(\lambda_{sdl}^{-4} + \lambda_J^{-4})^{1/4}} \\ &\propto \frac{\lambda_{sdl}}{[1 + (\lambda_{sdl}/\lambda_J)^4]^{1/4}}. \end{aligned} \tag{5.22}$$

Given the power law dependence on λ_{sdl}/λ_J one expects a rapid transition between regimes dominated by small λ_{sdl} or small λ_J. Also,

$$\begin{aligned} \mathbf{M} &= \mathbf{M}_p + \frac{\partial \mathbf{M}}{\partial x}\Delta x \\ \mathbf{M}\times\mathbf{M} &= \mathbf{M}\times(\mathbf{M}_{p\parallel}+\mathbf{M}_{p\perp}) + \mathbf{M}\times\frac{\partial \mathbf{M}}{\partial x}\Delta x \\ \mathbf{M}\times\mathbf{M}_{p\perp} &= -\mathbf{M}\times\frac{\partial \mathbf{M}}{\partial x}\Delta x \\ |\,\mathbf{M}_{p\perp}\,| &\propto |\,\frac{\partial \mathbf{M}}{\partial x}\,|\,. \end{aligned} \tag{5.23}$$

To a first approximation this determines the magnitude of μ_x from equations (5.12) and (5.18)

$$\frac{|\,\mathbf{m}_\perp\,|}{|\,\mathbf{M}_{p\perp}\,|} \propto \frac{\lambda_{sdl,\ J}}{|\,\partial\mathbf{M}/\partial x\,|}. \tag{5.24}$$

The above equation shows that at least the transport parameters and $|\,\partial\mathbf{M}/\partial x\,|$ strongly affect the validity of spin torque coefficients used in standard form of micromagnetic model, in particular because $|\,\partial\mathbf{M}/\partial x\,|$ is spatially varying. Thus one arrives at a simple criterion for determining the magnitude of the micromagnetic coefficients in a way which should assist a more realistic comparison with experimental data at least in terms of a qualitative comparison of magnetic ($\partial\mathbf{M}/\partial x$) and transport ($\lambda_{sdl,\ J}$) properties. The influence of transport properties will be presented and discussed in more details later.

As a result of divergence, the non-physical behaviour of the empirical constants μ_x and β_x brings into question the use of the standard micromagnetic spin torque formalism. It strongly suggests that an approach based on the self-consistent solution of the spin accumulation and magnetisation is physically more realistic and, using the semi-analytical theory, numerically attractive since the determination of spin accumulation is relatively fast in relation, for example, to the determination of the local field. Subsequently, the spin torque investigation will be addressed by applying the spin accumulation formalism instead of using the spin torque coefficients as the following section.

5.3.4 Spin torque

The effect of total spin torque component and the contribution of the adiabatic (AST) and non-adiabatic torques (NAST) on the spatially continuous magnetisation in domain wall with the same material parameters in the previous section are investigated here. In this approach, equations (5.12), (5.18) and (5.19) allow to construct the spin torque terms in the usual micromagnetic form, but from the calculated spin accumulation rather than relying on empirical constants. Furthermore, the total spin torque is calculated as a sum of the adiabatic and non-adiabatic torques shown in figure 5.9. Its behaviour corresponds to the direction of magnetisation within domain wall. Therefore in this case it can be concluded that the spins of conduction electrons follow the direction of the local magnetisation known as an adiabatic process leading to AST. Figure 5.9 (a) shows clearly that the components of AST orient in the plane of magnetisation of domain wall and the maximum AST appears at the centre of the wall due to a strongly spatially varying magnetisation, $\mid \partial\mathbf{M}/\partial x \mid \rightarrow$ max, well consistent with previous studies [9, 67, 84, 85] . It is found that the AST becomes the dominant torque of the system as $\mid \mathrm{ST}_{\mathrm{total}} \mid \approx \mid \mathrm{AST} \mid$.

On the other hand, the NAST arising from the deviation of conduction electrons from the adiabatic process acts on domain wall as another source of the external field. The enhancement of NAST indicates the weak coupling between conduction electrons and local magnetisation. Its magnitude is a few times smaller than that of AST as illustrated in figure 5.9 (a) and (b). Nevertheless, it may give rise to the out-of-plane domain wall observed from the appearance of the z component.

As can be seen in the results, both AST and NAST components are oscillatory within the domain wall owing to the *s-d* exchange interaction causing a precession of conduction electrons around the local magnetisation [85–88]. As depicted in figure 5.9 (c), the results seem to provide evidence that the total spin-transfer torque is significantly dominated by the adiabatic torque consisting of x and y components, meanwhile the out-of-plane component arises from the non-adiabatic torque.

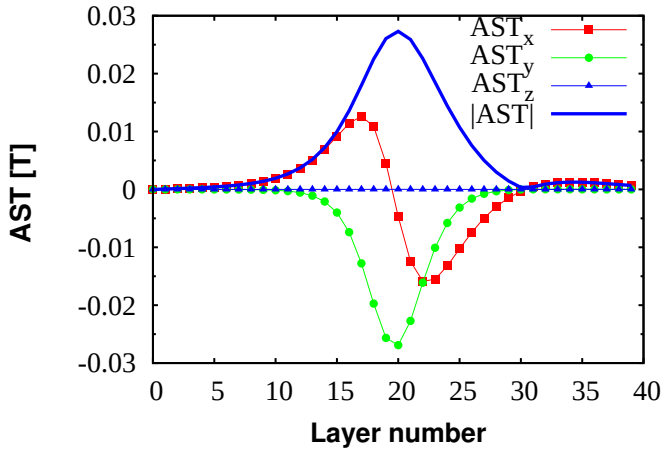

(a)

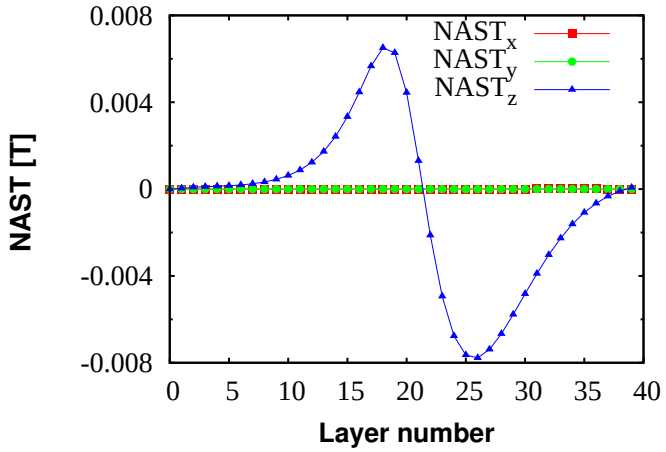

(b)

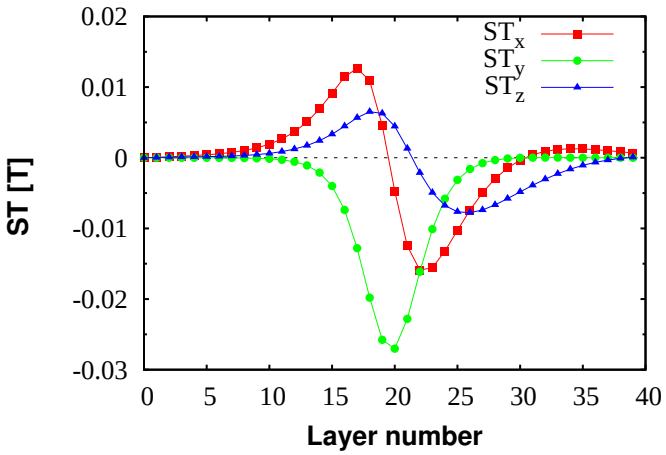

(c)

Figure 5.9: (a) Adiabatic spin torque (AST) (b) non-adiabatic spin torque (NAST) (c) total spin torque (ST) at any position of the domain wall in the free layer

5.4 Effect of spin diffusion length (λ_{sdl})

As mentioned earlier, the transport properties strongly influence the spin transport behaviour in the magnetic system. The spin accumulation is associated with not only the relative orientation of magnetisation but also the length scale of λ_{sdl} and λ_J. The following investigation will give useful insight into the effect of the spin diffusion length on the spin transport behaviour: spin current, spin accumulation, spin torque parameters and spin torque. It should be noted that the results in the rest of this chapter will be demonstrated in the rotated basis coordinate system.

5.4.1 Spin current and spin accumulation

Before discussing the behaviour of the spin accumulation and spin current as a function of the domain wall position, it is worthwhile to recall the formalism of spin accumulation to understand its behaviour. It should be noted that the spin accumulation is defined as $\mathbf{m} = n^{\uparrow} - n^{\downarrow}$. The system is driven to an equilibrium value $\mathbf{m}_{\infty} = n^{\uparrow}_{eq} - n^{\downarrow}_{eq}$ by the damping term as, $-(\mathbf{m} - \mathbf{m}_{\infty})/\tau_{sf}$, with the spin relaxation time of the conduction electrons (τ_{sf}). Therefore, this demonstrates that the spin diffusion length, proportional to the spin relaxation time, plays an important role on the behaviour of the spin accumulation.

Here, let us consider the spatial evolution of spin accumulation and spin current for multiple transport properties by varying the spin diffusion length while the length scale of λ_J representing the strength of the *s-d* exchange interaction is taken to be 4 nm [53]. As illustrated in figure 5.10, for small values of λ_{sdl}, the accumulation is able to respond to the magnetisation, relaxing to the equilibrium value faster corresponding to the stronger interaction between the conduction electrons and the magnetisation. However, large values of λ_{sdl} result in the development of non-equilibrium values of $\mathbf{m}$ on traversing the DW. Essentially, for large λ_{sdl} the spin accumulation and spin current interact weakly with the local magnetisation; the results demonstrate that for large λ_{sdl} the spin current and spin accumulation traverse the DW relatively unaffected. This is reflected in the magnitude and nature of the spin torque as described in the following section.

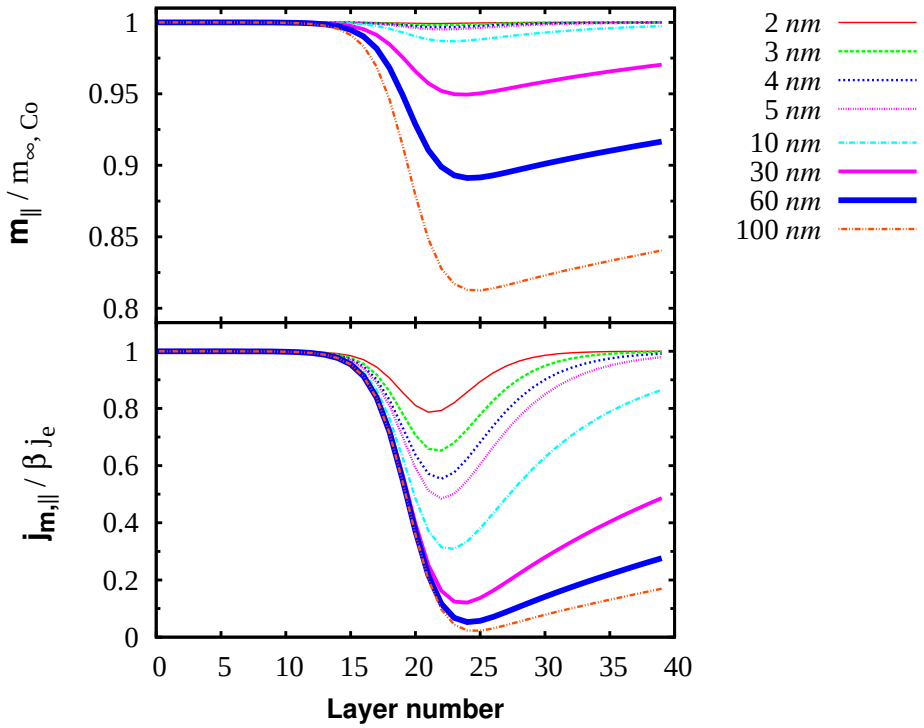

Figure 5.10: The variation of spin accumulation and spin current as a function of the position within the domain wall with various spin diffusion lengths between 2 and 100 nm in the basis coordinate system

5.4.2 Adiabatic and non-adiabatic spin torques

As a result of spin accumulation, for large λ_{sdl} the transverse spin accumulation tends to increasingly develop across the domain wall especially in the centre of the wall since the spin accumulation deviates more from the equilibrium value. For convenience, the adiabatic and non-adiabatic torques can be considered in the basis coordinate system. Both AST and NAST arise from the transverse spin accumulation ($\mathbf{m}_{\perp}$) associated with the constants k_1 and k_2 as shown in equation (4.14). It is noted that $1/l_+ = (k_1 - ik_2) = \sqrt{\lambda_{sf}^{-2} - i\lambda_J^{-2}}$ and then it can be rewritten as follows

$$\begin{aligned} k_{1,2} &= \sqrt{\frac{\pm\lambda_{sf}^{-2} + \sqrt{\lambda_{sf}^{-4} + \lambda_J^{-4}}}{2}} \\ &= \frac{1}{\sqrt{2}\lambda_{sf}} \sqrt{\pm 1 + \sqrt{1 + (\lambda_{sf}/\lambda_J)^4}}. \end{aligned}$$

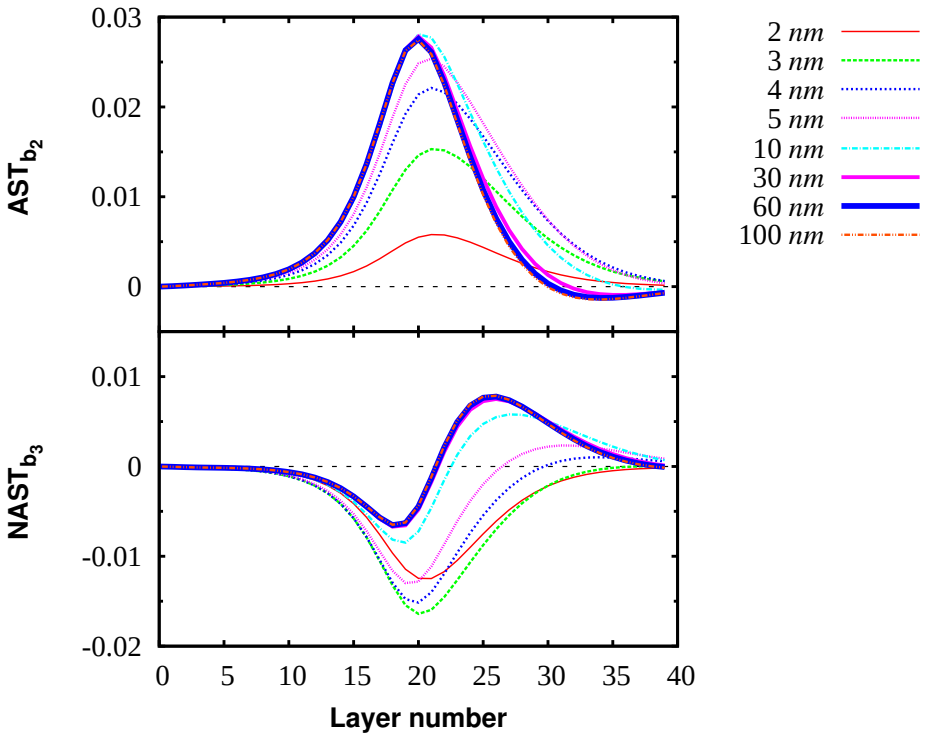

Figure 5.11: The spatial variation of the adiabatic (AST) and non-adiabatic (NAST) torques in the basis coordinate system: AST is in-plane spin torque along the basis $\hat{\mathbf{b_2}}$ whereas NAST is out-of-plane torque oriented in the direction of basis $\hat{\mathbf{b_3}}$.

Therefore, it is important to consider the ratio of λ_{sf}/λ_J to describe the response of spin torque in each regime. The oscillatory behaviour of AST and NAST can be seen in the regime $\lambda_{sf} > \lambda_J$ whereas there is no oscillation of both torques in the regime $\lambda_{sf} < \lambda_J$. Consequently, the critical value of the spin relaxtion length can be determined in the regime $\lambda_{sf} = \lambda_J$. In the case of $\lambda_J = 4\ nm$, it is found that the critical value of spin diffusion length ($\lambda_{sdl,crit}$) is about $3\ nm$, approximately consistent with $\lambda_{sf} = \lambda_J = 4\ nm$. As displayed in figure 5.11, in the regime $\lambda_{sdl} \leq 3\ nm$ both AST and NAST are relatively small as the spin accumulation is well able to follow the local magnetisation and reaches the equilibrium value with a short relaxation time. Furthermore, both torques tend to increase with increasing spin diffusion length in this regime. Obviously, it is observed that the transverse spin accumulation is mostly absorbed in the centre of the domain wall resulting in the highest spin torque in this position.

For the critical spin diffusion length $\lambda_{sdl,crit} = 3\ nm$ the spin torque is relatively small, with both AST and NAST terms of similar magnitude. However, with increasing

λ_{sdl}, the adiabatic term quickly becomes dominant. In the regime $\lambda_{sdl} \geq \lambda_{sdl,crit}$, spin torque exhibits the oscillatory behaviour of AST and NAST. The oscillation of both AST and NAST torques can be observed for large spin diffusion length. Also, the position in domain wall where AST and NAST change in sign for any given spin diffusion length corresponds to the phase angle as explained previously. The influence of spin diffusion length on spin torque parameters a and b will be considered next.

5.4.3 Spin torque parameters a and b

The effect of spin diffusion length on the spin torque parameters a and b is investigated and discussed here. Figure 5.12 shows the parameters a and b as a function of domain wall position for different spin diffusion lengths. Both parameters appear to be nonuniform corresponding to the nonuniform gradient of magnetisation within the domain wall. It also results in a nonuniform phase angle. These parameters are more nonuniform with increasing spin diffusion length, $\lambda_{sdl} > \lambda_J$.

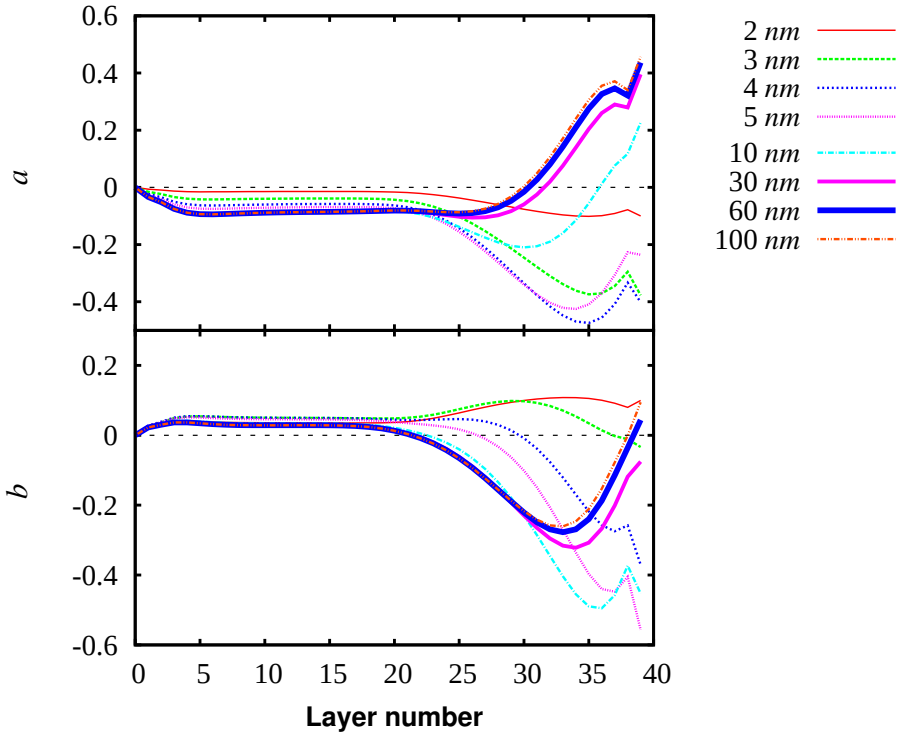

Figure 5.12: (top) The spin torque parameters a and (bottom) b as a function of the position in the domain wall responsible for the adiabatic and non-adiabatic spin torques for the system with different spin diffusion lengths

As seen in figure 5.13, increasing spin diffusion length gives rise to increasing in misalignment of transverse spin accumulation and transverse magnetisation as shown by the spatial variation of phase angle θ. For small spin diffusion length, $\lambda_{sdl} < \lambda_J$, the phase angle tends to be uniform and small. In contrast, the large spin diffusion length enhances the oscillation in the ratio of $\frac{|\mathbf{m}_\perp|}{|\mathbf{M}_{p\perp}|}$ and subsequently in spin torque parameters. The coefficients μ_x and β_x in the usual micromagnetic approach will be next discussed to observe the effect of λ_{sdl} on the coefficient divergence.

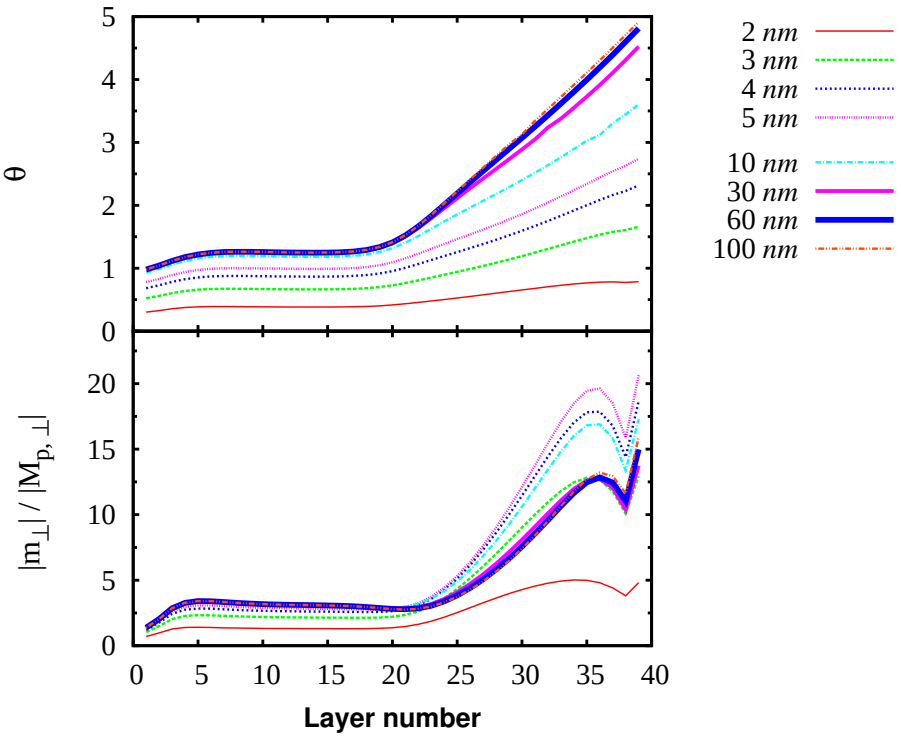

Figure 5.13: (top) The angle $\theta_{\mathbf{m}_\perp \mathbf{M}_{p,\perp}}$ between the transverse component of spin accumulation and that of magnetisation in previous layer as a function of domain wall position in the free layer with different spin diffusion lengths (bottom) The spatial variation of ratio $\frac{|\mathbf{m}_\perp|}{|\mathbf{M}_{p\perp}|}$

5.4.4 Coefficients β_x and μ_x in the standard form of usual micromagnetic approach

Consider first the behaviour of μ_x. In the first half of the DW, μ_x is essentially independent of position. It is also noted that in this region, μ_x increases with λ_{sdl}, as will

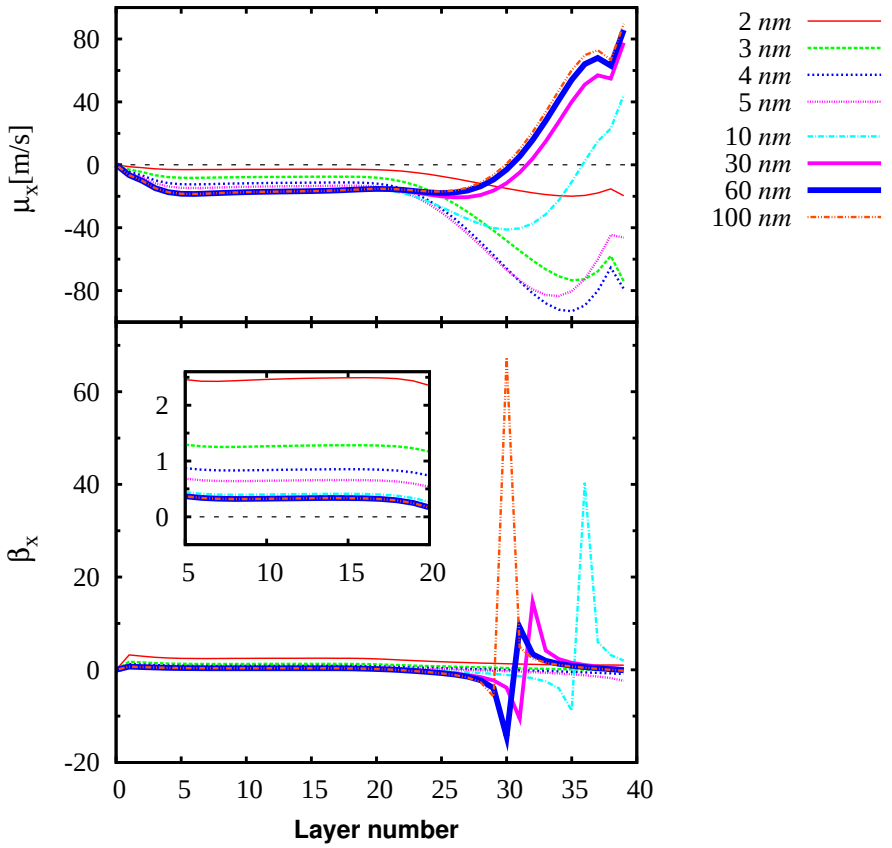

Figure 5.14: Spatial variation of spin torque coefficients μ_x and β_x within DW in the free layer for various spin diffusion lengths

be discussed further in section 5.5.1. This is consistent with the behaviour of the phase angle θ and $\frac{|\mathbf{m}_\perp|}{|\mathbf{M}_{p\perp}|}$ from figure 5.13. However, after the centre of the DW, μ_x begins to vary dramatically, an effect increasingly apparent for large λ_{sdl}. Similarly, for small λ_{sdl}, β_x is reasonably constant in the in the first part of the DW. For larger λ_{sdl}, β_x exhibits increasing spatial dependence, actually changing sign at large λ_{sdl}. It is also noted that β_x shows divergent behaviour at layer numbers dependent on λ_{sdl}. Claudio-Gonzalez *et al.* [67] have noted divergent behaviour, which was ascribed to the spatial decomposition of the spin accumulation. In this work it is found that the divergent behaviour is due to the zero value of a.

These results suggest that the usual micromagnetic approach is, in general, unsatisfactory for spin torque calculations. In the following sections I consider further the validity of the usual micromagnetic approach, that is with constant μ_x and β_x, by investigating the effect of the DW width. It is found that μ_x and β_x can be taken as constant

for magnetically soft material such as Fe, but this assumption is not valid for harder materials such as Co and FePt.

5.5 Effect of domain wall thickness

In this section, the value of the uniaxial anisotropy constant is varied for a parametric study of the effect of the DW width on the spin torque. The aim is to investigate the spatial evolution of the spin accumulation and spin torque as a function of the DW width, and also to investigate the limit of validity of the assumption of constant factors for the AST and NAST. The anisotropy constant ranges from K_u to $100K_u$ where K_u is the typical uniaxial anisotropy constant of cobalt, $4.2 \times 10^5 J/m^3$. This range includes materials such as FePt and other hard magnetic materials such as $SmCo_5$ and $Nd_2Fe_{14}B$.

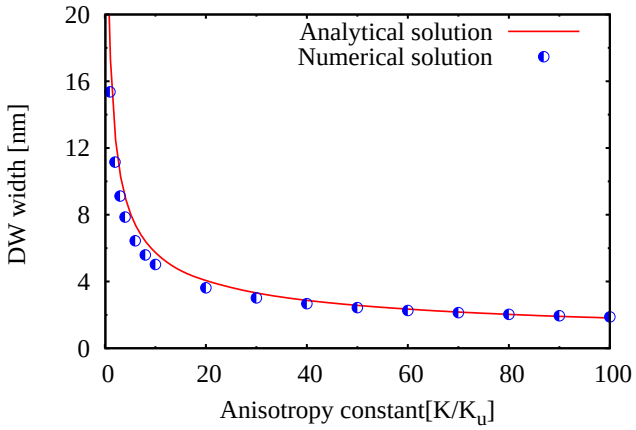

Figure 5.15: Domain wall width versus anisotropy constant: comparison between the analytical solution and the numerical solution

To observe the uniaxial anisotropy dependence of the spin transport behaviour, the formation of a Néel wall for different anisotropy is numerically calculated using the atomistic model as explained earlier. Initially a calculation of the DW width is presented as a function of the uniaxial anisotropy constant in order to verify the atomistic calculations in relation to the continuum (micromagnetic) theory. In figure 5.15, the numerically calculated DW widths for different anisotropy constants are compared with the analytical solutions calculated from equation (5.21) given by, $\delta = \pi\sqrt{A/K_u}$. As

expected the DW width decreases with increasing anisotropy constant and the numerical solution is consistent with the analytical result. This represents a useful test of the atomistic model in its prediction of the static magnetic properties. Subsequently, the equilibrium domain wall for various anisotropy constants is used for the spin accumulation calculation. The anisotropy dependence of the spin transport behaviour can be seen as follows.

5.5.1 Spin current and spin accumulation

Here the spin accumulation and spin current as a function of the DW width are investigated. The aim is to determine the effect of the magnetisation gradient, roughly characterised by the inverse of the DW width on the spin mistracking effect. The evidence of the breakdown of the assumption of constant μ_x and β_x for high anisotropy materials is also presented. I start by applying the modified formalism of spin accumulation to the domain wall and then calculating the spatial longitudinal spin current and spin accumulation as illustrated in figure 5.16. For convenience and clarity of representation all results are presented in the rotated basis system.

As discussed previously, the spin accumulation relaxes with the characteristic length scale of the spin diffusion length associated with the spin flip scattering toward the direction of magnetisation. The results shown in figure 5.16 clearly suggest that the spin mistracking is strongly dependent on the DW width. Recalling that the data are presented in the rotated basis, any mistracking is apparent as a deviation from unity of the normalised $\mathbf{m}_{\|}$ and $\mathbf{j}_{m,\|}$ values. With increasing anisotropy, there is a clear increase in the mistracking resulting from the inability of the spin accumulation to follow the increasingly rapid spatial magnetisation changes [85, 89–92]. In summary, a large uniaxial anisotropy decreases the inability of conduction electrons to adiabatically follow the strongly spatially varying magnetisation [93] causing the spin mistracking.

As previously mentioned, the domain wall width (δ) is a crucial parameter in the spin transport behaviour. Therefore, it is worthwhile to consider the magnitude of the transverse spin accumulation as a function of DW width, since the transverse spin accumulation induces a spin torque acting on the local magnetisation given by

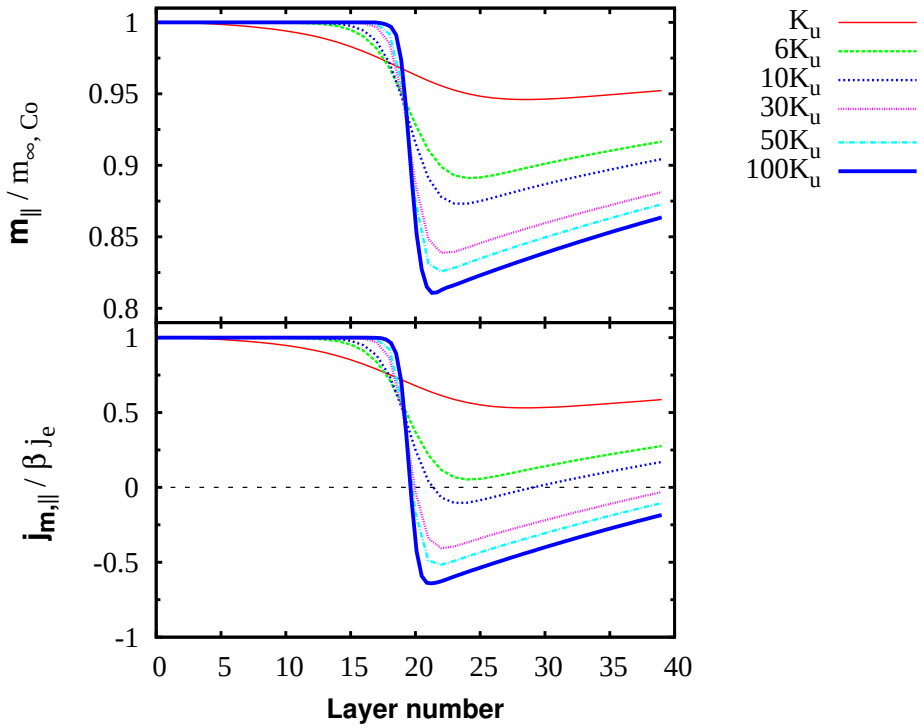

Figure 5.16: The unixial anisotropy dependence of the longitudinal spin accumulation and spin current: The spin diffusion length is taken as 60 nm.

$$
\begin{aligned}
|\,\mathbf{m}_{\perp}\,| &= \sqrt{|\,\mathbf{m}_{\perp,2}\,|^2 + |\,\mathbf{m}_{\perp,3}\,|^2} \\
&= 2e^{-k_1 x}\sqrt{[u\cos(k_2 x) - v\sin(k_2 x)]^2 + [u\sin(k_2 x) + v\cos(k_2 x)]^2} \\
&= 2e^{-k_1 x}\sqrt{u^2 + v^2}.
\end{aligned}
$$

As shown in equation (4.18), the unknown coefficients u and v are expressed in terms of λ_{sdl}/λ_J and $\partial\mathbf{m}/\partial\mathbf{x}$. However, it is found that the gradient of spin accumulation is proportional to the gradient of spin current associated with the magnetisation gradient as follows

$$
\begin{aligned}
\partial\mathbf{m}/\partial x &\propto \partial\mathbf{j}_{\mathbf{m}}/\partial x \\
&\propto \partial\mathbf{M}/\partial x
\end{aligned}
$$

and then one obtains

$$
|\,\mathbf{m}_{\perp}\,| \propto |\,\partial\mathbf{M}/\partial x\,| \frac{\lambda_{sdl}}{[1 + (\lambda_{sdl}/\lambda_J)^4]^{1/4}}. \tag{5.25}
$$

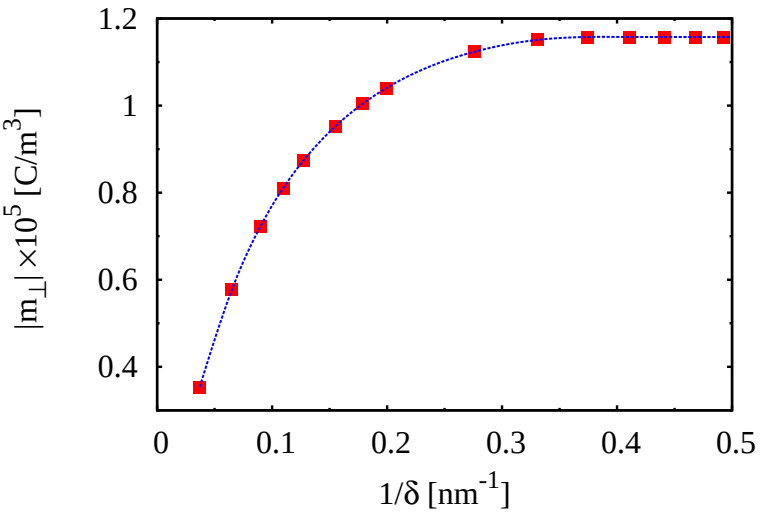

(a)

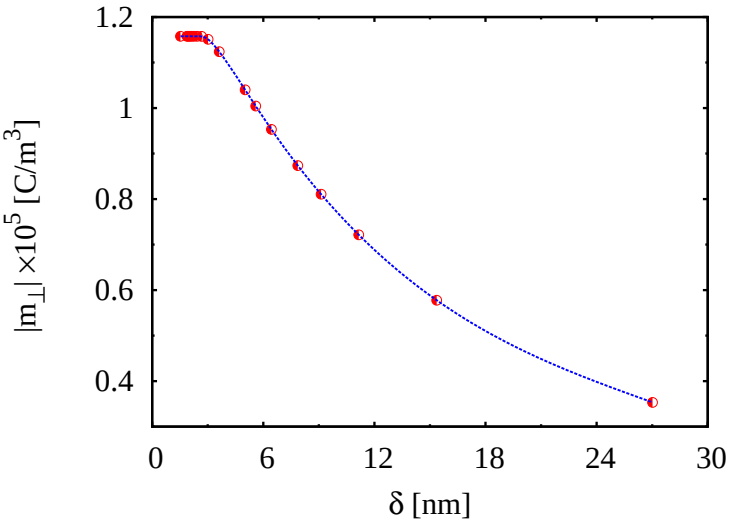

(b)

Figure 5.17: (a) The magnitude of transverse spin accumulation as a function of $1/\delta$ associated with the gradient magnetisation ($\nabla_x \mathbf{M}$) and (b) that as a function of domain wall width(δ)

The above equation shows that the transverse spin accumulation strongly depends on the gradient of magnetisation within the domain wall, inversely proportional to the domain wall width ($1/\delta$). In figure 5.17, the magnitude of the transverse spin accumulation at the center of domain wall is observed as a function of DW width and the gradient of magnetisation via $1/\delta$. Interestingly, there is an indication of a linear variation for small $\mid \mathbf{m}_\perp \mid$, consistent with equation (5.25). However, the exploration of this region

would require simulation of large DW widths, which is beyond the current investigation.

For a narrow DW, conduction electrons flow with spins largely undeviated across the strongly spatially varying magnetisation (large $\nabla_x \mathbf{M}$) giving rise to a large transverse spin accumulation. In turn, the transverse spin accumulation decreases with increasing DW width resulting from a weak spin mistracking as depicted in figure 5.17 (a) and (b). Interestingly, A saturation of transverse spin accumulation is observed at DW width about $\delta \approx \lambda_{sdl} = 3\ nm$ due to the finite system size. The result implies that mistracking of the conduction electrons with the local magnetisation increases significantly for smaller DW width. Also, this result can be used to describe the spin torque exerted on a DW as it originates from the transverse spin accumulation which will be shown in the next section.

5.5.2 Spin-transfer torque

In figure 5.18, the total spin torque, AST and NAST are plotted as a function of DW width. The effect of DW width on the adiabatic and non-adiabatic spin torques is larger in a narrow wall due to the larger magnetisation gradient resulting from a strong uniaxial anisotropy as expected. The contribution of AST is expected to prevail for a wide DW, whereas the NAST is supposed to be more effective in the narrow wall. Obviously, the oscillation of NAST about the DW centre can be observed for a very narrow wall due to the abrupt change in local magnetisation consistent with the previous work in Ref. [86,88]. As discussed in relation to the transverse spin accumulation in the previous section, the explanation of the behaviour of spin torque created within the DW follows from the fact that decreasing the DW width by increasing anisotropy leads to a stronger mistracking of conduction electrons and magnetisation. Similarly to the effect of the spin diffusion length, the AST is still the main contribution to the total spin torque. In addition, the AST can be a few orders of magnitude larger than that in NAST particularly in the regime of large anisotropy.

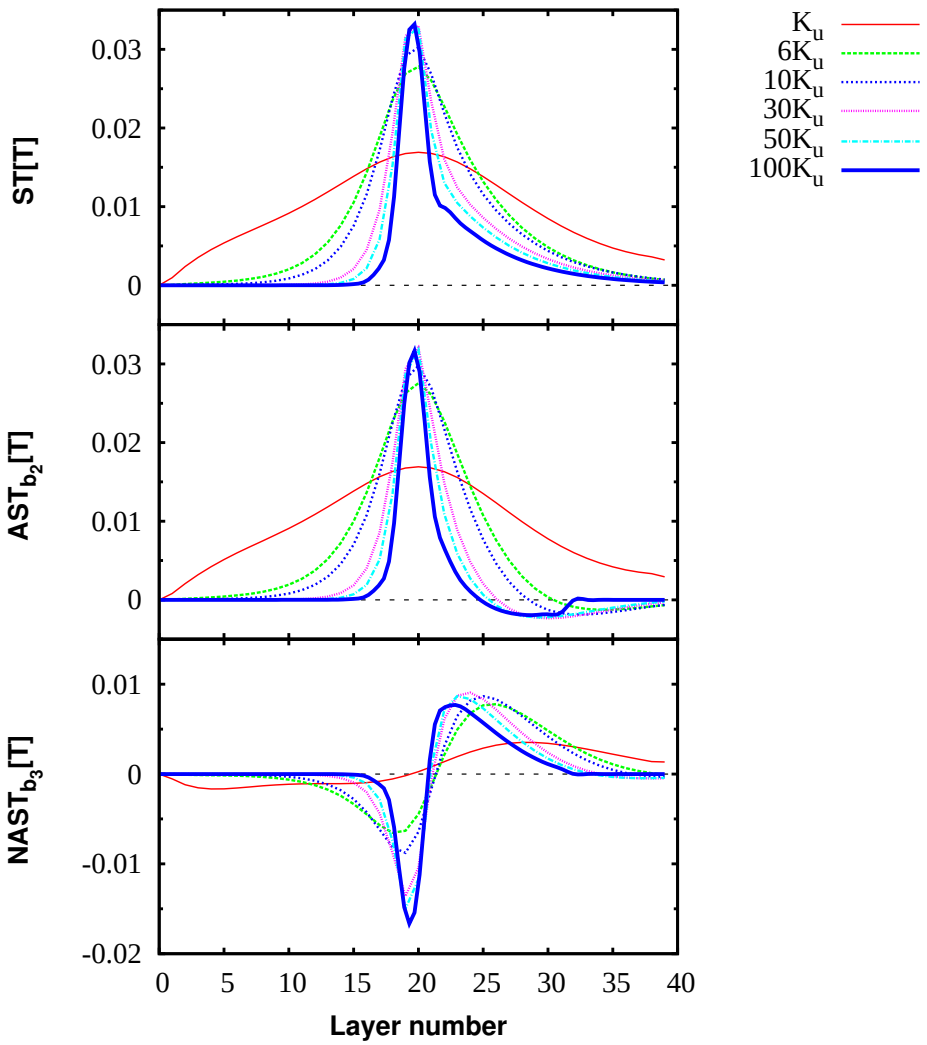

Figure 5.18: Spatial total spin torque, AST and NAST within DW for different anisotropy constants: K_u is the typical uniaxial anisotropy constant of cobalt, $4.2 \times 10^5 J/m^3$.

5.5.3 Validity of the spin torque coefficients in usual micromagnetic approach

The earlier results in sections 5.4 and 5.5 clearly show the effect of the spin diffusion length and the gradient of magnetisation within DW on the spin transport behaviour. It can be concluded that conduction electrons cannot reach equilibrium, that is collinearity with the local magnetisation, within the spatial extent of the DW in a narrow wall with a large spin diffusion length. However, the coefficients μ_x and β_x are possibly applicable to

a very wide DW of which width is comparable to λ_{sdl}. This results in uniform spin torque coefficients as illustrated in figure 5.19. To study the criterion of applicability of the spin torque coefficients in the usual micromagnetic approach, the static domain wall pattern with a small anisotropy of $K_u = 4.2 \times 10^4\ J/m^3$ is considered. This anisotropy value gives rise to domain wall width of about 27 nm, much greater than the spin diffusion length of 2 nm.

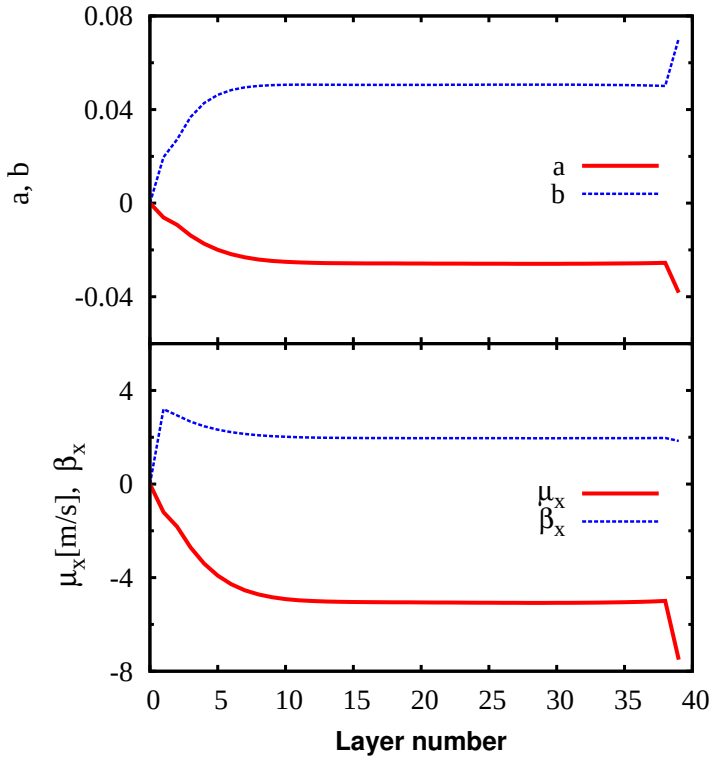

Figure 5.19: Spatial variation of the spin torque coefficients within a wide DW with the uniaxial anisotropy of $4.2 \times 10^4 J/m^3$ and the spin diffusion length at 2 nm

As shown in figure 5.19, the spin torque coefficients tend to be uniform throughout the DW. The effect of pinning as well as the finite size effect cause the kink at the boundary of the DW. The results indicate that the spin torque coefficients used in usual micromagnetic approach are probably applicable to describe the behaviour of spin transport in the magnetic system with a large DW width and a small spin diffusion length in the regime of $\lambda_{sdl} < \lambda_J$. Nevertheless, the typical value of the spin diffusion length is large, for instance, 60 nm for Co.

Consequently, I also consider the criterion for the validity of spin torque coefficients used in the usual micromagnetic model for a realistic system with a large spin diffusion length, taken to be 60 nm. For comparison, the magnetic systems Fe, Co and FePt of which the domain wall width are 200 nm, 18 nm and 4 nm respectively [94–98] are investigated.

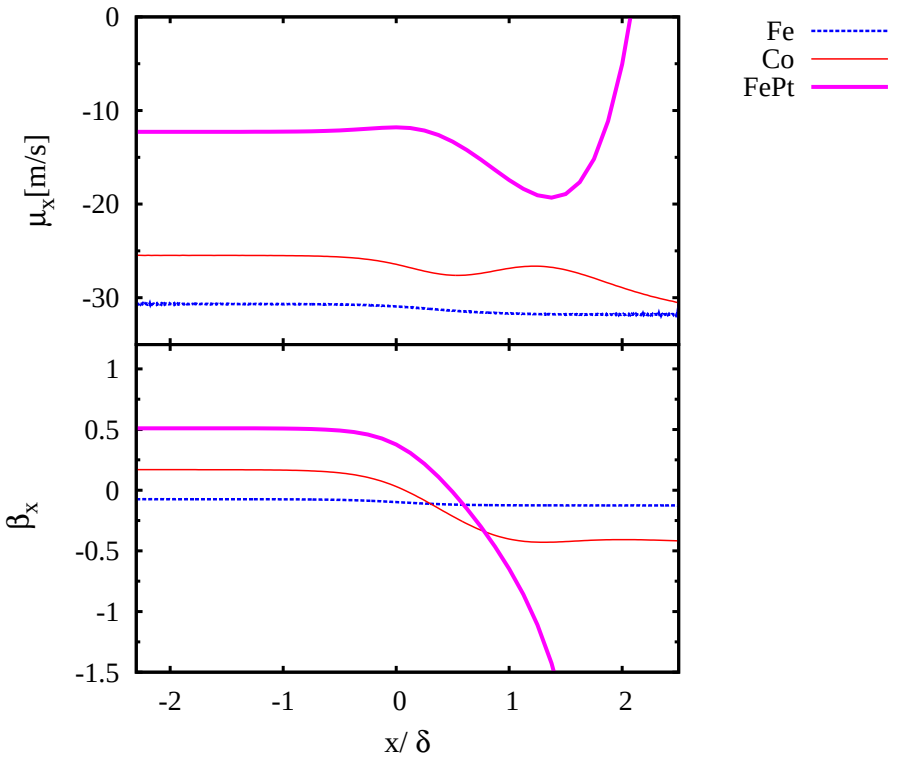

Figure 5.20: The spin torque coefficients used in the usual micromagnetic model as a function of x/δ: x is the position of the magnetic system and δ is the DW width.

The spin torque coefficients μ_x and β_x of the magnetic systems Fe, Co and FePt are plotted as a function of x/δ where x is distance from the centre of the DW and δ is the DW width. As illustrated in figure 5.20, the spin torque coefficients used in the micromagnetic model are applicable to describe the spin transport behaviour for the case of $\delta > \lambda_{sdl}$. For the case of Fe, the DW width is much larger than the spin diffusion length giving rise to the uniform spin torque coefficients. This is because of the slowly varying magnetisation within DW allowing the spin accumulation to closely follow the magnetisation. Interestingly, the value of the coefficient β_x becomes negative for this soft material. The nonuniform coefficients can be observed in Co for which the DW

width is smaller than the spin diffusion length. Interestingly, in the case of FePt, where the DW width is much smaller than the spin diffusion length, the coefficients exhibit a strong spatial dependence and a sign change in both μ_x and β_x. Clearly, the spin torque coefficients in the standard form are probably valid for the magnetic system of which the DW width is larger than the spin diffusion length. For both the harder magnetic materials, the variation of the coefficients, especially β_x, becomes very significant.

5.6 Summary

In summary of this chapter, the possible way to calculate the spin torque parameters a, b and coefficients μ_x, β_x used to describe AST and NAST in the standard form of the usual micromagnetic approach is studied. These spin torque parameters can be calculated directly from the spin accumulation. The model developed here is applied to the static domain wall pattern obtained from an atomistic model. It allows us to study the behaviour of the conduction electron spins travelling across the DW. Interestingly, it is found that the spin torque coefficients are spatially dependent and their divergence can be significantly observed at a very small angle between magnetisation leading to a tiny gradient of magnetisation. Therefore, it is strongly suggested to calculate the spin torque directly from the spin accumulation instead. The investigations presented in this chapter indicate an important limitation of the micromagnetic approach. It was shown that μ_x and β_x can be taken as approximately constant for DW widths comparable to the spin diffusion length. Given typical values of λ_{sdl} of tens of nm, the micromagnetic approach can only be justified for application to soft magnetic materials.

The proposed model will be more realistic in case that the diffuse interface is taken into account in the model. The nature of the interface is an important factor in spin injection and consequently in the phenomenon of spin torque but it still has received little attention. Therefore, the inclusion of diffuse interface will be considered in the following chapter.

CHAPTER VI

Modelling of spin injection across diffuse interfaces

Injection of spin polarised current is of great interest for potential new spintronic devices. In particular, the spin transport across interfaces has become increasingly important since the discovery of the giant magnetoresistance (GMR) and tunneling magnetoresistance (TMR). The GMR effect is associated with the spin-dependent scattering both at the interfaces and within the magnetic layers [40,99–101] since the magnitude of GMR is strongly dependent on the spin-dependent resistivity. The concept of spin injection across the interface between a ferromagnet and a non-magnet was first suggested by Aronov [41] and experimentally observed by Johnson and Silsbee [42]. Injecting an electric current into a ferromagnet results in a spin-polarised current, which subsequently flows across the interface into a non-magnet giving rise to a spin current in the nonmagnet and spin accumulation close to the interfacial region. The spin accumulation diffuses into the nonmagnet from the interface with a length scale associated with the spin relaxation time [47–49].

Clearly, the nature of the interface is an important factor in spin injection, and consequently in the phenomenon of spin torque [67, 87], which relies on spin injection. However, the effect of diffuse interfaces has received relatively little attention. Zhang, Levy and Fert (ZLF) [38] studied the spin accumulation arising from the injection of a polarised current produced by a pinned Ferro-Magnetic (FM) layer into a second FM layer, which results in a discontinuity of the spin accumulation across the interface. Shpiro, Levy and Zhang [53] used a similar formalism to develop a semi-analytical approach to diffuse interfaces in which the degree of continuity of the spin accumulation was determined by an effective interface resistance.

In this work, I generalise these approaches in two important ways. Firstly, I use a definition of the spin accumulation based on the spin-up and spin-down density of states rather than deviations from the equilibrium value as detailed in chapter 4. While this does not affect the spin torque it does provide a physically sound basis for the treatment of interfaces between FM layers of different materials. Secondly a simple model of the

behavior of diffused interfaces is proposed. The model is applied to the study of the transmission of spin current and the development of spin accumulation between two FM layers of different properties and also between FM/Non-Magnetic (NM) layers.

6.1 Model of the interfacial layer

6.1.1 Diffuse interface concentration profile

The structure of the interface between the different materials is modelled with the diffused concentration profile. The interface region is considered as a layer where the interdiffusion of species follows Fick's law. For computational simplicity, the diffusion in the magnetic system used in this work is one dimensional propagation, along the x direction. The solution of Fick's law suggested to describe the characteristic of the interface is obtained by solving the following properties.

Fick's first law: the diffusion flux (J) across the layer is proportional to the concentration gradient.

$$J = -D_{ion}\frac{\partial C}{\partial x} \tag{6.1}$$

Fick's second law: the concentration (C), which is time and position dependent, can be expressed as a function of second derivative of the concentration gradient through the ion diffusion constant (D).

$$\begin{aligned} \frac{\partial C}{\partial t} &= -\frac{\partial J}{\partial x} \\ \frac{\partial C}{\partial t} &= D_{ion}\frac{\partial^2 C}{\partial x^2} \end{aligned} \tag{6.2}$$

The system including the interface is divided into many thin layers each of thickness t_F, and using Fick's law, I model the diffusion of the local magnetic ion concentration for each layer i at any given position x of the system and over time t as

$$C_i(x,t;T) = \frac{t_F C_0}{\sqrt{\pi}x_0}\cdot exp\left[-(x/x_0)^2\right]. \tag{6.3}$$

Here C_0 is the initial atom concentration, $x_0 = 2\sqrt{D_{ion}t}$, with D_{ion} the ion diffusion constant which depends on the system temperature. These parameters characterise the width of the interface region (t_{IF}). The simple model assumes that the structure is fabricated at elevated temperatures and consequently the width of the interface depends on the deposition temperature (through D_{ion}) and the time t. Here I treat x_0 in

a parametric study in order to investigate the effect of the interface diffusion on the spin current and spin accumulation. The concentration profile can be obtained by using the superposition of the local concentrations,

$$C(x,t) = \sum_i C_i(x,t). \tag{6.4}$$

To give an example, the system of ferromagnet and nonmagnet (FM/NM) is first considered by dividing into many thin layers. Then the local concentration (C_i) equation (6.3) has been applied to each thin layer i with $x_0 = 0.2\ nm$ as illustrated in figure 6.1. Consequently, the total concentration (C) of the ferromagnetic ion at any position of the system can be achieved by using the superposition of the local concentration in equation (6.4).

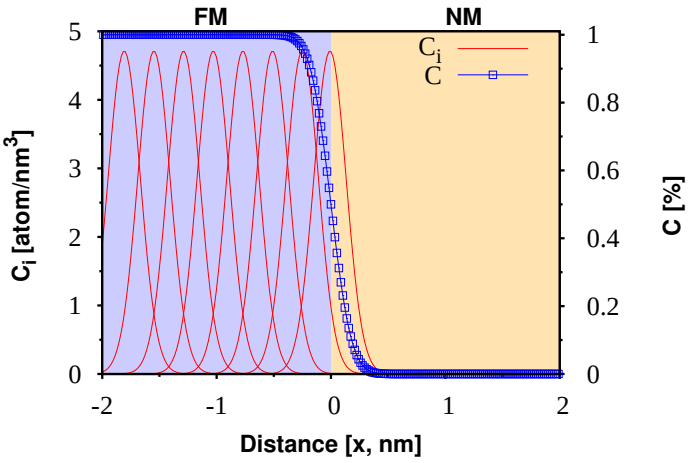

Figure 6.1: The local and total concentration of cobalt atom at any position of the Co/Cu system with $x_0 = 0.2\ nm$: Red lines show the contribution of the Co atom diffusion in each layer. Blue square shows the net concentration of Co arising from the contribution of all local concentrations.

Similarly, the concentration of the nonmagnetic ion (Cu) can be calculated in the same way as Co. Figure 6.2 (a) shows the concentration of the Co and Cu atoms at any position. In the interfacial region with the thickness of t_{IF}, the interface mixing of the Co and Cu atoms is enhanced. It is proportional to the width of the diffuse interface which is controlled by x_0.

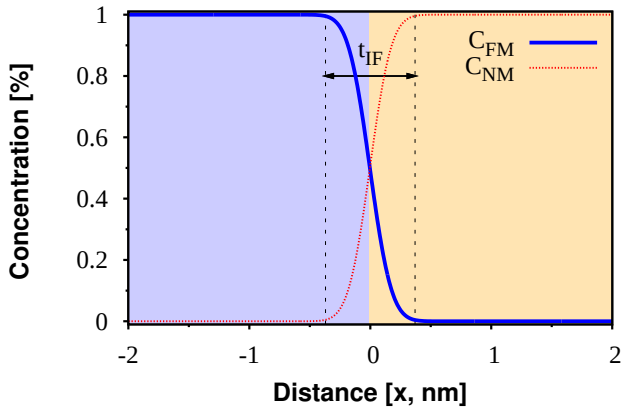

(a)

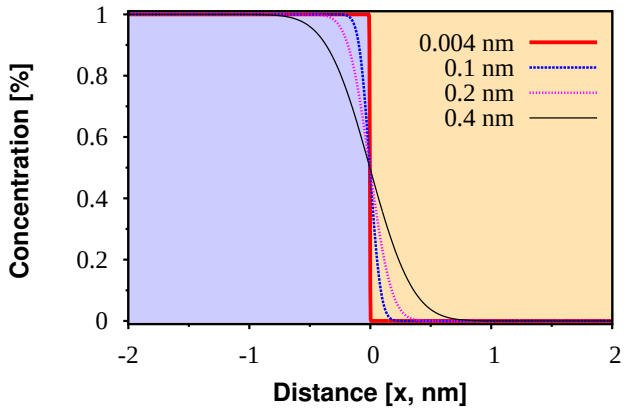

(b)

Figure 6.2: (a) The concentration of Co and Cu atoms at any position of the FM/NM system with the thickness of the interface of t_{IF} (b) The concentration of the Co ion at any position with different width of interface controlled by varying x_0

In experiment, the parameter x_0 involved the ion diffusion constant (D_{ion}) and the time t can be measured via the thickness of interface. Therefore, it is possible to model the interface region for a realistic system. Compared with the experimental results, the ion concentration profile is a good method to describe the interdiffusion of ions in the interface. The computational result as illustrated in figure 6.2 is consistent with several experimental works [102–105]. To investigate the influence of the interface thickness on the spin transport behaviour, the parameter x_0 is varied giving rise to different width of the interfaces as seen in figure 6.2 (b). In practice, the degree of intermixing, resulting from controlling the ion diffusion between layers, could be governed by changing the growth temperature [103, 106]. Evidently, increasing growth temperature broadens the interface region.

6.1.2 Transport parameters

Next, the calculated concentration profiles are used to model the spatial variation within the interface of the transport parameters: the spin polarisations β, β', the spin diffusion length λ_{sdl}, the exchange s-d integral J and $m_{\parallel}(\infty)$ as illustrated in figure 6.3. In this initial study I make the simplifying assumption that the local parameters can be taken as a linear combination of the bulk parameters weighted by the local concentrations. Thus, for 2 materials (a, b) of a given structure,

$$P(x) = P_a C(x)_a + P_b C(x)_b, \tag{6.5}$$

where $P(x)$ is any transport parameter at position x. $P_{a,b}$ is the transport parameter of (a, b) and $C(x)_{a,b}$ is the concentration of each atomic species obtained from equations (6.3) and (6.4).

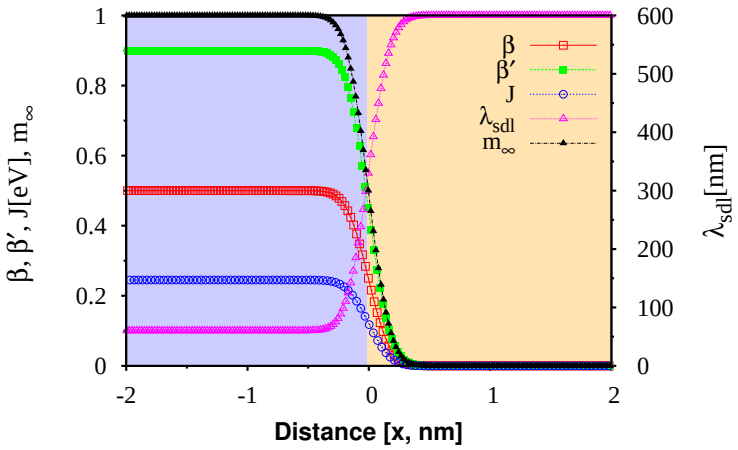

Figure 6.3: The transport parameters at any position of the system Co/Cu with $x_0 = 0.2\ nm$: The position $x = 0$ is the centre of the interface. The positions $x < 0$ and $x > 0$ show the layer of Co and Cu respectively.

6.2 Spin injection in FM/NM bilayers

To investigate the spin accumulation and spin current at any position, the modified formalism in equation (4.1) has been employed for simulating spin transport in each layer. The boundary condition is that the spin current is continuous across the interface. ZLF [38] assumed an atomically sharp interface, giving rise to a discontinuity in spin accumulation. Shpiro, Levy and Zhang [53] developed a semi-analytical approach

to diffuse interfaces in which the effect of the interface on the spin accumulation was incorporated through an effective interface resistance. Here, I calculate the spin accumulation and spin current across the diffusive interface directly, and for different interface thicknesses, which are controlled by varying parameter x_0.

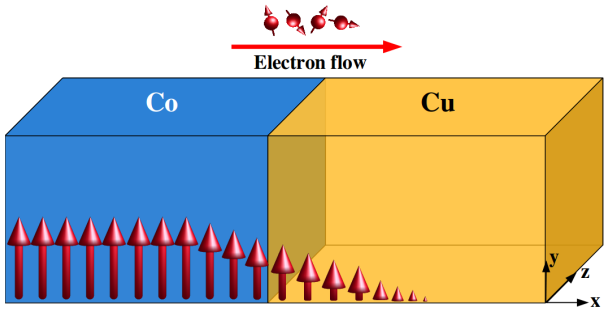

Figure 6.4: Schematic of the FM/NM bilayer (Co/Cu) with collinear magnetisation: The magnitude of the magnetisation is gradully decreased in the interface region due to the interdiffusion between Co and Cu ions.

We first consider the effects of diffuse interfaces in FM/NM bilayers as shown in figure 6.4. The calculation starts with the layer discretisation and then the concentration profile is calculated by employing equation (6.3). The transport parameters at any position are shown in figure 6.3 using the values of $m_{\parallel}(\infty) = 3.945 \times 10^7\ C/m^3$, $\beta = 0.5$, $\beta' = 0.9$ and $\lambda_{sdl} = 60\ nm$ for Co [53]. The spin polarisation of Cu is zero due to $N^{\uparrow}(E_F) = N^{\downarrow}(E_F)$ as shown in several works, for instance see Ref. [107]. This gives rise to zero equilibrium value $m_{\parallel}(\infty) = 0$ and the spin diffusion length is taken to be 600 nm.

Subsequently, the spin accumulation and the spin current are investigated by using the modified solution as described in chapter 4. The results for an FM/NM bilayer are shown in figure 6.5 (a) and (b). Typically, in the modified solution, the spin accumulation consists of longitudinal and transverse components. In this case no transverse components of $\mathbf{m}$ and $\mathbf{j_m}$ develop. It can be seen in figure 6.5 (a) that the spin accumulation follows the direction of the magnetisation and the degree of continuity, $\Delta m \equiv m(0^+) - m(0^-)$, is governed by the "*degree of interface mixing*". Specifically, for $x_0 = 0$, m is discontinuous across the interface($x = 0$). With increasingly diffuse interfaces characterised by large values of x_0 the degree of discontinuity in m at $x = 0$ decreases.

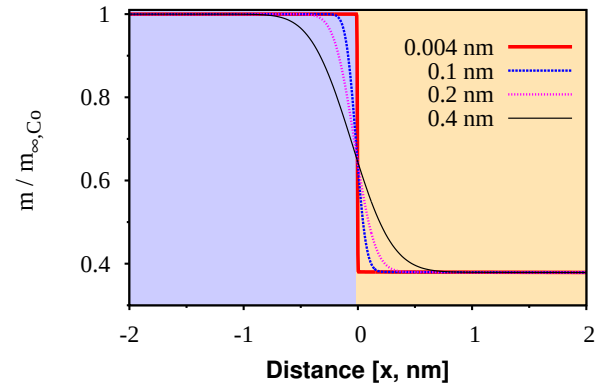

(a)

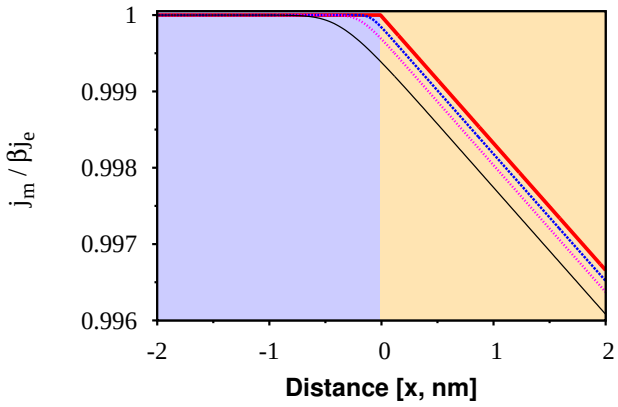

(b)

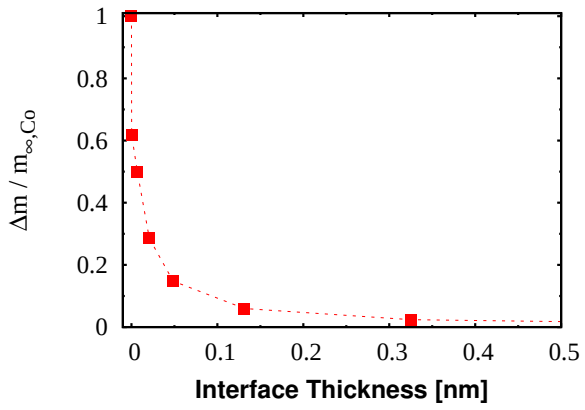

(c)

Figure 6.5: (a) The spin accumulation m and (b) spin current j_m at any position of the Co/Cu system with different x_0: The position $x = 0$ is the center of the interface. The positions $x < 0$ and $x > 0$ show the layer of Co and Cu respectively. m will eventually decay to 0 in the NM for $x > \lambda_{sdl}^{Cu}$. (c) The degree of the discontinuity of the spin accumulation as a function of the interface thickness

This is demonstrated in figure 6.5 (c), which shows the rapid decrease in the discontinuity of m with x_0. Importantly, even modest interface roughness of the order of 1 monolayer is sufficient to ensure continuity of $\mathbf{m}$. It is interesting to note the very slow decrease of $\mathbf{m}$ and $\mathbf{j_m}$ in the NM. This is consistent with a decay over the length scale of the spin diffusion length of the nonmagnet, i.e., $\lambda_{sdl}^{Cu} = 600\ nm$ in agreement with a previous study [107].

6.2.1 Semi-analytical calculation

It is possible to simplify the formalism for a FM/NM bilayer where the magnetisation at any point is collinear. This is an important special case since it relates to the injection of a spin current into a non-magnet. In the following I develop an expression allowing the direct semi-analytical calculation of the spin accumulation and spin current for this geometry. In this case there are no transverse components of $\mathbf{m}$, which remains parallel to the magnetisation and of magnitude

$$m = m(\infty) + [m(0) - m(\infty)]e^{-x/\lambda_{sdl}}. \tag{6.6}$$

Because of the spatial variation of the transport parameters, equation (6.6) is not convenient to express the overall spatial variation of m. Instead a local solution is sought based on

$$\frac{dm}{dx} = \frac{-[m_0 - m(\infty)]}{\lambda_{sdl}} e^{-x/\lambda_{sdl}}. \tag{6.7}$$

The spin current is given by

$$\mathbf{j}_m = \beta j_e \mathbf{M} - 2D_0 \left[\frac{d\mathbf{m}}{dx} - \beta\beta' \mathbf{M}(\mathbf{M} \cdot \frac{d\mathbf{m}}{dx}) \right],$$

and for the case of $\mathbf{m}$ collinear with $\mathbf{M}$ this becomes

$$j_m = \beta j_e - 2D_0(1 - \beta\beta')\frac{dm}{dx}. \tag{6.8}$$

Consider the boundary condition at the interface which requires the imposition of continuity of spin current, $j_{m,i+1}(0^-) = j_{m,i+1}(0^+)$, where

$$\begin{aligned} j_{m,i+1}(0^-) &= \beta_i j_e - 2D_0^i(1 - \beta_i\beta_i')\frac{dm_{i+1}(0^-)}{dx} \\ j_{m,i+1}(0^+) &= \beta_{i+1} j_e - 2D_0^{i+1}(1 - \beta_{i+1}\beta_{i+1}')\frac{dm_{i+1}(0^+)}{dx}, \end{aligned}$$

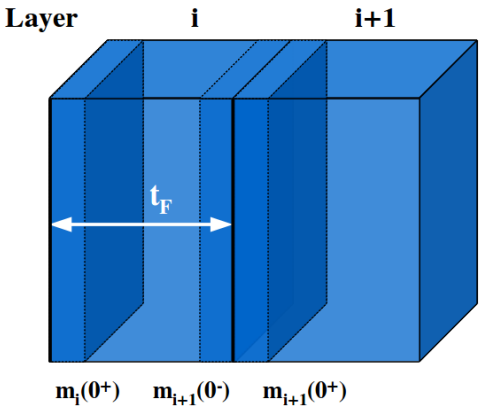

Figure 6.6: Schematic of the numerical approach to the calculation of m for a FM/NM bilayer. 0^- and 0^+ define values entering and leaving the interface.

and, the derivative of the spin accumulation at the interface

$$\begin{aligned}\frac{dm_{i+1}(0^-)}{dx} &= \frac{-[m_i(0^+)-m_i(\infty)]}{\lambda^i_{sdl}}e^{-t_F/\lambda^i_{sdl}} \\ \frac{dm_{i+1}(0^+)}{dx} &= \frac{-[m_{i+1}(0^+)-m_{i+1}(\infty)]}{\lambda^{i+1}_{sdl}}.\end{aligned}$$

Therefore, one obtains;

$$m_{i+1}(0^-) = m_i(\infty)+[m_i(0^+)-m_i(\infty)]e^{-t_F/\lambda^i_{sdl}} \tag{6.9}$$

$$\begin{aligned}m_{i+1}(0^+) &= -\lambda^{i+1}_{sdl}\left[\frac{(\beta_{i+1}-\beta_i)j_e+2D^i_0(1-\beta_i\beta'_i)\frac{dm_{i+1}(0^-)}{dx}}{2D^{i+1}_0(1-\beta_{i+1}\beta'_{i+1})}\right] \\ &= \frac{(\beta_{i+1}-\beta_i)j_e\lambda^{i+1}_{sdl}}{2D^{i+1}_0(1-\beta_{i+1}\beta'_{i+1})}+\frac{D^i_0(1-\beta_i\beta'_i)\lambda^{i+1}_{sdl}}{D^{i+1}_0(1-\beta_{i+1}\beta'_{i+1})\lambda^i_{sdl}}[m_{i+1}(0^-)-m_i(\infty)]\end{aligned} \tag{6.10}$$

Equations (6.9) and (6.10) allow to propagate the solution across a given layer and into the next. Continuous application of the equations describes the variation of m and subsequently j_m for the entire structure. These equations allow a simple treatment of the important case of spin injection from a ferromagnet into a nonmagnet. It is verified that calculations using equations (6.9) and (6.10) reproduce the full numerical results in figure 6.5, including the result that the spin accumulation after traversing the interface is (in the approximations used here) independent of the interface width. This suggests that the spin injection into a non-magnet is relatively unaffected by the variation in transport properties due to interface diffusion, but may be increased by other factors such as scattering at the interface, which could easily be introduced into the current

approach. In addition, the continuity of the spin accumulation strongly depends on the transport parameters of the materials in between the interface.

6.3 Spin injection in FM/FM bilayers

6.3.1 Collinear configuration

I now use the modified formalism to study the case of two collinear ferromagnets, each having a different, and non-zero, value of $m_{\|}(\infty)$. Specifically I investigate the spin accumulation and spin current across a Co/NiFe interface with the magnetisation of both layers collinear in the y direction. The concentration of Co and NiFe ions are determined first using the solution of Fick's law. The transport parameters at any position are calculated as previously, and are shown in figure 6.7. The value of transport parameters of Co and NiFe are taken from Ref. [53]. For NiFe the transport parameters are used as the following values $\beta = 0.7$, $\beta' = 0.95$ and $\lambda_{sdl} = 5\ nm$.

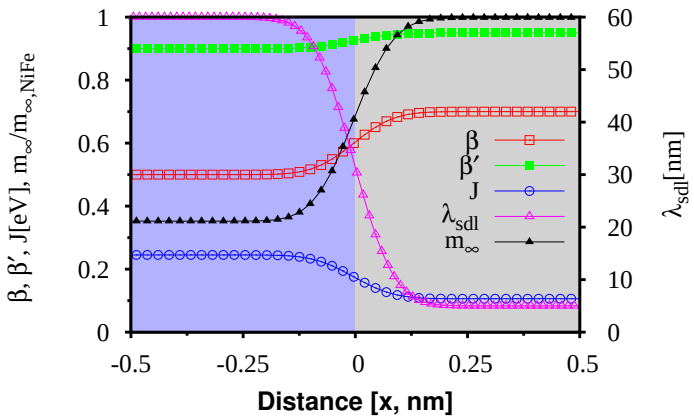

Figure 6.7: The transport parameters at any position of the system of two ferromagnets (Co/NiFe) corresponding to the concentration profile with $x_0 = 0.1\ nm$

Importantly, the nonzero equilibrium values of spin accumulation of Co and NiFe are calculated by employing equation (4.8) from *ab-initio* information provided by Dr. R Cuadrado. The *fcc* and *bcc* lattice parameters of the Co and NiFe bulk, respectively, are used in this work as the following values: a_{Co}=3.46 Å and a_{NiFe}=2.72 Å. In figure 6.8 the DOS of both materials are shown, and as relevant main characteristic for this study, one can observe that the values of the minority-spin states at the Fermi level are higher than the majority-spin ones in both cases which are in good agreement with the work

of Park *et al.* [62]. The calculated values are: $N_{\uparrow}(E_F) - N_{\downarrow}(E_F) = 1.02$ states/eV·atom and $N_{\uparrow}(E_F) - N_{\downarrow}(E_F) = 1.41$ states/eV·atom or $m_{\parallel}(\infty) = 3.945 \times 10^7\ C/m^3$ and $m_{\parallel}(\infty) = 1.118 \times 10^8\ C/m^3$ for Co and NiFe respectively. As a result in figure 6.7, the equilibrium value, m_{∞}, at any position of the system is likely to vary from the value of Co to the value of NiFe.

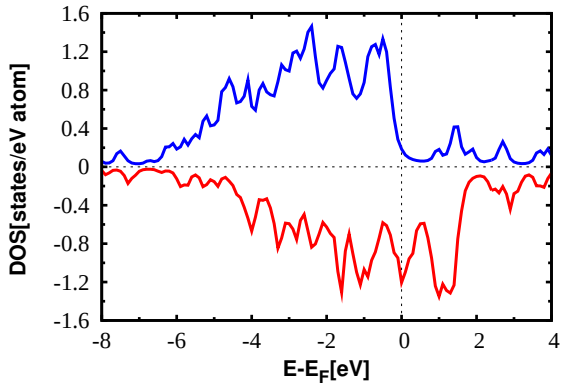

(a)

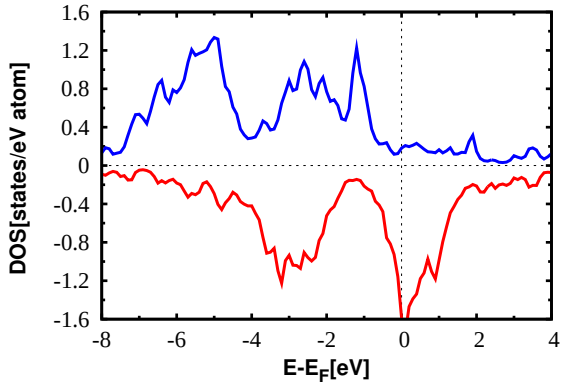

(b)

Figure 6.8: (a) Spin density of states of Co and (b) NiFe bulk provided by Dr. R Caudrado [61, 62]

Let us consider $x_0 = 0.1\ nm$. As shown in figure 6.9, the spin accumulation increases in NiFe, reflecting its higher spin polarisation. Also, the spin current increases in the NiFe layer because of the high spin polarisation β of the conductivity in NiFe. In addition, both spin accumulation and spin current reach the equilibrium values in the second ferromagnet (NiFe) over the spin diffusion length. This increase in **m** in NiFe is accessible only on the introduction of the modified damping term in equation (4.1) allowing the evolution to a non-zero value of $m_{\parallel}(\infty)$, consistent with treating the

spin accumulation as the difference of the spin up and spin down density of states. The formalism allows the complete description of any multilayer system including the polarising effect of a pinned layer on an incoming non-polarised current.

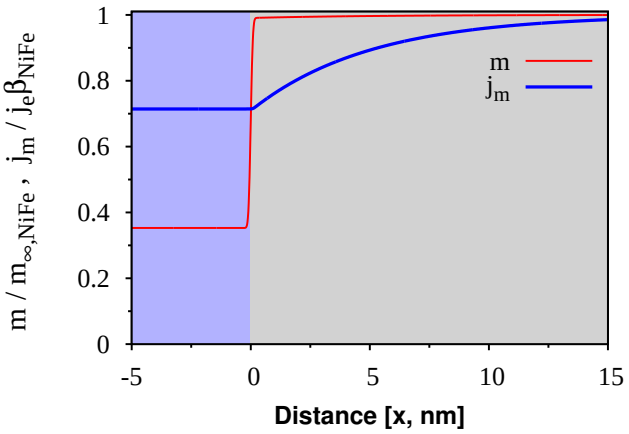

Figure 6.9: The spin accumulation and spin current at any position of the Co/NiFe bilayer system

6.3.2 Non-collinear configuration

Finally let us illustrate the components of spin accumulation induced by a non-collinear structure in a Co/NiFe bilayer as shown in figure 6.10 by injecting a spin current, $j_e = 5 \times 10^{11}\ A/m^2$, along the x direction. The magnetisation in Co and NiFe layers are oriented at 60° and the magnetisation direction rotates linearly in the interface region. The magnetisation of Co is in the y direction, whereas that of NiFe is in yz plane. The magnetisation profile can be seen in figure 6.11 (top) and the width of interface is approximately 0.325 nm.

The spin accumulation at any position of the non-collinear system is possible to be calculated using the proposed model including the diffuse interface as previously. It can be seen in figure 6.11 (bottom) that the spin accumulation follows the direction of magnetisation as the y and z components develop. Interestingly, the y component of spin accumulation is oscillatory in the interfacial region arising from the appearance of the x or out-of-plane component of the spin accumulation. The oscillation decreases with decreasing the angle between magnetisations in Co and NiFe.

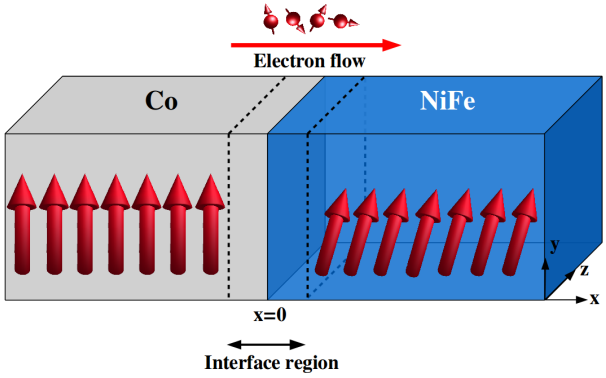

Figure 6.10: The non-collinear magnetisation configuration in a Co/NiFe system: Magnetisation in NiFe layer is oriented at 60° of that in Co layer.

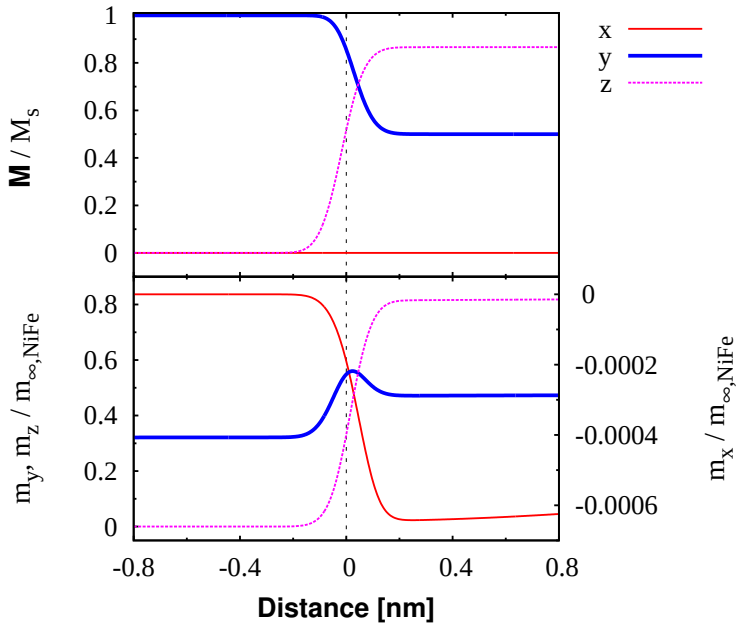

Figure 6.11: (top) The non-collinear magnetisation configuration in a Co/NiFe system with 60°: The direction of magnetisation in the interface region gradually rotates to 60° compared with that in Co layer. (bottom) The spin accumulation at any position of the system

The out-of-plane component of spin accumulation tends to develop from the interface and decays to zero over the length scale at 10 *nm* which is the transverse relaxation length. It is very small compared with the in-plane component but significant. Note that the spin-transfer torque created on the local magnetisation arises from the transverse

component. Therefore the x component of the spin accumulation gives rise to the spin torque in the interfacial layer. Subsequently, the spin torque at any position of the system is calculated directly from the transverse spin accumulation ($\mathbf{m}_\perp$), $ST = J(\mathbf{M} \times \mathbf{m}_\perp)$. The component of the spin torque is illustrated in figure 6.12 (bottom). The maximum value of the spin torque exists in the interface corresponding to the angle between magnetisation and spin accumulation (θ_{Mm}) as shown in figure 6.12 (top). It becomes zero at about 10 nm corresponding to the transverse relaxation length. The contribution of the y and z components is regarded as the "*adiabatic spin torque*" and the out-of-plane component, x, is referred to the " *non-adiabatic spin torque*".

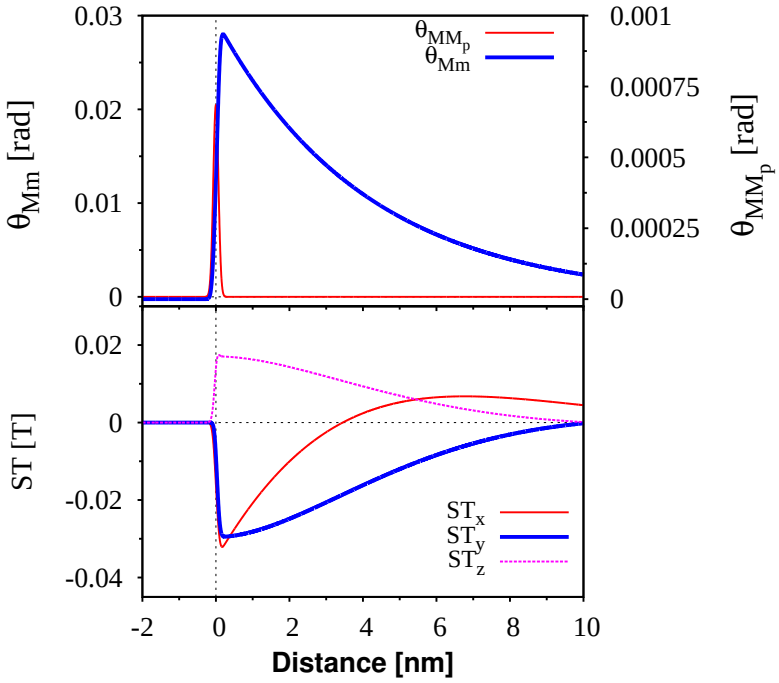

Figure 6.12: (top) The angle of magnetisation between layers(θ_{MM_p}) and that between magnetisation and spin accumulation(θ_{Mm}) (bottom) The component of total spin-transfer torque at any position of the non-collinear structure

Importantly, out of the interface region $x > 0.1625\ nm$, the magnetisations between discretisation layers are oriented in the same direction. In principle, the spin torque should be zero in this region since it is calculated from the following equation,

$$ST = J(\mathbf{M} \times \mathbf{m}_\perp) = a(\mathbf{M} \times (\mathbf{M}_p \times \mathbf{M})) + b(\mathbf{M} \times \mathbf{M}_p).$$

As the above equation, the spin torque can be obtained in 2 alternative ways: it is

calculated directly from the spin accumulation which I suggested and from the coefficients a and b as in the previous study [12,13,38,63]. The coefficients a and b are not significant for the collinear magnetisation as $\mathbf{M} \times \mathbf{M}_p = 0$, leading to zero spin-transfer torque. This formalism is used to estimate the spin torque in the magnetic system under the assumption that the spin accumulation completely follows the magnetisation direction for the collinear magnetisation. In other words, the collinear magnetisation, $\mathbf{M}//\mathbf{M}_p$, results in the collinear between $\mathbf{M}$ and $\mathbf{m}$, $\mathbf{M} \times \mathbf{m}_\perp = 0$. In this study (chapter 5), it is found that the spin torque calculated from the coefficients a and b is not appropriate to describe the behaviour of the spin transport especially in the system with gradual variation of magnetisation in the interface.

6.4 Summary

In conclusion, the equation of spin accumulation is generalised to describe its behavior at any position within a magnetic multilayer and the effect of interface diffusion is modelled using Fick's law. The model was applied to study ferromagnet/non-magnet (FM/NM) bilayers as well as between two ferromagnets (FM/FM). In the case of FM/NM bilayers a simple semi-analytic approach of the spin accumulation was formulated. This approach links the behavior of spin accumulation at the interface, in a physically transparent way, to a degree of interface mixing determined by known physical parameters, principally the ion diffusion constant D_{ion}. It is found that relatively modest amounts of interface diffusion give rise to continuity of $\mathbf{m}$. Importantly, this formalism allows to directly simulate the sharp variation of $\mathbf{m}$ due to the interface.

Now, the spin transport behaviour within the domain wall explained in chapter 5 and the inclusion of the diffuse interface discussed in this chapter are well understood. Next, it is essential to study the spin transport behaviour with time evolution as it is extensively applied to the spintronic devices based on current-induced domain wall motion. The detail will be discussed in the following chapter.

CHAPTER VII

Magnetisation dynamics including the effect of spin torque

The manipulation of magnetisation using a spin-polarised current, the so-called "*current-induced domain wall motion*" has been intensively studied [9–17] due to possible applications in DW-based magnetic devices such as race-track memory [108, 109] and logical operation in devices such as magnetic random access memory (MRAM) [110,111]. The key advantage of this technique is that the current-induced magnetisation reversal can be confined to a small spatial area leading to many potential applications and the possibility to reduce the size of devices, unlike the conventional technique of *field-induced* domain wall motion. Therefore, this chapter will deal with the topic of how to control the magnetic domain wall by means of spin injection. It will become necessary to understand the dynamics of magnetisation in the presence of spin-transfer torque extending from chapter 5 which explains the mechanism of spin transport in the static domain wall pattern.

The first part of this chapter will outline the implementation employed here to observe the dynamics of magnetisation within a domain wall. The appearance of spin-transfer torque is taken into account in the atomistic model via the *s-d* exchange interaction between the spin accumulation and the local magnetisation as an additional field. The usual Landau-Lifshitz-Gilbert (LLG) equation of motion at the atomistic level is then modified by including the effect of the spin transfer torque. The second part will provide the details of numerical technique used in this work to investigate the response of the magnetisation within domain wall in the application of spin injection with time evolution.

The final part of this thesis will mainly deal with investigating the magnetisation dynamics of a bilayer magnetic system consisting of two ferromagnets separated by a nonmagnetic spacer layer in the presence of spin-transfer torque. In this work, I investigate not only the effect of the spin polarized current on the dynamics of the magnetisation in a single domain wall of the free layer, but also the complicated dynamic behaviour of the response of the domain wall displacement due to the spin transfer

torques. Furthermore, current-induced domain wall motion is studied by injecting a current with different magnitudes perpendicular to the plane of the bilayer system. This allows the investigation of effects such as the critical current density (the minimum spin current required to move the domain wall), the domain wall displacement, domain wall velocity, domain wall width as well as the degree of nonadaibaticity. All details will be discussed as the following.

7.1 Basic idea of current-induced domain wall motion

The current-induced domain wall motion can be simply explained in the head-to-head domain wall pattern as shown in figure 7.1. It is noteworthy that the magnetic domain is the region within which all elementary magnetic moments align in the same direction. Therefore, the DW is the transition region between two magnetic domains. As can be seen in the figure below, the arrow in the DW shows the direction of the local magnetisation and its direction gradually changes throughout the DW.

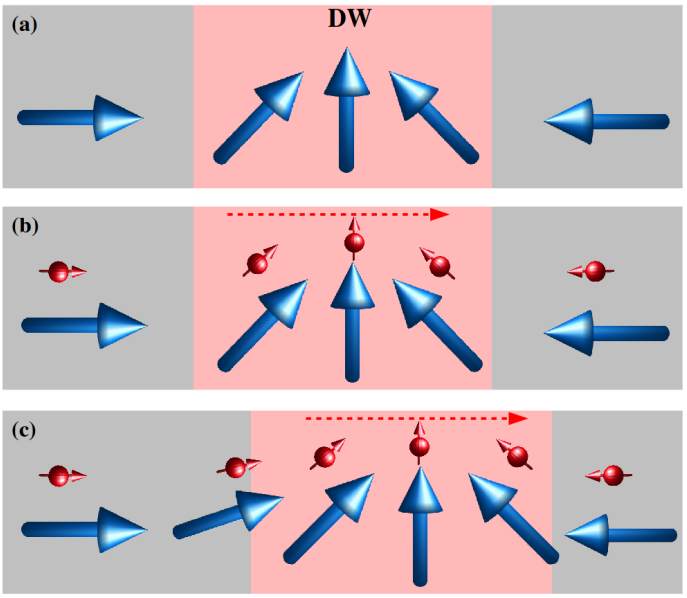

Figure 7.1: Schematic illustration of current-induced DW motion: (a) A head-to-head DW pattern (b) The spin of conduction electron follows the direction of the local magnetisation due to *s-d* exchange interaction. (c) As a result of the reaction torque acting on the local magnetisation, the local magnetisation is reoriented and consequently the DW is displaced by injecting spin current. [112].

The mechanism of the spin-transfer torque in slowly varying magnetisation structure, i.e., domain wall, starts with injecting the spin current carried by the conduction electron into the magnetic domain wall. It then flows through the DW resulting in the s-d exchange interaction between spin current and local magnetisation. As a consequence, spin-transfer torque acts on the spin current to adiabatically align itself in the direction of local magnetisation. Simultaneously, a reaction torque proportional to the spin current density is created on the local magnetisation within DW causing the magnetisation reorientation as illustrated in figure 7.1. In the case of a sufficiently large spin current density, domain wall can be translated easily in the direction of the electron flow [112].

7.2 Atomistic model

I will begin with discussion of the atomistic model underlying the spin-transfer torque effect. To model the magnetic system including the effect of spin-transfer torque, it is important to first consider the classical spin Hamiltonian used to describe the energetics of magnetic system and then the modified usual LLG equation, modelling approach to describe the dynamic motion of magnetisation at an atomistic level, will be derived. Finally, the numerical technique used to investigate the dynamic behaviour will be detailed.

7.2.1 Classical spin Hamiltonian ($\mathcal{H}$)

The spin system is modelled using a classical spin Hamiltonian, with the parameters of cobalt. The classical spin Hamiltonian using the Heisenberg ($\mathcal{H}$) form of exchange can be written as follows [113]

$$\mathcal{H} = \mathcal{H}_{\text{exc}} + \mathcal{H}_{\text{ani}} + \mathcal{H}_{\text{app}}, \tag{7.1}$$

denoting terms for the exchange interaction, magnetic anisotropy and externally applied magnetic field respectively. The contribution of each term to the total free energy are given as the following.

7.2.1.1 The exchange interaction and energy

The interaction between magnetic moments in a magnetic system can be classified into three main types: direct exchange, indirect exchange and superexchange. In this work,

the short-range exchange interaction will be included in the Heisenberg form. The exchange energy for the system of interacting atomic moments can be represented by the Heisenberg Hamiltonian form summing over the nearest neighbours only as follows

$$\mathcal{H}_{\text{exc}} = -\sum_{i \neq j} J_{ij} \mathbf{S}_i \cdot \mathbf{S}_j \tag{7.2}$$

where J_{ij} is the nearest neighbour exchange integral between the spin site i and j, $\mathbf{S}_i$ is the local normalised spin moment and $\mathbf{S}_j$ is the normalised spin moment of neighbouring atom at site j. The normalised spin is taken from the actual spin moment, $\mathbf{S}_i = \mu_{\mathbf{s}} / \mid \mu_{\mathbf{s}} \mid$.

Importantly, the sign of the exchange integral significantly corresponds to the orientation of neighbouring spins with minimum exchange energy. According to the Bethe-Slater curve [82, 83], $J_{ij} > 0$ for ferromagnetic materials where neighboring spins align in parallel, for instance, Fe, Co and Ni. For anti-ferromagnets the spins prefer to align anti-parallel, $J_{ij} < 0$. The exchange energy results in the magnetic ordering meanwhile the preferred direction of spin moments is dominated by the magnetic anisotropy which will be presented as the following.

7.2.1.2 The magnetocrystalline anisotropy energy

The intrinsic property of the material playing an important role in the shape of the hysteresis loop is magnetic anisotropy. In principle, there are several kinds of anisotropy, but only intrinsic anisotropy known as magnetocrystalline anisotropy will be considered here. Its effect arises from the interaction between the spin and orbital motion of each electron, which generally favours lying in a specific lattice direction in the absence of external field, a so-called easy direction [83].

The most common form of anisotropy in the materials of interest is uniaxial anisotropy, where the spin moments tend to align along a single axis, namely the easy axis ($\mathbf{e}$). It is found that the anisotropy energy depends only on the relative orientation of the magnetisation with respect to easy axis. For uniaxial anisotropy the energy can be written as a function of the angle θ between magnetisation and easy axis in the following form.

$$\mathcal{H}_{\text{ani}} = K_0 + K_1 \sin^2\theta + K_2 \sin^4\theta + \ldots \tag{7.3}$$

where K_0, K_1, K_2, ... are the anisotropy constants which measure the strength of anisotropy with the dimensions of energy per unit volume (J/m^3).

From the expansion in equation (7.3), the first term is usually ignored due to its angular independence and the small higher order terms in this series can be neglected. Therefore the anisotropy energy can be simplified to

$$\mathcal{H}_{\text{ani}} = K_1 \sin^2\theta \tag{7.4}$$

but $\cos\theta = \mathbf{S} \cdot \mathbf{e}$, where $\mathbf{S}$ is normalised spin and $\mathbf{e}$ is the unit vector of easy axis. Also K_1 in the above equation represents the uniaxial anisotropy, therefore one can substitute K_1 with K_u as follows

$$\begin{aligned} \mathcal{H}_{\text{ani}} &= K_u \sin^2\theta = K_u(1-\cos^2\theta) \\ &= K_u(1-\cos^2\theta) = K_u(1-(\mathbf{S}\cdot\mathbf{e})^{\mathbf{2}}) \\ &= K_u - K_u(\mathbf{S}\cdot\mathbf{e})^{\mathbf{2}}. \end{aligned}$$

The first term of above equation can be negligible as it is angular independent. Subsequently, the uniaxial anisotropy of the magnetic system at the atomistic level can be consider by summing the anisotropy of all spins given by

$$\mathcal{H}_{\text{ani}} = -K_u \sum_i (\mathbf{S}_i \cdot \mathbf{e})^2 \tag{7.5}$$

where K_u is the anisotropy energy per atom.

7.2.1.3 The applied field energy

In the case of the magnetic system subject to the external applied field denoted as $\mathbf{H}_{\text{app}}$, the interaction between the magnetic system and the external applied field arises. This interaction energy is referred to as Zeeman energy given by

$$\mathcal{H}_{\text{app}} = -\mu_s \sum_i \mathbf{S}_i \cdot \mathbf{H}_{\text{app}} \tag{7.6}$$

In equation (7.1), the spin Hamiltonian represents the energies in the magnetic system including the exchange energy in the first term, the anisotropy energy and the external applied field respectively. It can be rewritten by substituting equations (7.2)-(7.6) into equation (7.1), then the final form of spin Hamiltonian is given by

$$\mathcal{H} = -\sum_{i \neq j} J_{ij} \mathbf{S}_i \cdot \mathbf{S}_j - K_u \sum_i (\mathbf{S}_i \cdot \mathbf{e})^2 - \mu_s \sum_i \mathbf{S}_i \cdot \mathbf{H}_{\text{app}}. \tag{7.7}$$

Besides the energetics of the magnetic system provided in the spin Hamiltonian, the demagnetising field and the thermal fluctuation field should be taken into account in the model. The inclusion of the demagnetising field is determined separately in order to reduce the computational time for the large-scale atomistic calculation by using a technique developed by Boerner *et al.* [114] based on a macrocell approximation. As the thermal fluctuation is temperature dependent, the Langevin Dynamics [83, 115] will be used to include the effect of temperature to the model. The demagnetising field and thermal field will be detailed in the following sections although this work will concentrate on the current-induced domain wall motion with athermal case. The nonzero temperature case will be studied comprehensively for future work.

7.2.1.4 The demagnetising energy

The demagnetising energy is connected with the magnetic created by the magnetic body itself. The dipole consisting of the north and south poles is established on the magnetised body generating magnetic fields both inside and outside itself. In general, the demagnetising or dipolar field arises in the opposite direction to magnetisation and its value depends on the geometry of the magnetic body. The demagnetising energy can be calculated by an integral over the volume (V) of the magnetic body as the following equation [83, 116]

$$\mathcal{H}_{\mathrm{dip}} = -\frac{1}{2}\int \mathbf{M}\cdot\mathbf{H}_{\mathrm{d}}\mathbf{dV} \tag{7.8}$$

where the demagnetising or dipolar field is defined as $\mathbf{H}_d = -N_d\mathbf{M}$, N_d is demagnetising factor which is dependent on the shape of material, μ_0 is permeability of free space and $\mathbf{M}$ is the unit vector of the magnetisation.

In general, the demagnetising energy at position r of the magnetic system arises from the contribution from all the *other* magnetic moments and from itself. However, in the small and symmetric magnetic systems consisting of a single domain, the self-demagnetising field is often neglected. Therefore, in this work the demagnetising field contributed from all the other magnetic moments is calculated. The calculation of demagnetising field is time consuming due to the long-ranged interaction. In the following, the calculation of the demagnetising energy is considered based on the technique developed by Boerner *et al.* [114] to accelerate the calculation.

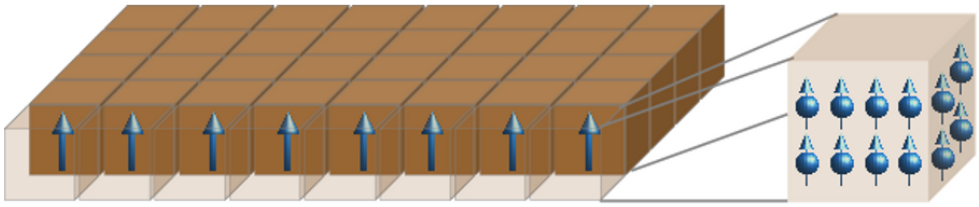

Figure 7.2: Schematic representation of the supercell approach used to calculate the demagnetisation field: The system is discretised into many supercells. Each supercell consisting of several spins is represented by the averaged moment.

This approach proceeds by first dividing the thin sample into many small cells known as a "supercell". The magnetic moment in each supercell is then calculated by averaging over the spins within the cell. Finally, the averaged moments are used to calculate the local dipolar field within each cell which is taken as representative of all spins within that cell as shown in figure 7.2. The demagnetising energy expressed in terms of the contribution from all the magnetic moments is given by

$$\mathcal{H}_{\mathrm{dip},i} = -\sum_{j\neq i}\left[\frac{3(\vec{\mu}_i\cdot\vec{r}_{ij})(\vec{\mu}_j\cdot\vec{r}_{ij})}{|\vec{r}_{ij}|^5} - \frac{\vec{\mu}_i\cdot\vec{\mu}_j}{|\vec{r}_{ij}|^3}\right]$$

where $\vec{\mu}_i$ is the magnetic moment of a supercell site i, $\vec{\mu}_j$ is the magnetic moment of a supercell site j and $\vec{r}_{ij}$ and and $\mid \vec{r}_{ij} \mid$ are the vector and the distance between the supercells i and j respectively. But a unit vector between supercells is $\mathbf{r}_{ij} = \frac{\vec{r}_{ij}}{|\vec{r}_{ij}|}$, and then substitute into the above equation as follows

$$\mathcal{H}_{\mathrm{dip},i} = -\sum_{j\neq i}\left[\frac{3(\vec{\mu}_i\cdot\mathbf{r}_{ij})(\vec{\mu}_j\cdot\mathbf{r}_{ij}) - \vec{\mu}_i\cdot\vec{\mu}_j}{|\vec{r}_{ij}|^3}\right].$$

The demagnetising or dipolar field can be calculated as the first derivative of the dipolar interaction energy ($\mathcal{H}_{\mathrm{dip},i}$) with respect to the magnetic moment i therefore

$$\mathbf{H}_{\mathrm{dip},i} = -\frac{\partial\mathcal{H}_{\mathrm{dip},i}}{\partial\vec{\mu}_i} = \sum_{j\neq i}\left[\frac{3(\vec{\mu}_j\cdot\mathbf{r}_{ij})\mathbf{r}_{ij} - \vec{\mu}_j}{|\vec{r}_{ij}|^3}\right]$$

but the magnetic moment in the supercell site j is $\vec{\mu}_j = \mu_s\boldsymbol{\mu}_j$, then the dipolar field of the supercell site i can be written as the following

$$\mathbf{H}_{\mathrm{dip},i} = \mu_s \sum_{i \neq j} \left[\frac{3(\boldsymbol{\mu}_j \cdot \mathbf{r}_{ij})\mathbf{r}_{ij} - \boldsymbol{\mu}_j}{|\vec{r}_{ij}|^3} \right]$$

where μ_s is the magnitude of the spin moment and $\boldsymbol{\mu}_j$ is a unit vector of the magnetic moment of the supercell site j.

The above expression is the dipolar field in CGS units, therefore the dipolar interaction field strength can be written in the SI unit of tesla as

$$\mathbf{H}_{\mathrm{dip},i} = \frac{\mu_0 \mu_s}{4\pi a^3} \sum_{i \neq j} \left[\frac{3(\boldsymbol{\mu}_j \cdot \mathbf{r}_{ij})\mathbf{r}_{ij} - \boldsymbol{\mu}_j}{|\vec{r}_{ij}|^3} \right] \tag{7.9}$$

where $\boldsymbol{\mu}_j = \sum_{i=1}^{n_{atom}} \mathbf{S}_i$ is a unit vector of the magnetic moment in the supercell site j which is found from the summation of spin moments in the supercell j, μ_0 is the permeability of free space, a is the atomic lattice spacing, $|\vec{r}_{ij}|$ is the distance between the supercell sites calculated from their integer coordinates and n_{atom} is the number of atoms in each supercell.

7.2.1.5 Thermal field

The thermal fluctuation of the spin moments arising from the effect of temperature can be taken into account in the atomistic model using Langevin Dynamics in the formalism of Brown [115], under the assumption that the inclusion of temperature can be represented by a random field term [117–121]. The introduction of the thermal fluctuation into the atomistic model enables to study the ferromagnetic-paramagnetic transition. The statistical properties of the fluctuation field ($\mathbf{H}^i_{\mathrm{th}}(t)$) represented by a Gaussian distribution are given by the following equation

$$\begin{aligned} \left\langle \mathbf{H}^i_{\mathrm{th}}(t) \right\rangle &= 0 \\ \left\langle \mathbf{H}^i_{\mathrm{th}}(t) \mathbf{H}^j_{\mathrm{th}}(t') \right\rangle &= \frac{2\alpha k_B T}{\mu_s \gamma} \delta_{ij} \delta(t - t'), \end{aligned} \tag{7.10}$$

where i, j are the Cartesian components, $\mathbf{H}_{\mathrm{th}}$ is a random field with the Gaussian fluctuations, $2\alpha k_B T/(\mu_s \gamma)$ is the factor measuring the strength of thermal fluctuation, k_B is the Boltzmann constant, T is the system temperature in Kelvin, α is the damping parameter describing the coupling of the spin system to the heat bath phenomenologically and γ is the absolute value of the gyromagnetic ratio. In this thesis I use $\gamma = 1.76 \times 10^{11} s^{-1} T^{-1}$ and the units of μ_s are in JT^{-1}.

To observe the spin dynamics including the effect of temperature in the atomistic model, the thermal fluctuation is represented by a Gaussian distribution $\mathbf{\Gamma}(t)$ in three dimensions with a mean of zero. The thermal field on each spin site i at each time step (Δt) can be calculated as follows

$$\mathbf{H}^i_{\text{th}}(t) = \mathbf{\Gamma}(t)\sqrt{\frac{2\alpha k_B T}{\gamma \mu_s \Delta t}}. \tag{7.11}$$

Consequently the effective local field which includes Zeeman, exchange, anisotropy, demagnetisation contributions and a random thermal field acting on the spin site i in the atomistic model is given by

$$\mathbf{H}^i_{\text{eff}} = -\frac{1}{\mu_s}\frac{\partial \mathcal{H}}{\partial \mathbf{S}_i} + \mathbf{H}_{\text{dip},i} + \mathbf{H}^i_{\text{th}} \ , \tag{7.12}$$

where $\mathcal{H}$ denotes the spin Hamiltonian as seen in equation (7.7),

$$\mathcal{H} = -\sum_{i \neq j} J_{ij}\mathbf{S}_i \cdot \mathbf{S}_j - K_u \sum_i (\mathbf{S}_i \cdot \mathbf{e})^2 - \mu_s \sum_i \mathbf{S}_i \cdot \mathbf{H}_{\text{app}}.$$

In the following section, the atomistic simulation will be outlined. The energetics of the magnetic system will be described by using the spin Hamiltonian as mentioned previously. The effect of spin-transfer torque will be represented as an additional field. Therefore, all possible fields acting on the spin will be linked with the standard Landau-Lifshitz-Gilbert (LLG) equation to investigate the dynamics of spin moments in the introduction of spin-transfer torque. It is noted that the rest of this work will only investigate the effect of spin-transfer torque on DW motion at zero temperature as the following details.

7.2.2 Introduction of the spin-transfer torque

To investigate the effect of the spin-transfer torque in the atomistic model, the *s-d* model is used to present the a qualitative description of the spin-transfer torque acting on the spin moment via the spin accumulation. The exchange energy due to the *s-d* exchange interaction of the spin accumulation and the local spin moment can be described as, $\mathcal{H}_{\text{sd}} = -J\mathbf{m} \cdot \mathbf{S}$, where J is the *s-d* exchange integral. The effect of the spin torque on the dynamic motion of spin moment can be accounted into the standard Gilbert form as an additional field, $J\mathbf{m}$, given by [38, 52, 53]

$$\frac{\partial \mathbf{S}}{\partial t} = -\gamma \mathbf{S} \times (\mathbf{H}_{\text{eff}} + J\mathbf{m}) + \alpha \mathbf{S} \times \frac{\partial \mathbf{S}}{\partial t}. \tag{7.13}$$

For convenient numerical integration, equation (7.13) can be converted into Landau-Lifshitz-Gilbert (LLG) form, giving the final form

$$\frac{\partial \mathbf{S}}{\partial t} = -\frac{\gamma}{(1+\alpha^2)}\mathbf{S}\times(\mathbf{H}_{\text{eff}}+J\mathbf{m}) - \frac{\gamma\alpha}{(1+\alpha^2)}\left[\mathbf{S}\times(\mathbf{S}\times(\mathbf{H}_{\text{eff}}+J\mathbf{m}))\right] , \tag{7.14}$$

where γ is the absolute gyromagnetic ratio, α is the damping constant, $\mathbf{S}$ is the local normalised spin and $\mathbf{H}_{\text{eff}}$ is the effective field contributed from the exchange field, the anisotropy field, the external applied field, thermal field as well as the demagnetising field as mentioned previously.

According to equation (7.14), the first and second terms represent the precessional and damping motions of the spin moment respectively. The local effective field $\mathbf{H}_{\text{eff}}$ leads to damped precessional motion into the direction of the local effective field. Interestingly, the additional field due to the presence of the injected spin current, $J\mathbf{m}$, gives rise to the contribution of adiabatic and non-adiabatic torques. This term describes the spin torque effect on the spin motion and indicates that the additional field due to the spin-transfer torque can be another source of precessional and damping terms [12, 40].

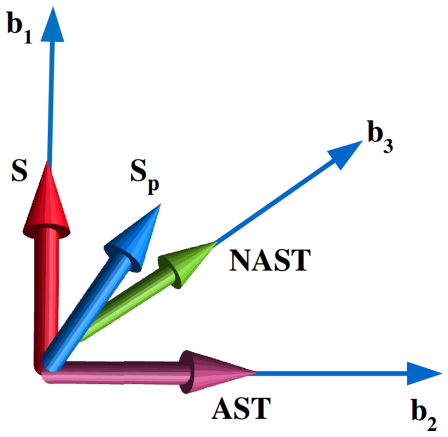

Figure 7.3: Schematic representation of the spin-transfer torque consisting of the AST and NAST in the rotated basis system

To calculate the adiabatic (AST) and non-adiabatic spin torques (NAST), let us consider the rotated basis system in which the spin moment in the current layer ($\mathbf{S}$) is along $\hat{\mathbf{b}}_1$ direction whereas that in the previous layer ($\mathbf{S}_p$) is oriented in the plane $\hat{\mathbf{b}}_1\hat{\mathbf{b}}_2$. In this basis system as shown in figure 7.3, the adiabatic and non-adiabatic torques can

be determined from the total spin torque via *s-d* exchange interaction as follows

$$\begin{aligned} \mathrm{ST} &= S \times J\mathbf{m} \\ &= \hat{\mathbf{b}}_1 \times J(m_{\parallel}\hat{\mathbf{b}}_1 + m_{\perp,2}\hat{\mathbf{b}}_2 + m_{\perp,3}\hat{\mathbf{b}}_3) \\ &= -Jm_{\perp,3}\hat{\mathbf{b}}_2 + Jm_{\perp,2}\hat{\mathbf{b}}_3. \end{aligned} \tag{7.15}$$

As previously mentioned in chapter 5, the AST is the in-plane torque whereas the NAST is introduced as the field-like torque or the out-of-plane torque. Therefore, the spin moments in the rotated basis system as illustrated in figure 7.3 result in the AST and NAST along the directions of $\hat{\mathbf{b}}_2$ and $\hat{\mathbf{b}}_3$ respectively. As a consequence, the AST and NAST in the rotated basis system are given by

$$\begin{aligned} \mathrm{AST} &= -Jm_{\perp,3}\hat{\mathbf{b}}_2 \\ \mathrm{NAST} &= Jm_{\perp,2}\hat{\mathbf{b}}_3. \end{aligned} \tag{7.16}$$

The above equation shows that the AST and NAST can be achieved directly via the spin accumulation. Subsequently, the dynamics of spin motion including the effect of the spin-transfer torque can be investigated by employing equation (7.14). Various numerical techniques [122–125] have been developed to solve the LLG equation in the presence of the spin injection. In this work, the Heun scheme will be used to investigate the spin motion as described in the following.

7.2.3 Numerical technique

The dynamics of spins in the presence of the spin-transfer torque can be observed by means of the standard LLG equation with the additional field due to spin torque as shown in equation (7.14). Due to the nonlinear behaviour, it is necessary to solve this equation numerically as the analytical solutions cannot be derived in the general case. Primitively, Euler's method is commonly used for the time integration of LLG equation by considering the spin motion in a single discretised time step, Δt. It assumes a linear change in the spin direction in each time step. The predicted point considered by the Euler's method can be underestimated or overestimated therefore a small time step is required in order to get small error. However, even if the small time step is used, not only does the computational cost tend to increase but also the numerical error starts to accumulate due to a large number of time steps [113].

In this work, I will apply the Huen scheme which is an improved integration scheme. To reduce the error of Euler's method and to allow the use of a larger time step, a predictor-corrector algorithm will be applied. It starts with predicting the new spin direction in the next time step based on the standard Euler integration referred as "*predictor algorithm*" given by

$$\mathbf{S}_{t+1,\text{Euler}} = \mathbf{S}_t + \Delta t \mathbf{S}'_t \tag{7.17}$$

and the derivative of spin moment at time t is as follows

$$\mathbf{S}'_t = \frac{-\gamma}{(1+\alpha^2)} \left[\mathbf{S}_t \times \mathbf{H} + \alpha \mathbf{S}_t \times (\mathbf{S}_t \times \mathbf{H})\right] \tag{7.18}$$

where the effective field including the additional field due to spin-transfer torque is $\mathbf{H} = \mathbf{H}_{\text{eff}} + J\mathbf{m}_\perp$.

It should be noted that the new spins are renormalised after both the predictor and corrector steps since the Huen scheme does not preserve the spin unit vector length. Also the effective field and the spin torque field must be recalculated as the spin positions have changed. Subsequently, the predicted spin position and revised local effective field ($\mathbf{H}_{\text{new}}$) are used to calculate the final spin position, a so-called "*corrector algorithm*". The correction of predicted spin position is performed in the Heun scheme by using the average derivative at the old spin($\mathbf{S}'$) and new spin($\mathbf{S}'_{t+1,\text{Euler}}$) positions to obtain more accurate direction of the spin moments as the following

$$\mathbf{S}_{t+1,\text{Heun}} = \mathbf{S}_t + \frac{\Delta t}{2}[\mathbf{S}'_t + \mathbf{S}'_{t+1,\text{Euler}}] \ , \tag{7.19}$$

where

$$\mathbf{S}'_{t+1,\text{Euler}} = \frac{-\gamma}{(1+\alpha^2)} \left[\mathbf{S}_{t+1,\text{Euler}} \times \mathbf{H}_{\text{new}} + \alpha \mathbf{S}_{t+1,\text{Euler}} \times (\mathbf{S}_{t+1,\text{Euler}} \times \mathbf{H}_{\text{new}})\right].$$

The Heun scheme is a simple but powerful numerical technique. In a complete integration time step, every spin moment in the magnetic system is simulated. The dynamic motion of spin moments can be investigated by repeating the predictor-corrector algorithm for the system many times.

7.3 Current-induced domain wall motion

In this work, the dynamics of magnetisation in the bilayer system consisting of two ferromagnets (FMs) as explained in Sec. 5.3.1 is investigated. The current-induced domain wall motion can be studied by injecting a spin current perpendicular to the plane of the bilayer. In this computational study, the investigation is presented in two sections. Firstly the effect of the spin transfer torque on the domain wall dynamics, the time evolution of domain wall displacement as well as DW velocity is investigated. Furthermore, the effect of the current density (j_e) is also studied by injecting a current with different magnitudes. This allows the investigation of the critical current density which is the minimum spin current required to move the domain wall. Secondly, the effect of DW width on the time evolution of the DW displacement and DW velocity is then considered.

7.3.1 Time evolution of magnetisation and spin torque

A bilayer structure is modelled with the dimension of the free layer of $60 \times 30 \times 1.5\ nm^3$. As mentioned earlier, in order to calculate the spin accumulation and spin torque the system is discretised into cells with a size of $1.5 \times 1.5 \times 1.5\ nm^3$. A domain wall is forced into the free layer by fixing the antiparallel magnetisation at the boundaries as illustrated in figure 7.4. The DW profile is transverse the xy plane.

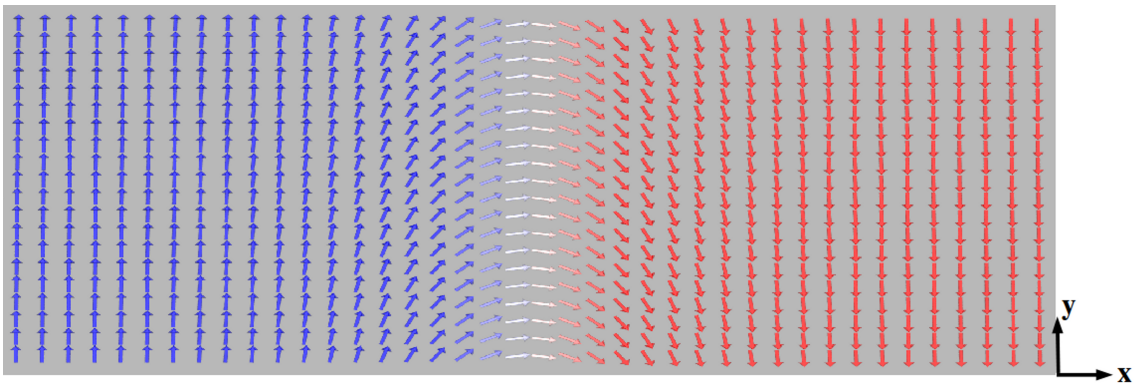

Figure 7.4: The tail-to-tail domain wall contained in the second ferromagnet of the bilayer system with the uniaxial anisotropy constant of $K_u = 2.52 \times 10^6\ J/m^3$: The arrows indicate the direction of magnetisation. The magnetisation along the y direction is represented by blue color. In contrast, the red color shows the orientation of magnetisation in the $-y$ direction.

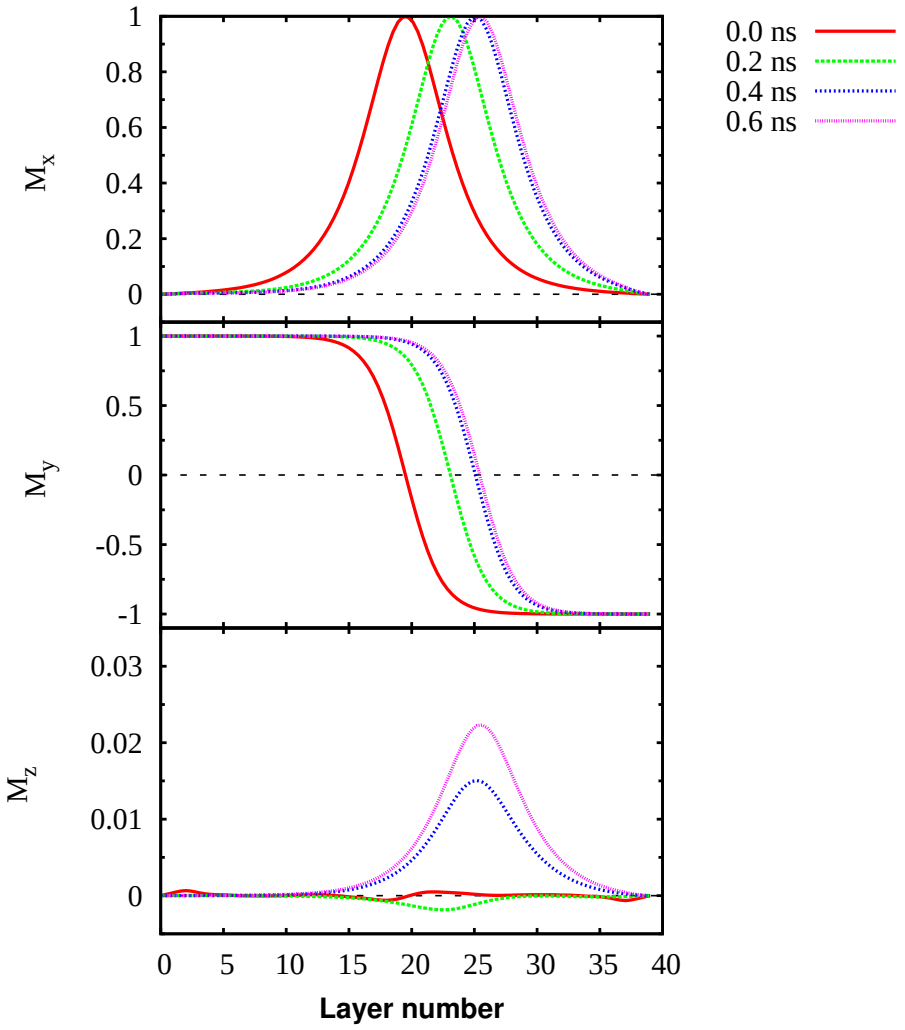

Figure 7.5: Schematic representation of the magnetisation component with time evolution from 0 ns to the equilibration time of 0.6 ns: The current density injected into the bilayer system containing the DW is 50 MA/cm^2.

The first investigation of interest is the effect of the spin-transfer torque on the domain wall motion by introducing the current density of 50 MA/cm^2 into the bilayer system. The current-induced domain wall motion can be observed through the component of magnetisation. As depicted in figure 7.5, the variation of magnetisation with time is investigated in order to understand the effect of the spin-torque. In the absence of the spin-transfer torque at $t = 0$ ns, the DW is situated centrally and the position of the DW centre is defined by the maximum magnetisation of the x component and zero of the y component. The DW initially moves when the spin current is injected above

the critical value. DW has the translational motion into the right which is the direction of the injected current and it tends to stop moving at the equilibration time $t = 0.6\ ns$ with the finite DW displacement. Specifically, an out-of-plane or z component slightly develops during the propagation time. Its appearance comes from the fact that the domain wall interacts with the strong pinning site. It is evidence of DW deformation due to interaction with the pinning site.

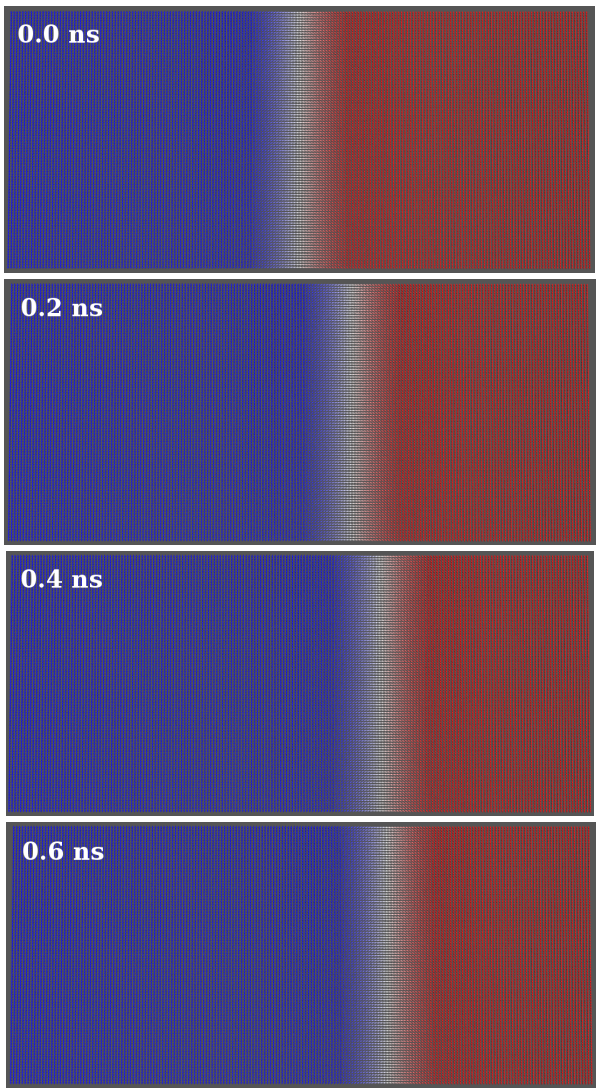

Figure 7.6: Visualisation of the current-induced domain wall motion with time evolution from 0 ns to the equilibration time of 0.6 ns with the current of 50 MA/cm^2

It is also illustrative to investigate the domain wall motion driven by the spin-transfer torque via the visualisation as demonstrated in figure 7.6. This figure shows the top view of the spin direction at the atomic resolution. The blue and red colours represent the spin direction along y and $-y$ directions respectively. The white area indicates the domain wall region. For this current density, it is found that the domain wall is slightly displaced from the initial position and the domain wall width does not decrease. This is because the spin current density is not sufficiently high.

In order to investigate the origin of the oscillatory behaviour, the current density injected into the DW must be high enough. Therefore, a current density of 1000 MA/cm^2 is chosen. The magnetisation component at the initial DW centre at layer number of 20 is investigated in its time evolution after the introduction of the spin-transfer torque. Figure 7.7 clearly shows that the spin-transfer torque acting on magnetisation causes the deformation of DW leading to precessional motion of x and z components. This is the precession of the equilibrium magnetisation about the effective field determined by the interaction with the pinning site.

Also, it is interesting to consider the time variation of the spin-transfer torque naturally including the adiabatic and non-adiabatic torques to understand its evolution. The x and y components of the spin torque are regarded as the adiabatic torque tending to develop towards the direction of magnetisation meanwhile the z component of spin torque arises from the contribution of the non-adiabatic torque or the out-of-plane torque. The spin torque acting on the local magnetisation due to the spin-polarised current results in the translation of the DW. As a consequence, the spatial spin torque at different times as illustrated in figure 7.8 corresponds to the time variation of magnetisation in figure 7.5. It is found that the equilibrium is established after the introduction of spin injection for 0.6 ns. In addition, it is evidently shown that the magnitude of the adiabatic and non-adiabatic torques remain constant with time evolution and the domain wall width is not significantly decreased from the initial state as the spin current density of 50 MA/cm^2 is not high enough to force the DW against the pinning sites.

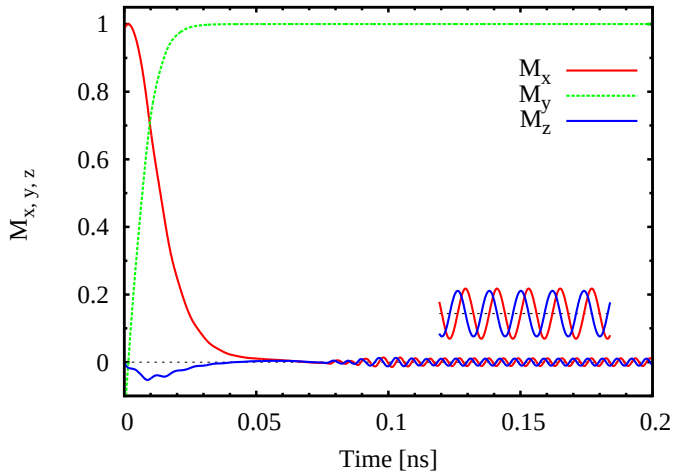

Figure 7.7: The magnetisation component of the intial DW centre with time evolution after injecting the spin current with the density of 1000 MA/cm^2

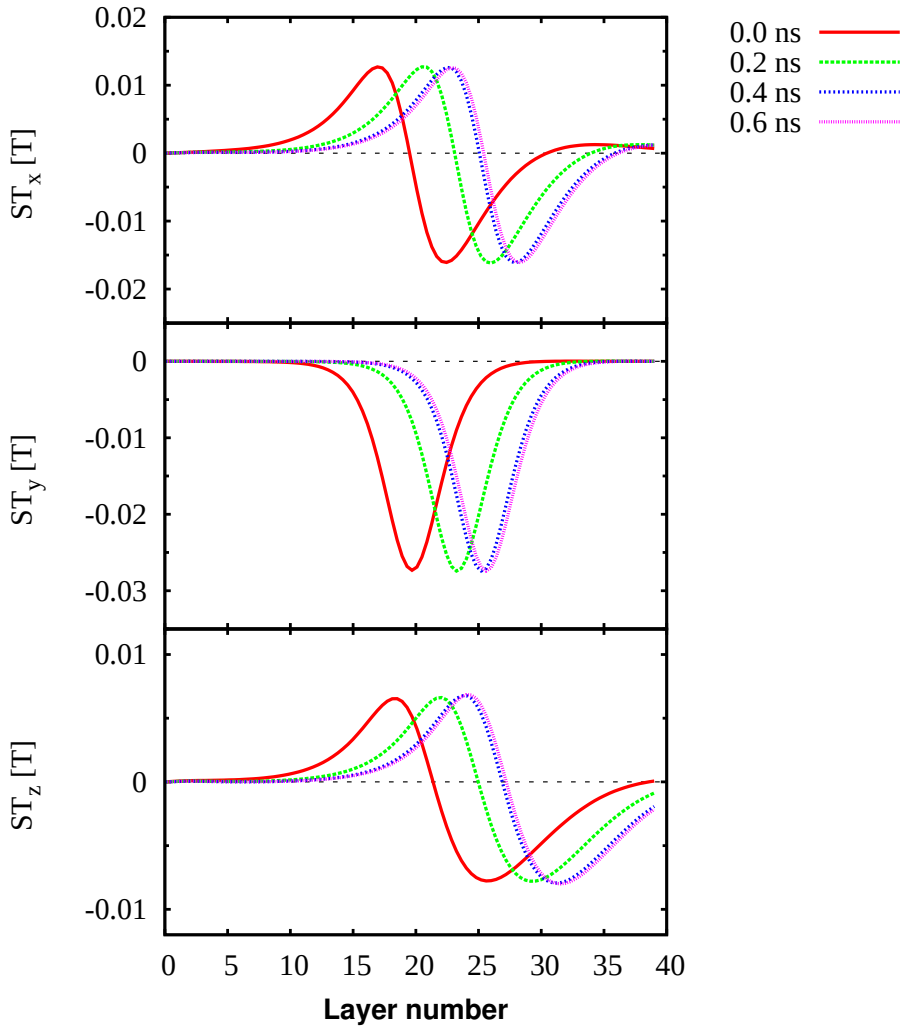

Figure 7.8: The time evolution of the spatial spin-transfer torque with $j_e = 50\ MA/cm^2$

7.3.2 DW displacement and velocity

The next investigation of interest is the effect of the current density on the domain wall motion. The strength of the spin-transfer torque can be controlled by varying the magnitude of the current density. This leads to the investigation of the critical spin current density (j_e), which is the minimum value to initiate domain wall motion. It is first noted that the calculation in this section observed the domain wall motion in the bilayer system with the anisotropy constant of $K_u = 2.52 \times 10^6\, J/m^3$ giving rise to the domain wall width of approximately 6.86 nm. The application of the spin-polarised current induces a displacement of the DW position with time evolution, as shown in figure 7.9 (top panel). DW displacement is monitored by observing the shift of the DW centre from the initial position at each time step. It can be seen that the DW displacement is time dependent and increases linearly in the first time period before reaching a steady state with finite displacement due to the interaction with the pinning site. The equilibration time of DW displacement tends to decrease with increasing spin current density.

To describe the behaviour of the DW displacement with different regimes of the spin current density, it is important to consider the critical current density, which can be evaluated through the initial DW velocity. The initial velocity is calculated by determining the rate of change of the DW displacement in the first 0.1 ns as the DW shows uniform translational motion during that period. The relation between the initial DW velocity as a function of the current density is plotted on a semi-logarithmic scale as shown in figure 7.9 (bottom panel). It is found that the critical current density causing the DW motion is 0.5 MA/cm^2. For a small current density $j_e < j_e^{crit}$, the domain wall motion does not occur. The spin-transfer torque acting on the magnetisation within the domain wall created by the spin current below the critical value is not sufficiently strong to move the domain wall.

On increasing the current density above the critical value, the domain wall moves uniformly without any precession along the direction of the injected spin current. This motion induced by the spin current is due to the conservation of the angular momentum. Furthermore, the domain wall motion is accompanied by oscillatory behaviour, which tends to be observed with a high current density over 100 MA/cm^2. The oscillation of DW displacement indicates the forth and back motion of DW before reaching the equilibrium state. Interestingly, as a result of increasing current density to an extremely

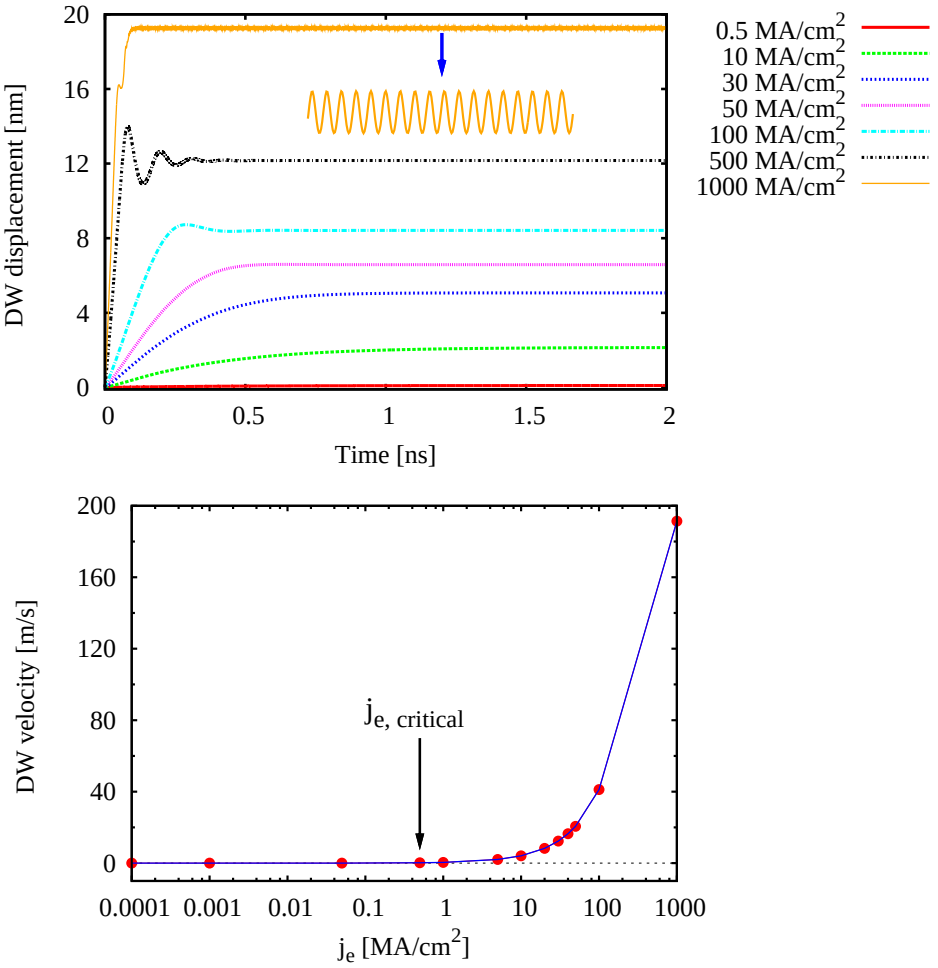

Figure 7.9: (top) The time variation of domain wall displacement with different current densities in the dimension of MA/cm^2 (bottom) The initial DW velocity as a function of current density: The critical current density, minimum current density required to move DW is 0.5 MA/cm^2.

high value $j_e = 1000\ MA/cm^2$, the dynamic behaviour of the DW is also oscillatory, but exhibits a stable precessional state deviating around a finite wall displacement. At equilibrium, the DW displacement oscillates at a high frequency of 300 GHz since the pinned DW essentially acts as a spin-torque oscillator. This also implies the appearance of the out-of-plane component of magnetisation resulting from the non-adiabatic torque, consistent with the previous study in Ref. [14]. In addition, the non-adiabatic torque driving the DW in the stable precessional state is strong enough to deform the Néel wall so as to have a significant out-of-plane component, which results in the oscillatory propagation.

7.4 Current-induced DW motion: the effect of the domain wall width

In this section, the effect of the domain wall width on the magnetisation dynamics is investigated. This is done by introducing a spin-polarised current into a bilayer system containing a domain wall whose width is varied by changing the anisotropy constant. The domain wall profile with different anisotropy constants can be seen in figure 7.10. The magnetisation is allowed to continuously vary throughout the layer with the pinning sites at the boundaries. The width of the domain wall is varied by increasing the uniaxial anisotropy constant to investigate the influence of the magnetic anisotropy to the spin-transfer torque emerged in the domain wall. The anisotropy constant is varied from the typical anisotropy value of cobalt $K_u = 4.2 \times 10^5\, J/m^3$ up to 100 times of that value. The x and y components of DW profile can be used to characterise the centre of DW and the DW width. The z component of the magnetisation is zero according to the usual properties of the Néel wall for the thin sample.

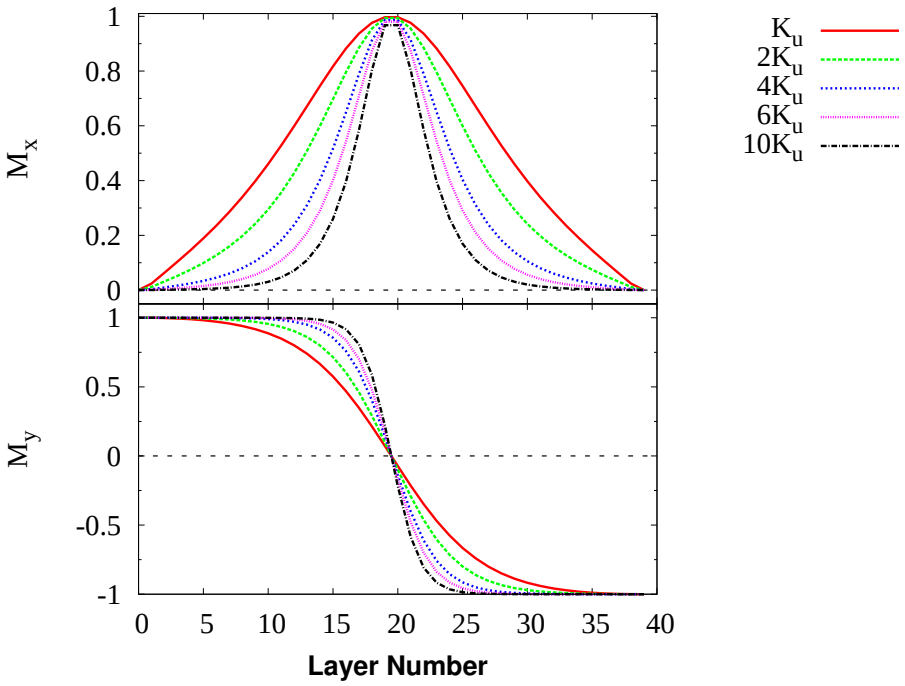

Figure 7.10: The domain wall profile transverse in the xy plane with various anisotropy constants: The uniaxial anisotropy constant of cobalt is $K_u = 4.2 \times 10^5\, J/m^3$. The distance between layer is given in units of cells, corresponding to 5 atomic spacings.

A detailed qualitative investigation of the current-induced DW motion with the effect of anisotropy constant will be discussed in the following.

7.4.1 DW displacement and velocity

Firstly, a spin current with the density of 50 A/m^2 is injected into the bilayer system along the x direction in order to observe the manipulation of the magnetisation within the DW with different anisotropy constants. The magnetisation configuration is illustrated in figure 7.11 after the introduction of the spin current for 1 ns. It shows that the DW motion is initiated after injecting the spin current into the system. The centre of the domain wall moves from the initial position along the direction of the spin current. This arises from the exchange interaction between the spin current and the local magnetisation within the DW. The system with high anisotropy is easily displaced due to a larger gradient of magnetisation within the DW giving rise to a high magnitude of spin torque acting on it. Interestingly, the DW centre of the system with the anisotropy constant of K_u is unchanged. This implies that the density of spin current injected to the system is below the critical value. For a wide domain wall, the high current density is required to initiate the DW motion. In contrast, the DWs with high anisotropy are able to move, which implicitly indicates that the critical current density of the narrow DW is lower. In addition, the out-of-plane component is likely to be large for high anisotropy.

Furthermore, it is also worthwhile to observe the dynamic behaviour of the DW motion via the DW displacement and the initial DW velocity. As illustrated in figure 7.12 (top panel), the DW displacement is not noticeable for a very wide wall, specifically for uniaxial anisotropy constants of K_u and $2K_u$. The DW exhibits transient oscillatory behaviour back to its initial position. Hence, a higher spin current density is needed in order to initiate the translation of DW for these cases. On the other hand, displacement of the narrow DW tends to be more easily initiated than the wide DW. This is because of the strong interaction between the spin current and the local magnetisation gradient within the DW giving rise to a large spin-transfer torque. For a low anisotropy, the linear response of the DW displacement occurs in the first 0.1 ns and then reaches the equilibrium state. For a high anisotropy, the DW displacement deviates from linear behaviour and the precessional motion is enhanced for several cycles in the first ns before reaching the equilibrium state. The deviation from the linear behaviour in the first period becomes stronger for higher anisotropy. In the case of this spin current

density, the stable precessional state is not established as the current density is not high enough to push the DW against the pining sites.

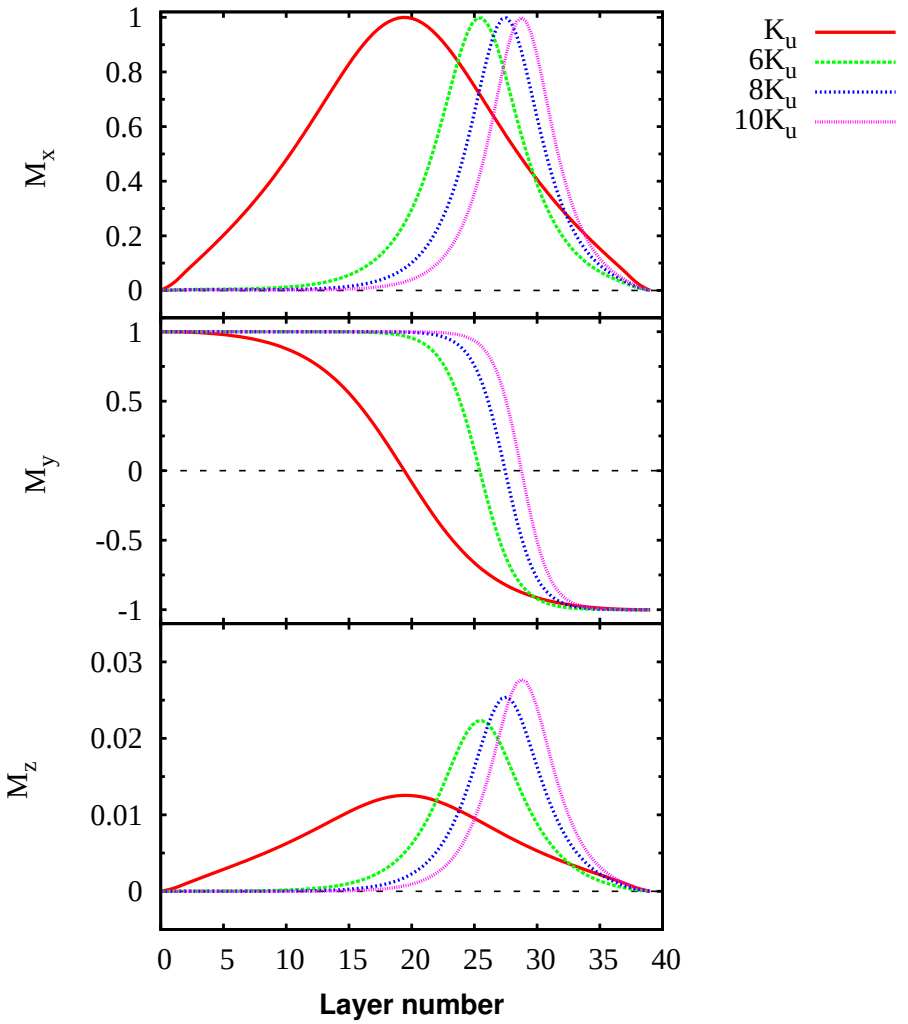

Figure 7.11: The component of magnetisation in the second FM with various anisotropy constants after the introduction of the spin current for 1 ns: The centre of the DWs are displaced in the direction of the injected spin current. The system with high anisotropy constant leading to a large gradient of magnetisation within domain wall results in a large displacement of the DW.

In addition, the initial DW velocity as a function of the DW width is subsequently considered. Obviously, the DW width becomes a sensitive parameter to the initial DW velocity as can be seen in figure 7.12 (bottom panel). The initial DW velocity is decreased with increasing DW width caused by the decreasing magnetisation gradient. This rela-

tion can be used to evaluate the critical DW width for each spin current density. The current density of 50 MA/cm^2 is able to move a DW along the direction of the injected spin current in case of the DW width less than 11.2 nm.

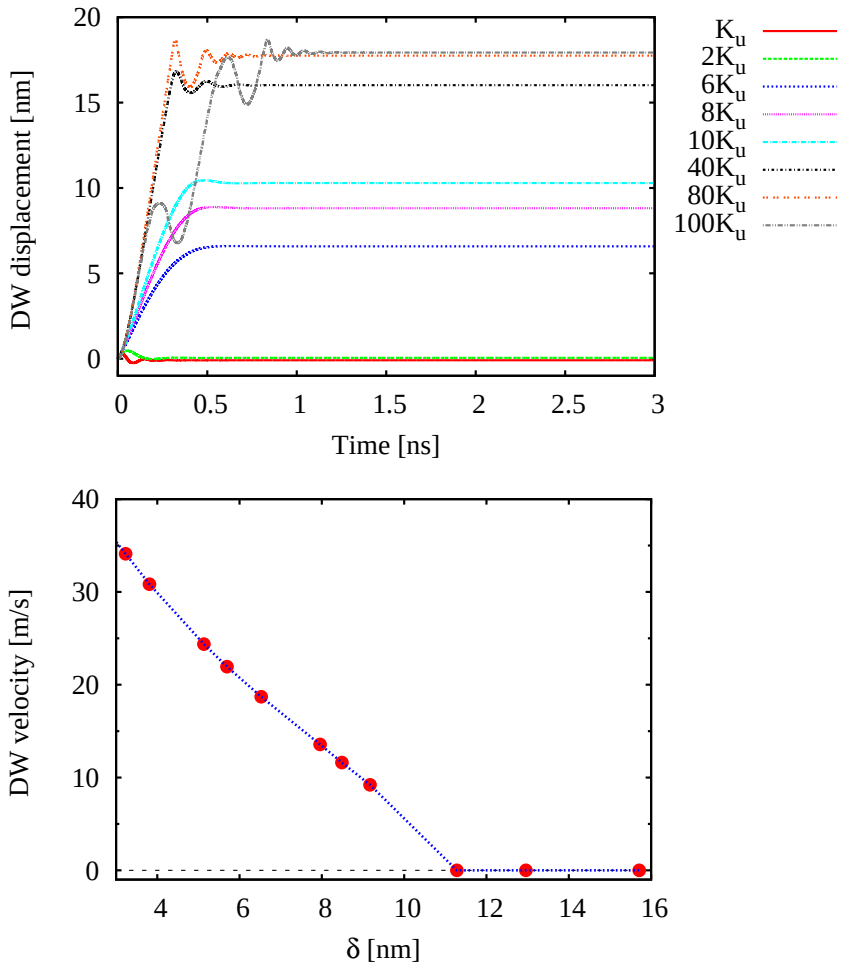

Figure 7.12: (top) The time-dependent variation of the domain wall displacement and (bottom) the initial domain wall velocity of different uniaxial anisotropy systems with the spin current density of 50 MA/cm^2

7.4.2 Spin-transfer torque

In this part, the spin transfer torque consisting of adiabatic (AST) and non-adiabatic (NAST) components is investigated. As mentioned before, the total spin-transfer torque is mainly contributed by the AST resulting from the spin accumulation component following the direction of the local magnetisation whereas the out-of-plane torque comes from the NAST arising from the electron mistracking. The strength of the spin-transfer

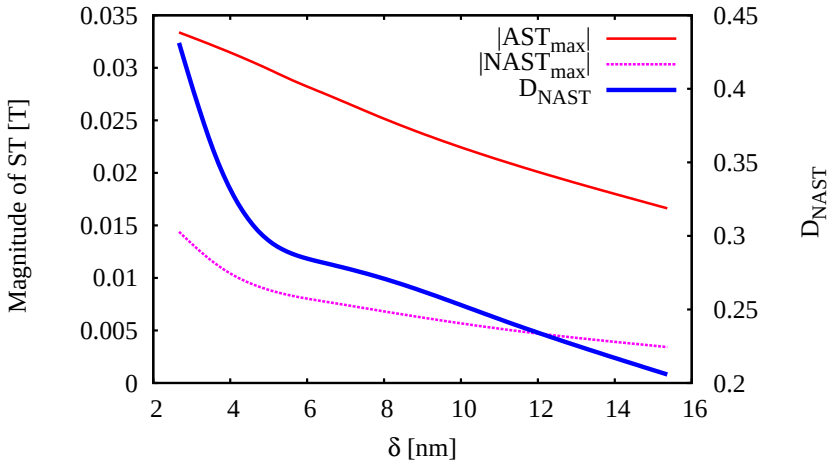

Figure 7.13: The thickness dependence of a maximum of adiabatic spin torque (AST), non-adiabatic spin torque (NAST) and the degree of nonadiabaticity (D_{NAST})

torque on the DW can be represented by considering the maximum value occurring at any position over the DW region given that its contribution is nonuniform throughout the DW. In addition, the degree of non-adiabatic torque or the so-called nonadiabaticity (D_{NAST}), which characterises the relative influence of the NAST on the DW compared with the AST, is also evaluated as the following equation.

$$D_{\mathrm{NAST}} = \frac{\mid \mathrm{NAST_{max}} \mid}{\mid \mathrm{AST_{max}} \mid} \tag{7.20}$$

where the nonadiabaticity is denoted as D_{NAST}. $\mid \mathrm{NAST_{max}} \mid$ and $\mid \mathrm{AST_{max}} \mid$ are the maximum value of adiabatic and non-adiabatic torques within DW.

Clearly, as shown in figure 7.13, both adiabatic and non-adiabatic torques tend to be more effective in narrow DW due to the large gradient of magnetisation. It can also be seen that the nonadaibaticity factor becomes more significant for a small DW width. This is schematically shown in figure 7.13. In contrast, the pure adiabatic torque is likely to dominate the total torque, with negligible non-adiabatic torque, for a large DW width. This is consistent with previous studies [9, 66].

7.5 Summary

In conclusion, in this chapter I applied the modified formalism of spin accumulation as explained in chapter 4 and an atomistic model, to study the dynamics of magnetisation

within the DW in the presence of a spin-transfer torque. The spin polarised current flowing into the ferromagnet leads to a spin accumulation exerting the torque on the local magnetisation. The results show the translation of the domain wall along the direction of the injected current. The total spin torque contributed by adiabatic and non-adiabatic torques at any position within the DW is considered here. The results in the final section indicate that both torques are inversely proportional to domain wall width. Furthermore, it is found that the adiabatic torque dominates the total spin torque meanwhile the adiabatic torque controls the out-of-plane component of spin torque. Finally, the nonadiabaticity factor is also determined to indicate the strength of the non-adiabatic torque. It tends to decay to zero as the DW width increases. The material with high anisotropy such as FePt giving rise to narrow domain wall is more effective for data storage application as the enhancement of high spin-transfer torque occurs.

Up to this point of the thesis, I proposed the modified formalism of the spin accumulation based on a generalisation of the previous work of ZLF. The modified solution of spin accumulation was applied to study the spin transport behaviour in the bilayer system including the effect of a diffuse interface. In addition, the implementation of modified solution and the atomistic model is used to study the dynamics of the magnetisation as discussed in this chapter. The final chapter discussed next will summarise all results presented previously and then outline the future prospects for the modified approach.

CHAPTER VIII

Conclusions and future work

8.1 Conclusions

In conclusion, the modified spin accumulation model based on diffusive transport is proposed to describe the behaviour of spin transport in the magnetic bilayer system. It is verified that the general solution of spin accumulation in this work reduces to the specific case of the previous work of ZLF. The modified model is also applicable for the multilayer structure with different materials leading to the different nonzero equilibrium values of spin accumulation. It is applied to the bilayer system with both collinear and non-collinear configurations to observe the spin transport properties. The results show that the spin current and spin accumulation tend to follow the direction of the local magnetisation. Interestingly, an out-of-plane component of spin accumulation can be observed owing to the mistracking of the conduction electrons.

The spin-transfer torque contributions from the adiabatic and non-adiabatic torques can be described directly by the spin accumulation. The adiabatic and non-adiabatic torques parameters in the standard form, μ_x and β_x, can be solved and expressed in terms of the spin accumulation. In general, these coefficients are assumed to be constant throughout the layers. However, it is found that they strongly depend on the spatial variation of magnetisation giving rise to the nonuniform behaviour throughout the layers. The angular dependence causes the divergence of the coefficients at the small angle between magnetisation. Importantly, it was concluded that the constants μ_x and β_x used in the standard micromagnetic model do not provide a good description of the spin torque phenomenon due to the non-physical behaviour except for the case of soft materials with large domain wall widths. Instead, the approach based on the self-consistent solution of spin accumulation is suggested. As a result of spin torque calculations, it was shown that the adiabatic torque significantly controls the total spin-transfer torque in the system compared to the non-adiabatic torque. However, the non-adiabatic torque causes the out-of-plane component of the total spin-transfer torque.

According to the results in chapter 5, there are two important factors affecting the spin transport properties. The first significant factor is the spin diffusion length. The mistracking of conduction electrons increases with increasing spin diffusion length. For a large spin diffusion length, a weak interaction between the conduction electron and the local magnetisation is exhibited. This also results in the oscillatory behaviour in spin-transfer torque. The second crucial factor is the domain wall width controlled by varying the anisotropy constant. The magnitude of transverse spin accumulation which interprets the mistracking of the conduction electrons with the local magnetisation increases significantly in a narrow DW. The results indicate that the spin torque coefficients used in the usual micromagnetic approach are probably applicable to describe the behaviour of spin transport in the magnetic system with a large DW width but this approach is not valid for harder magnetic materials. In the final section of chapter 5, the coefficients μ_x and β_x tend to be uniform and valid to describe the spatial spin torques in Fe system where the DW width is comparable with the spin diffusion length.

Subsequently, the effect of a diffuse interface is taken into account, by applying the solution of Fick's law to describe the interface. The current approach links the behaviour of spin accumulation at the interface, in a physically transparent way, to a degree of interface mixing determined by known physical parameters, principally the ion diffusion constant D_{ion}. In practice it is noted that many spintronic applications such as STM-RAM (Spin Torque Magnetoresistive Random Access Memory) and ST nano-oscillators require high current densities and any interface diffusion at elevated temperatures could be expected to give rise to a larger penetration of the spin accumulation $\mathbf{m}$ from the interface. It is found that relatively modest amounts of interface diffusion give rise to continuity of $\mathbf{m}$. Importantly, the formalism outlined in this thesis allows to directly simulate the sharp variation of $\mathbf{m}$ due to the interface. Finally, it is noted that the approach proposed here provides a rather general framework for the study of interface effects. In particular, it is assumed that the local properties are a linear combination of the bulk properties weighted by the concentration of species. Generalisation of this aspect is relatively easy and may be used to improve matching to experimental conditions. The findings in this work are relevant to fundamental physics and technological applications.

Finally, the current-induced domain wall motion in a bilayer system was investigated theoretically using an atomistic model based on the standard LLG equation

including the effect of the spin transfer torque. The spin polarised current leads to a spin accumulation which exerts a torque on the local magnetisation. It results in the translation of the domain wall in the direction of the injected conduction electrons. The spin torque contributed by adiabatic and non-adiabatic torques is considered. Their magnitudes are inversely proportional to the domain wall width. Furthermore, it is found that the adiabatic torque dominates the total spin torque whereas the non-adiabatic torque controls the out-of-plane component of the total spin torque. The domain wall width becomes the important parameter relative to the transport length scales. Finally, the nonadiabaticity factor is also determined to indicate the strength of non-adiabatic torque. It tends to decay to zero as the thickness increases. The material with high anisotropy giving rise to narrow domain wall is more effective for data storage application.

8.2 Future work

Spin torque-induced magnetisation switching is a possible technique to control and manipulate the orientation of the magnetisation. The spin-transfer torque arising from the spin polarised current flowing through a spin valve or MTJ structures enables the magnetisation switching. This phenomenon provides a new concept for the development of advanced MRAM, nonvolatile logics and readers in hard disk drives.

This work not only generates interesting results, but also the modified spin accumulation model is applicable to investigate the spin transport behaviour in real devices such as the read head in hard disk drive. In general, the computational models of read sensors are based on micromagnetic approaches. Although successful, micromagnetic approach is limited in a number of ways which makes the formalism inappropriate for spin transport investigation with further scaling of device dimensions, which increases the influence of the interface roughness. Therefore, one proposal for further work is aimed at developing a model of spin accumulation and spin transport in multilayer systems for GMR calculation at the atomistic level. The theory will be employed in an atomistic model to simulate GMR and spin torque effects in readers taking into account the interface roughness and nonzero temperatures. Furthermore, the effect of elevated temperatures produced by the heating effect of the current would be worth investigation. This includes studies of the enhanced magnetisation fluctuations at the interface and to determine its level of significance as a noise source.

Another possible future work is to develop a model of calculation of TMR in magnetic tunnel junctions (MTJs). MTJs using a MgO tunnel barrier gives rise to a high ratio of tunnel magnetoresistance. Given that CoFeB is magnetically soft, it is well known that the perpendicular anisotropy in CoFeB-MgO MTJs arises due to the interfacial anisotropy. Evidently, the perpendicular magnetic anisotropy (PMA) arises at the interface between the ferromagnetic transition metal and insulator. Ohno's group at Tohoku university experimentally studied the magnetic properties of CoFeB/MgO structure of which the PMA exhibits at the interface [37]. It results in a giant tunnel magnetoresistance ratio in MTJs. Therefore, understanding the thickness, size and temperature dependent magnetic properties of CoFeB-MgO MTJs is an important step towards optimization of this system for spintronics applications. Subsequently, the spin transport in MTJ could be studied by using the atomistic model coupled with the modified spin accumulation model.

In the respect of model development, the improvement of the interface model is of great interest for future work. This may give rise to a better explanation of the scattering mechanism within the interface region. Also the model is possibly developed for the case of the non-uniform currents.

PUBLICATIONS AND PRESENTATIONS

Publications

- *" Modeling spin injection across diffuse interfaces "*, **P. Chureemart**, R Cuadrado, I D'Amico and RW Chantrell, Physical Review B 87 (19), 195310, 2013

- *" Dynamics of domain wall driven by spin-transfer torque "*, **P. Chureemart**, RFL Evans and RW Chantrell, Physical Review B 83 (18), 184416, 2011

- *" Magnetic orientation in advanced recording media "*, J. Chureemart, **P. Chureemart**, RFL Evans, RW Chantrell and K O' Grady, J. Phys. D: Appl. Phys. 44 455002, 2011

Papers under preparation

- *" Self-Consistent Calculation of Adiabatic and Non-adiabatic Spin Torque "*, **P. Chureemart**, I. D'Amico, and R. W. Chantrell, to be submitted to Physical Review Letters

- *" Influence of uniaxial anisotropy on domain wall motion driven by non-local spin torque "*, **P. Chureemart**, R. F. L. Evans, I. D'Amico, and R. Chantrell, to be submitted to Physical Review B

- *" Atomistic calculation of the temperature dependent anisotropy of CoFeB-MgO magnetic tunnel junctions "*, **P. Chureemart**, R. F. L. Evans, H. Sato, H. Ohno and R.W. Chantrell, to be submitted to Applied Physics Letters

Invited talk

- *" Self-Consistent Calculation of Adiabatic and Non-adiabatic Spin Torque "*, **P. Chureemart**, R. F. L. Evans, I. D'Amico, and R. W. Chantrell, 9th RIEC International Workshop on SPINTRONICS, June 2012, Tohoku University, Japan

Oral presentations

- *" A model of spin injection including the effect of interface diffusion "*, **P. Chureemart**, R. Cuadrado, I. D'Amico and R. W. Chantrell, The 12th Joint MMM/Intermag Conference, January 2013, Chicago, Illinois, USA

- *" Atomistic modelling of magnetization dynamics with spin accumulation "*, **P. Chureemart**, R. F. L. Evans, I. D'Amico, and R. Chantrell, INTERMAG 2012, May 2012, Vancouver, Canada

- *" Atomistic modelling of magnetization dynamics with spin torque "*, **P. Chureemart**, R. F. L. Evans, I. D'Amico, and R. Chantrell, THE 19th INTERNATIONAL CONFERENCE ON MAGNETISM, July 2012, Busan, Korea

- *"Study of Spin Torque in Multilayer Structures Including Combined Drift Diffusion and Effect of Diffuse Interfacial Layer "* **P. Chureemart**, J. L. Gay, I. D'Amico and R.W. Chantrell, INTERMAG 2011, April 2011, Taipei, Taiwan

- *" Study of spin torque in multilayer structures via combined drift diffusion and atomistic modelling techniques "* **P. Chureemart**, J. L. Gay, I. D'Amico and R.W. Chantrell, 55th MMM, November 2010, Atlanta, USA

- *" Study of spin torque in multilayer structures via combined drift diffusion and atomistic modelling techniques "*, J. L. Gay, **P. Chureemart**, I. D'Amico, R. W. Chantrell, JEMS10, August 2010, Krakow, Poland.

Poster presentation

- *" Atomistic calculation of the temperature dependent anisotropy of CoFe-MgO magnetic tunnel junctions "*, **P. Chureemart**, R. F. L. Evans and R.W. Chantrell, The 12th Joint MMM/Intermag Conference, January 2013, Chicago, Illinois, USA

LIST OF SYMBOLS

$\mid \vec{r}_{ij} \mid$	Distance between supercell i and j
α	Damping constant
β	Spin polarisation parameter for conductivity
β'	Spin polarisation parameter for diffusion constant
β_x	Spin torque coefficient used to explain non-adiabatic toque in the standard form
δ	Domain wall width
γ	Absolute gyromagnetic ratio given by $\gamma = g\mu_B/\hbar = 1.76 \times 10^{11}\ rad\ s^{-1}T^{-1}$
$\hat{\mathbf{b}}$	Basis coordinate system comprising $\hat{\mathbf{b}}_1$, $\hat{\mathbf{b}}_2$ and $\hat{\mathbf{b}}_3$ which are parallel and perpendicular to the local magnetisation
$\hat{\mathbf{e}}$	Global coordinate system comprising $\hat{\mathbf{e}}_x$, $\hat{\mathbf{e}}_y$ and $\hat{\mathbf{e}}_z$ which are along the x, y and z directions respectively.
$\hat{\sigma}$	2×2 matrix of conductivity
$\hat{D}$	2×2 matrix of diffusion constant
$\hat{j}$	2×2 matrix of current
$\hat{n}$	2×2 matrix of accumulation
$\hbar$	Reduced Planck constant
λ_J	Length scale given by, $\sqrt{2\hbar D_0/J}$
λ_{mfp}	Electron mean free path
λ_{sdl}	Spin diffusion length
λ_{sf}	Spin relaxation length given by, $\sqrt{D\tau_{sf}}$
$\mathbf{E}$	Electric field
$\mathbf{j}$	Current density
$\mathbf{j}_e$	Charge current density

$\mathbf{j}_m$ Spin current density

$\mathbf{M}$ Normalised magnetisation

$\mathbf{m}$ Spin accumulation

$\mathbf{M}_{\text{eq}}$ Equilibrium magnetisation

$\mathbf{m}_{\parallel}$ Longitudinal spin accumulation

$\mathbf{m}_{\perp}$ Transverse spin accumulation

$\mathbf{M}_p$ Unit vectors of magnetisation in the pinned layer

$\mathbf{m}_{\perp,2}$ Transverse spin accumulation along the direction $\hat{\mathbf{b}}_2$

$\mathbf{m}_{\perp,3}$ Transverse spin accumulation along the direction $\hat{\mathbf{b}}_3$

$\mathbf{M}_{p,\perp}$ Transverse magnetisation in the pinned layer

$\delta\mathbf{m}$ Nonequilibrium spin density of state

$\mathcal{H}$ Classical spin Hamiltonian

μ Electrochemical potential

$\mu^{\uparrow(\downarrow)}$ Electrochemical potential for spin-up(down) electrons

μ_{ch} Chemical potential

μ_B Bohr magneton, $\mu_B = 9.274 \times 10^{24}\ J/T$

μ_x Spin torque coefficient used to explain adiabatic toque in the standard form

ρ Resistivity

$\rho^{\uparrow(\downarrow)}$ Spin-dependent resistivities of the spin-up(down) channels

σ Conductivity of the ferromagnet

$\sigma^{\uparrow(\downarrow)}$ Spin-dependent conductivities of the spin-up(down) channels

$\tau^{\uparrow\downarrow(\downarrow\uparrow)}$ Spin-relaxation time at which the spin-up(down) electrons scatter to the spin-down(up) electrons

τ_{sf} Average spin-relaxation time of the conduction electron

AP Antiparallel state

AST Adiabatic spin torque

CIP Current in plane

CPP Current Perpendicular to the plane

DW Domain wall

ECP Electrochemical potential

FM Ferromagnet

GMR Giant magnetoresistance

MRAM Magnetic random access memory

MTJ Magnetic tunnel junction

NAST Non-adiabatic spin torque

NM Nonmagnet

PMA Perpendicular magnetic anisotropy

P Parallel state

TMR Tunnelling magnetoresistance

T_F Field-like torque or perpendicular spin torque

T_S Slonczewski torque

θ Angle between the magnetisation of the pinned layer and that of the free layer

$\vec{r}_{ij}$ Vector between supercell i and j

a Parameter describing the strength of adiabatic torque(AST)

b Parameter describing the strength of non-adiabatic torque(NAST)

C Atom concentration

D Diffusion constant

$D^{\uparrow(\downarrow)}$ Spin-dependent diffusion constants

D_{NAST} Nonadiabaticity

D_{ion} Ion diffusion constant

e Absolute value of the electron charge

J Exchange energy between the electron spin and the local magnetization

$j^{\uparrow(\downarrow)}$ Current density of spin-up(down) channels

J_{ij} Nearest neighbor exchange integral between the spin site i and j

j_{mx} x component of spin current

j_{my} y component of spin current

j_{mz} z component of spin current

k_B Boltzmamn constant

K_u Anisotropy energy per atom

$k_{1,2}$ Length scale given by $(k_1 \pm ik_2) = \sqrt{\lambda_{sf}^{-2} \pm i\lambda_J^{-2}}$

$l_{\mp}$ Length scales given by $1/l_{\mp} = \sqrt{(1/\lambda_{sf}^2) \pm (i/\lambda_J^2)}$

M_s Saturation magnetisation

m_x x component of spin accumulation

m_y y component of spin accumulation

m_z z component of spin accumulation

$N(E_F)$ Density of state at the Fermi energy

$n^{\uparrow(\downarrow)}$ Local spin-up(down) carrier densities

$N_i^{\uparrow(\downarrow)}(E_F)$ Spin-up(down) density of state at the Fermi energy

$n_{eq}^{\uparrow(\downarrow)}$ Equilibrium(bulk) populations of spin-up(down) density of states

P_i Spin polarisation of the ferromagnet

$R_{\downarrow}$ High resistance

$R_{\uparrow}$ Low resistance

R_P Resistance of parallel state(P)

R_{AP} Resistance of anti-parallel state(AP)

T Temperature

T_{non} Nonconservation of the spin angular momentum

V Unit cell volume

$\mathbf{S}_i$ Local normalised spin moment

$\mathbf{S}_j$ Normalised spin moment of neighbouring atom at site j

$\mathbf{m}_\infty$ Equilibrium value of spin accumulation

$\vec{\mu}_{i,\,j}$ Magnetic moment of supercell site $i,\ j$

BIBLIOGRAPHY

[1] J. C. Slonczewski, "Current-driven excitation of magnetic multilayers," *Journal of Magnetism and Magnetic Materials*, vol. 159, no. 1-2, pp. L1 – L7, 1996.

[2] L. Berger, "Emission of spin waves by a magnetic multilayer traversed by a current," *Phys. Rev. B*, vol. 54, no. 13, pp. 9353–9358, Oct 1996.

[3] J. A. Katine, F. J. Albert, R. A. Buhrman, E. B. Myers, and D. C. Ralph, "Current driven magnetization reversal and spin wave excitations in co/cu/co pillars," *Phys. Rev. Lett.*, vol. 84, pp. 4212–4215, 2000.

[4] M. Tsoi, A. G. M. Jansen, J. Bass, W.-C. Chiang, V. Tsoi, and P. Wyder, "Generation and detection of phase-coherent current-driven magnons in magnetic multilayers," *Nature*, vol. 406, pp. 46–48, 2000.

[5] S. I. Kiselev, J. C. Sankey, I. N. Krivorotov, N. C. Emley, R. J. Schoelkopf, R. A. Buhrman, and D. C. Ralph, "Microwave oscillations of a nanomagnet driven by a spinpolarized current," *Nature*, vol. 425, pp. 380–383, 2003.

[6] C. Burrowes, A. P. Mihai, D. Ravelosona, J.-V. Kim, C. Chappert, L. Vila, A. Marty, Y. Samson, F. Garcia-Sanchez, L. D. Buda-Prejbeanu, I. Tudosa, E. E. Fullerton, and J.-P. Attane, "Non-adiabatic spin-torques in narrow magnetic domain walls," *Nat Phys*, vol. 6, 2010.

[7] D. P. Bernstein, B. Bräuer, R. Kukreja, J. Stöhr, T. Hauet, J. Cucchiara, S. Mangin, J. A. Katine, T. Tyliszczak, K. W. Chou, and Y. Acremann, "Nonuniform switching of the perpendicular magnetization in a spin-torque-driven magnetic nanopillar," *Phys. Rev. B*, vol. 83, p. 180410, May 2011.

[8] C. T. Boone, J. A. Katine, M. Carey, J. R. Childress, X. Cheng, and I. N. Krivorotov, "Rapid domain wall motion in permalloy nanowires excited by a spin-polarized current applied perpendicular to the nanowire," *Phys. Rev. Lett.*, vol. 104, p. 097203, Mar 2010.

[9] J. Xiao, A. Zangwill, and M. D. Stiles, "Spin-transfer torque for continuously variable magnetization," *Phys. Rev. B*, vol. 73, no. 5, p. 054428, Feb 2006.

[10] M. D. Stiles, W. M. Saslow, M. J. Donahue, and A. Zangwill, "Adiabatic domain wall motion and Landau-Lifshitz damping," *Phys. Rev. B*, vol. 75, p. 214423, Jun 2007.

[11] S. Zhang and Z. Li, "Roles of nonequilibrium conduction electrons on the magnetization dynamics of ferromagnets," *Phys. Rev. Lett.*, vol. 93, p. 127204, Sep 2004.

[12] Z. Li and S. Zhang, "Magnetization dynamics with a spin-transfer torque," *Phys. Rev. B*, vol. 68, no. 2, p. 024404, Jul 2003.

[13] Z. Li and S. Zhang , "Domain-wall dynamics driven by adiabatic spin-transfer torques," *Phys. Rev. B*, vol. 70, no. 2, p. 024417, Jul 2004.

[14] Z. Li and S. Zhang, "Domain-wall dynamics and spin-wave excitations with spin-transfer torques," *Phys. Rev. Lett.*, vol. 92, no. 20, p. 207203, May 2004.

[15] A. Rebei and O. Mryasov, "Dynamics of a trapped domain wall in a spin-valve nanostructure with current perpendicular to the plane," *Phys. Rev. B*, vol. 74, p. 014412, Jul 2006.

[16] A. V. Khvalkovskiy, K. A. Zvezdin, Y. V. Gorbunov, V. Cros, J. Grollier, A. Fert, and A. K. Zvezdin, "High domain wall velocities due to spin currents perpendicular to the plane," *Phys. Rev. Lett.*, vol. 102, p. 067206, Feb 2009.

[17] C. T. Boone and I. N. Krivorotov, "Magnetic domain wall pumping by spin transfer torque," *Phys. Rev. Lett.*, vol. 104, no. 16, p. 167205, Apr 2010.

[18] A. Shpiro, "Two problems in spin-dependent transport in metallic magnetic multilayers," Ph.D. dissertation, Department of Physics, New York University, 2004.

[19] S. D. Sarma, "Spintronics: A new class of device based on electron spin, rather than on charge, may yield the next generation of microelectronics," *American Scientist*, vol. 89, no. 6, pp. pp. 516–523, 2001.

[20] M. N. Baibich, J. M. Broto, A. Fert, F. N. Van Dau, F. Petroff, P. Etienne, G. Creuzet, A. Friederich, and J. Chazelas, "Giant Magnetoresistance of (001)Fe/(001)Cr Magnetic Superlattices," *Phys. Rev. Lett.*, vol. 61, pp. 2472–2475, Nov 1988.

[21] G. Binasch, P. Grünberg, F. Saurenbach, and W. Zinn, "Enhanced magnetoresistance in layered magnetic structures with antiferromagnetic interlayer exchange," *Phys. Rev. B*, vol. 39, pp. 4828–4830, Mar 1989.

[22] A. Fert, "Nobel lecture origin, development, and future of spintronics," *Rev. Mod. Phys.*, vol. 80, pp. 1517–1530, Dec 2008.

[23] M. Julliere, "Tunneling between ferromagnetic films," *Physics Letters A*, vol. 54, no. 3, pp. 225–226, 1975.

[24] A. Schuhl and D. Lacour, "Spin dependent transport: GMR and TMR," *C. R. Physique*, vol. 6, 2005.

[25] B. Dieny, V. S. Speriosu, S. S. P. Parkin, B. A. Gurney, D. R. Wilhoit, and D. Mauri, "Giant magnetoresistive in soft ferromagnetic multilayers," *Phys. Rev. B*, vol. 43, pp. 1297–1300, Jan 1991.

[26] N. F. Mott and H. H. Wills, "The electrical conductiviey of transition metals," *Proc. R. Soc.*, vol. 153, no. 880, p. 699, 1936.

[27] N. F. Mott and H. H. Wills, "The resistance and thermoelectric properties of the transition metals," *Proc. R. Soc.*, vol. 156, no. 888, p. 368, 1936.

[28] N. F. Mott, "Electrons in transition metals," *Adv. Phys.*, vol. 13, no. 51, p. 325, 1964.

[29] E. Tsymbal and D. Pettifor, "Perspectives of giant magnetoresistance," ser. Solid State Physics, H. Ehrenreich and F. Spaepen, Eds. Academic Press, 2001, vol. 56, pp. 113–237.

[30] S. M. Thompson, "The discovery, development and future of GMR: The Nobel Prize 2007," *Journal of Physics D: Applied Physics*, vol. 41, no. 9, p. 093001, 2008.

[31] T. Valet and A. Fert, "Theory of the perpendicular magnetoresistance in magnetic multilayers," *Phys. Rev. B*, vol. 48, pp. 7099–7113, Sep 1993.

[32] J. Mathon and A. Umerski, "Theory of tunneling magnetoresistance in a junction with a nonmagnetic metallic interlayer," *Phys. Rev. B*, vol. 60, pp. 1117–1121, Jul 1999.

[33] T. Miyazaki and N. Tezuka, "Giant magnetic tunneling effect in $Fe/Al_2O_3/Fe$ junction," *Journal of Magnetism and Magnetic Materials*, vol. 139, no. 3, pp. L231–L234, 1995.

[34] J. S. Moodera, L. R. Kinder, T. M. Wong, and R. Meservey, "Large magnetoresistance at room temperature in ferromagnetic thin film tunnel junctions," *Phys. Rev. Lett.*, vol. 74, pp. 3273–3276, Apr 1995.

[35] S. Yuasa and D. D. Djayaprawira, "Giant tunnel magnetoresistance in magnetic tunnel junctions with a crystalline MgO(001) barrier," *Journal of Physics D: Applied Physics*, vol. 40, no. 21, p. R337, 2007.

[36] S. Ikeda, J. Hayakawa, Y. Ashizawa, Y. M. Lee, K. Miura, H. Hasegawa, M. Tsunoda, F. Matsukura, and H. Ohno, "Tunnel magnetoresistance of 604300 K by suppression of Ta diffusion in CoFeB/MgO/CoFeB pseudo-spin-valves annealed at high temperature," *Applied Physics Letters*, vol. 93, no. 8, p. 082508, 2008.

[37] S. Ikeda, K. Miura, H. Yamamoto, K. Mizunuma, H. D. Gan, M. Endo, S. Kanai, J. Hayakawa, F. Matsukura, and H. Ohno, "A perpendicular-anisotropy cofebmgo magnetic tunnel junction," *Nat Mater*, vol. 9, 2010.

[38] S. Zhang, P. M. Levy, and A. Fert, "Mechanisms of spin-polarized current-driven magnetization switching," *Phys. Rev. Lett.*, vol. 88, no. 23, p. 236601, May 2002.

[39] I. Žutić, J. Fabian, and S. Das Sarma, "Spintronics: Fundamentals and applications," *Rev. Mod. Phys.*, vol. 76, pp. 323–410, Apr 2004.

[40] S. Takahashi and S. Maekawa, "Spin current, spin accumulation and spin hall effect," *Science and Technology of Advanced Materials*, vol. 9, no. 1, p. 014105, 2008.

[41] A. G. Aronov, "Spin injection in metals and polarisation of nuclei," *JETP Lett.*, vol. 24, no. 1, pp. 37–39, July 1976.

[42] M. Johnson and R. H. Silsbee, "Interfacial charge-spin coupling: Injection and detection of spin magnetization in metals," *Phys. Rev. Lett.*, vol. 55, pp. 1790–1793, Oct 1985.

[43] A. Fert and I. A. Campbell, "Two-current conduction in nickel," *Phys. Rev. Lett.*, vol. 21, pp. 1190–1192, Oct 1968.

[44] P. C. van Son, H. van Kempen, and P. Wyder, "Boundary resistance of the ferromagnetic-nonferromagnetic metal interface," *Phys. Rev. Lett.*, vol. 58, pp. 2271–2273, May 1987.

[45] F. J. Jedema, M. S. Nijboer, A. T. Filip, and B. J. van Wees, "Spin injection and spin accumulation in all-metal mesoscopic spin valves," *Phys. Rev. B*, vol. 67, p. 085319, Feb 2003.

[46] S. Bandyopsdhyay and M. Cahay, *Introduction to spintronics*. CRC Press, 2008.

[47] M. Johnson and R. H. Silsbee, "Ferromagnet-nonferromagnet interface resistance," *Phys. Rev. Lett.*, vol. 60, pp. 377–377, Jan 1988.

[48] M. Johnson and R. H. Silsbee, "Thermodynamic analysis of interfacial transport and of the thermomagnetoelectric system," *Phys. Rev. B*, vol. 35, pp. 4959–4972, Apr 1987.

[49] M. Johnson and R. H. Silsbee, "Coupling of electronic charge and spin at a ferromagnetic-paramagnetic metal interface," *Phys. Rev. B*, vol. 37, pp. 5312–5325, Apr 1988.

[50] C. Heide, "Effects of spin accumulation in magnetic multilayers," *Phys. Rev. B*, vol. 65, p. 054401, Dec 2001.

[51] S. Hershfield and H. L. Zhao, "Charge and spin transport through a metallic ferromagnetic-paramagnetic-ferromagnetic junction," *Phys. Rev. B*, vol. 56, pp. 3296–3305, Aug 1997.

[52] P. M. Levy, "The role of spin accumulation in current-induced swithcing of magnetic layers, or the first $10^{-12}s$ in a magnetic multilayer after the current is switched on," *J. Phys. D: Appl. Phys.*, vol. 35, pp. 2448–2451, 2002.

[53] A. Shpiro, P. M. Levy, and S. Zhang, "Self-consistent treatment of nonequilibrium spin torques in magnetic multilayers," *Phys. Rev. B*, vol. 67, no. 10, p. 104430, Mar 2003.

[54] J. Grollier, D. Lacour, V. Cros, A. Hamzic, A. Vaurès, A. Fert, D. Adam, and G. Faini, "Switching the magnetic configuration of a spin valve by current-induced domain wall motion," *Journal of Applied Physics*, vol. 92, no. 8, pp. 4825–4827, 2002.

[55] M. Kläui, P.-O. Jubert, R. Allenspach, A. Bischof, J. A. C. Bland, G. Faini, U. Rüdiger, C. A. F. Vaz, L. Vila, and C. Vouille, "Direct observation of domain-wall configurations transformed by spin currents," *Phys. Rev. Lett.*, vol. 95, no. 2, p. 026601, Jul 2005.

[56] F. Bonell, T. Hauet, S. Andrieu, F. Bertran, P. Le Fèvre, L. Calmels, A. Tejeda, F. Montaigne, B. Warot-Fonrose, B. Belhadji, A. Nicolaou, and A. Taleb-Ibrahimi, "Spin-polarized electron tunneling in bcc FeCo/MgO/FeCo(001) magnetic tunnel junctions," *Phys. Rev. Lett.*, vol. 108, p. 176602, Apr 2012.

[57] C. Heide, "Spin currents in magnetic films," *Phys. Rev. Lett.*, vol. 87, p. 197201, Oct 2001.

[58] M. D. Stiles and A. Zangwill, "Anatomy of spin-transfer torque," *Phys. Rev. B*, vol. 66, p. 014407, Jun 2002.

[59] S. Zhang and P. M. Levy, "Time dependence of spin accumulation and magnetoresistance in magnetic multilayers," *Phys. Rev. B*, vol. 65, p. 052409, Jan 2002.

[60] J. Zhang and P. M. Levy, "Layer by layer approach to transport in noncollinear magnetic structures," *Phys. Rev. B*, vol. 71, p. 184426, May 2005.

[61] P. Chureemart, R. Cuadrado, I. D'Amico, and R. W. Chantrell, "Modeling spin injection across diffuse interfaces," *Phys. Rev. B*, vol. 87, p. 195310, May 2013.

[62] C. H. Park, B. C. Lee, and J. I. Lee, "Spin-asymmetry of the density of states for bulk and surface fe, co, and ni," *J. Korean Phys.Soc.*, vol. 47, pp. 655–665, Oct 2005.

[63] P. Chureemart, R. F. L. Evans, and R. W. Chantrell, "Dynamics of domain wall driven by spin-transfer torque," *Phys. Rev. B*, vol. 83, p. 184416, May 2011.

[64] R. Wieser, E. Y. Vedmedenko, and R. Wiesendanger, "Indirect control of antiferromagnetic domain walls with spin current," *Phys. Rev. Lett.*, vol. 106, no. 6, p. 067204, Feb 2011.

[65] H. Murakami, T. Komine, and R. Sugita, "Effect of non-adiabatic spin torque parameter on domain wall motion driven by pulse current in a magnetic nanowire," *Magnetics, IEEE Transactions on*, vol. 45, no. 10, pp. 3812 –3815, oct. 2009.

[66] M. Eltschka, M. Wötzel, J. Rhensius, S. Krzyk, U. Nowak, M. Kläui, T. Kasama, R. E. Dunin-Borkowski, L. J. Heyderman, H. J. van Driel, and R. A. Duine, "Nonadiabatic spin torque investigated using thermally activated magnetic domain wall dynamics," *Phys. Rev. Lett.*, vol. 105, p. 056601, Jul 2010.

[67] D. Claudio-Gonzalez, A. Thiaville, and J. Miltat, "Domain wall dynamics under nonlocal spin-transfer torque," *Phys. Rev. Lett.*, vol. 108, p. 227208, Jun 2012.

[68] G. Tatara, H. T. Ueda, K. Taguchi, Y. Sasaki, M. Nishijima, and A. Takeuchi, "Proposal for an active electromagnetic metamaterial based on spin-torque oscillators," *Phys. Rev. B*, vol. 87, p. 155102, Apr 2013.

[69] J. Slonczewski, "Excitation of spin waves by an electric current," *Journal of Magnetism and Magnetic Materials*, vol. 195, no. 2, pp. L261 – L268, 1999.

[70] T. Taniguchi, J. Sato, and H. Imamura, "Theory of spin accumulation and spin-transfer torque in a magnetic domain wall," *Phys. Rev. B*, vol. 79, no. 21, p. 212410, Jun 2009.

[71] Z. Z. Sun, J. Schliemann, P. Yan, and X. R. Wang, "Current-induced domain wall motion with adiabatic and nonadiabatic spin torques in magnetic nanowires," *The European Physical Journal B - Condensed Matter and Complex Systems*, vol. 79, pp. 449–453, 2011.

[72] J.-i. Kishine and A. S. Ovchinnikov, "Adiabatic and nonadiabatic spin-transfer torques in the current-driven magnetic domain wall motion," *Phys. Rev. B*, vol. 81, no. 13, p. 134405, Apr 2010.

[73] S. E. Barnes and S. Maekawa, "Current-spin coupling for ferromagnetic domain walls in fine wires," *Phys. Rev. Lett.*, vol. 95, no. 10, p. 107204, Sep 2005.

[74] Y. Tserkovnyak, H. J. Skadsem, A. Brataas, and G. E. W. Bauer, "Current-induced magnetization dynamics in disordered itinerant ferromagnets," *Phys. Rev. B*, vol. 74, no. 14, p. 144405, Oct 2006.

[75] H. Kohno, G. Tatara, and J. Shibata, "Microscopic calculation of spin torques in disordered ferromagnets," *Journal of the Physical Society of Japan*, vol. 75, no. 11, p. 113706, 2006.

[76] A. Bratass, A. D. Kent, and H. Ohno, "Current-induced torques in magnetic materials," *Nat Mater*, vol. 11, pp. 372–381, Apr 2012.

[77] A. Bratass, Y. Tserkovnyak, G. E. W. Bauer, and P. J. Kelly, "Spin pumping and spin transfer," in *Spin Current*, S. Maekawa, S. O. Valenzuela, E. Saitoh, and T. Kimura, Eds. Oxford: Oxford Science Publication, 2012.

[78] J. Sun, "Current-driven magnetic switching in manganite trilayer junctions," *Journal of Magnetism and Magnetic Materials*, vol. 202, no. 1, pp. 157 – 162, 1999.

[79] C. Heide, P. E. Zilberman, and R. J. Elliott, "Current-driven switching of magnetic layers," *Phys. Rev. B*, vol. 63, p. 064424, Jan 2001.

[80] L. Berger, "Low field magnetoresistance and domain drag in ferromagnets," *Journal of Applied Physics*, vol. 49, no. 3, pp. 2156–2161, 1978.

[81] A. Thiaville, Y. Nakatani, J. Miltat, and Y. Suzuki, "Micromagnetic understanding of current-driven domain wall motion in patterned nanowires," *EPL (Europhysics Letters)*, vol. 69, no. 6, p. 990, 2005.

[82] D. Jiles, *Introduction To Magnetism And Magnetic Materials*, 1st ed. Springer, 1990.

[83] B. D. Cullity and C. D. Graham, *Introduction to Magnetic Materials*, 2nd ed. John Wiley and Sons Inc., 2009.

[84] M. Thorwart and R. Egger, "Current-induced nonadiabatic spin torques and domain-wall motion with spin relaxation in a ferromagnetic metallic wire," *Phys. Rev. B*, vol. 76, p. 214418, Dec 2007.

[85] P. Baláž, V. K. Dugaev, and J. Barnaś, "Spin-transfer torque in a thick néel domain wall," *Phys. Rev. B*, vol. 85, p. 024416, Jan 2012.

[86] A. Vanhaverbeke and M. Viret, "Simple model of current-induced spin torque in domain walls," *Phys. Rev. B*, vol. 75, p. 024411, Jan 2007.

[87] A. Manchon, R. Matsumoto, H. Jaffres, and J. Grollier, "Spin transfer torque with spin diffusion in magnetic tunnel junctions," *Phys. Rev. B*, vol. 86, p. 060404, Aug 2012.

[88] S. Bohlens and D. Pfannkuche, "Width dependence of the nonadiabatic spin-transfer torque in narrow domain walls," *Phys. Rev. Lett.*, vol. 105, p. 177201, Oct 2010.

[89] P. M. Levy and S. Zhang, "Resistivity due to domain wall scattering," *Phys. Rev. Lett.*, vol. 79, pp. 5110–5113, Dec 1997.

[90] J. H. Franken, M. Hoeijmakers, H. J. M. Swagten, and B. Koopmans, "Tunable resistivity of individual magnetic domain walls," *Phys. Rev. Lett.*, vol. 108, p. 037205, Jan 2012.

[91] K. M. Seemann, F. Garcia-Sanchez, F. Kronast, J. Miguel, A. Kákay, C. M. Schneider, R. Hertel, F. Freimuth, Y. Mokrousov, and S. Blügel, "Disentangling the physical contributions to the electrical resistance in magnetic domain walls: A multiscale study," *Phys. Rev. Lett.*, vol. 108, p. 077201, Feb 2012.

[92] I. Garate, K. Gilmore, M. D. Stiles, and A. H. MacDonald, "Nonadiabatic spin-transfer torque in real materials," *Phys. Rev. B*, vol. 79, p. 104416, Mar 2009.

[93] Z. Yuan, Y. Liu, A. A. Starikov, P. J. Kelly, and A. Brataas, "Spin-orbit-coupling-induced domain-wall resistance in diffusive ferromagnets," *Phys. Rev. Lett.*, vol. 109, p. 267201, Dec 2012.

[94] P. Ho, G. C. Han, R. F. L. Evans, R. W. Chantrell, G. M. Chow, and J. S. Chen, "Perpendicular anisotropy L10-FePt based pseudo spin valve with Ag spacer layer," *Applied Physics Letters*, vol. 98, no. 13, p. 132501, 2011.

[95] J. Lyubina, I. Opahle, K.-H. Müller, O. Gutfleisch, M. Richter, M. Wolf, and L. Schultz, "Magnetocrystalline anisotropy in L10 FePt and exchange coupling in FePt/Fe 3 Pt nanocomposites," *Journal of Physics: Condensed Matter*, vol. 17, no. 26, p. 4157, 2005.

[96] H. J. Richter, O. Hellwig, S. Florez, C. Brombacher, and M. Albrecht, "Anisotropy measurements of FePt thin films," *Journal of Applied Physics*, vol. 109, no. 7, 2011.

[97] A. Aharoni and J. P. Jakubovics, "Magnetic domain walls in thick iron films," *Phys. Rev. B*, vol. 43, pp. 1290–1293, Jan 1991.

[98] M. Ohno and K. Yoh, "Micromagnetic simulation of magnetization reversal process and stray field behavior in fe thin film wire," *J. Appl. Phys.*, vol. 102, 2007.

[99] S. S. P. Parkin, "Origin of enhanced magnetoresistance of magnetic multilayers: Spin-dependent scattering from magnetic interface states," *Phys. Rev. Lett.*, vol. 71, pp. 1641–1644, Sep 1993.

[100] G. B. Rodrguez, L. Pereira, M. Miranda, A. Antunes, and M. Baibich, "Magnetotransport and coupling in nanostructured Co/Ag thin films," *Journal of Magnetism and Magnetic Materials*, vol. 214, no. 12, pp. 78 – 84, 2000.

[101] E. Ho, A. Petford-Long, and A. Cerezo, "The effect of interfacial regions on the giant magnetoresistance in as-grown and annealed Fe/Cr MLFs," *Journal of Magnetism and Magnetic Materials*, vol. 192, no. 3, pp. 431 – 442, 1999.

[102] J.-L. Tsai, H.-T. Tzeng, and B.-F. Liu, "Magnetic properties and microstructure of graded Fe/FePt films," *Journal of Applied Physics*, vol. 107, no. 11, p. 113923, 2010.

[103] D. Goll, A. Breitling, L. Gu, P. A. van Aken, and W. Sigle, "Experimental realization of graded L10-FePt/Fe composite media with perpendicular magnetization," *Journal of Applied Physics*, vol. 104, no. 8, p. 083903, 2008.

[104] J. Lee, V. Alexandrakis, M. Fuger, B. Dymerska, D. Suess, D. Niarchos, and J. Fidler, "FePt L10/A1 graded media with a rough interphase boundary," *Applied Physics Letters*, vol. 98, no. 22, p. 222501, 2011.

[105] Y. Choi, J. S. Jiang, Y. Ding, R. A. Rosenberg, J. E. Pearson, S. D. Bader, A. Zambano, M. Murakami, I. Takeuchi, Z. L. Wang, and J. P. Liu, "Role of diffused Co atoms in improving effective exchange coupling in Sm-CoFe spring magnets," *Phys. Rev. B*, vol. 75, p. 104432, Mar 2007.

[106] P. Ho, R. Evans, R. Chantrell, G. Han, G.-M. Chow, and J. Chen, "Atomistic Modeling of the Interlayer Coupling Behavior in Perpendicularly Magnetized-FePt/Ag/FePt Pseudo Spin Valves," *Magnetics, IEEE Transactions on*, vol. 47, no. 10, pp. 2646–2648, 2011.

[107] M. R. Sears and W. M. Saslow, "Spin accumulation at ferromagnet/nonmagnetic material interfaces," *Phys. Rev. B*, vol. 85, p. 014404, Jan 2012.

[108] S. S. P. Parkin, M. Hayashi, and L. Thomas, "Magnetic Domain-Wall Racetrack Memory," *Science*, vol. 320, no. 5873, pp. 190–194, 2008.

[109] L. Thomas, R. Moriya, C. Rettner, and S. S. P. Parkin, "Dynamics of Magnetic Domain Walls Under Their Own Inertia," *Science*, vol. 330, no. 6012, pp. 1810–1813, 2010.

[110] S. Tehrani, E. Chen, M. Durlam, M. DeHerrera, J. Slaughter, J. Shi, and G. Kerszykowski, "High density submicron magnetoresistive random access memory (invited)," *J. App. Phys.*, vol. 85, no. 8, p. 5822, 1999.

[111] H. Boeve, C. Bruynseraede, J. Das, K. Dessein, G. Borghs, J. De Boeck, R. Sousa, L. Melo, and P. Freitas, "Technology assessment for the implementation of magnetoresistive elements with semiconductor components in magnetic random access memory (MRAM) architectures," *Magnetics, IEEE Transactions on*, vol. 35, no. 5, pp. 2820 –2825, Sep. 1999.

[112] T. Ono, "Spin-transfer torque in nonuniform magnetic structures," in *Spin Current*, S. Maekawa, S. O. Valenzuela, E. Saitoh, and T. Kimura, Eds. Oxford: Oxford Science Publication, 2012.

[113] R. F. L. Evans,W. J. Fan, P. Chureemart, T. A. Ostler, J. Barker, M. O. A. Ellis, and R. W. Chantrell, "Atomistic spin model simulations of magnetic nanomaterials using VAMPIRE," *To be submitted to Physical Review E*, 2013.

[114] E. Boerner, O. Chubykalo-Fesenko, O. Mryasov, R. Chantrell, and O. Heinonen, "Moving toward an atomistic reader model," *IEEE Transactions on magnetic*, vol. 41, no. 2, pp. 936 – 940, Feb 2005.

[115] W. F. Brown, "Thermal fluctuations of a single-domain particle," *Phys. Rev.*, vol. 130, pp. 1677–1686, Jun 1963.

[116] A. Hubert and R. Schfer, *Magnetic Domains: The Analysis of Magnetic Microstructures*, 3rd ed. Springer, 2009.

[117] A. Lyberatos, D. V. Berkov, and R. W. Chantrell, "A method for the numerical simulation of the thermal magnetization fluctuations in micromagnetics," *Journal of Physics: Condensed Matter*, vol. 5, no. 47, p. 8911, 1993.

[118] A. Lyberatos and R. W. Chantrell, "Thermal fluctuations in a pair of magnetostatically coupled particles," *Journal of Applied Physics*, vol. 73, no. 10, pp. 6501–6503, 1993.

[119] J. L. Garcia-Palacios and F. J. Lázaro, "Langevin-dynamics study of the dynamical properties of small magnetic particles," *Phys. Rev. B*, vol. 58, pp. 14 937–14 958, Dec 1998.

[120] O. Chubykalo, J. D. Hannay, M. Wongsam, R. W. Chantrell, and J. M. Gonzalez, "Langevin dynamic simulation of spin waves in a micromagnetic model," *Phys. Rev. B*, vol. 65, p. 184428, May 2002.

[121] W. T. Coffey and Y. P. Kalmykov, "Thermal fluctuations of magnetic nanoparticles: Fifty years after brown," *Journal of Applied Physics*, vol. 112, no. 12, p. 121301, 2012.

[122] C. Serpico, I. D. Mayergoyz, and G. Bertotti, "Numerical technique for integration of the Landau-Lifshitz equation," *Journal of Applied Physics*, vol. 89, no. 11, pp. 6991–6993, 2001.

[123] M. d'Aquino, C. Serpico, G. Coppola, I. D. Mayergoyz, and G. Bertotti, "Midpoint numerical technique for stochastic Landau-Lifshitz-Gilbert dynamics," *Journal of Applied Physics*, vol. 99, no. 8, p. 08B905, 2006.

[124] R. Evans, "Atomistic modelling of nanogranular magnetic materials," Ph.D. dissertation, Department of Physics, University of York, 2008.

[125] D.-V. Dan and S.-E. Malureanu, "Modelling of the magnetization process based on the Landau-Lifshitz-Gilbert equation," in *Advanced Topics in Electrical Engineering (ATEE), 2011 7th International Symposium on*, 2011, pp. 1–4.